WCAP-6050
Reactor Technology
(TID-4500, 17th Ed.)

WCAP-6050

ANALYSIS OF THE REACTIVITY CHARACTERISTICS OF YANKEE CORE I

By

C. G. Poncelet
Nuclear Engineering Section
Reactor Development

Prepared for the New York Operations Office
U. S. Atomic Energy Commission
Under AEC Contract Number AT(30-1)-3017

January, 1963

Technical Approval:

H. W. Graves, Jr., Manager
Nuclear Engineering Section
Reactor Development

Project Manager Approval:

L. Chajson, Manager
Yankee Core Evaluation

Westinghouse Electric Corporation
Atomic Power Division
P. O. Box 355
Pittsburgh 30, Pennsylvania

DISCLAIMER

WESTINGHOUSE DISTRIBUTION

W. E. Johnson	1	L. B. Kramer	1
J. C. Rengel	1	E. L. Kuno	1
W. E. Abbott	1	F. L. Langford, Jr.	1
H. N. Andrews	1	S. M. Marshall	15
S. Bartnoff	1	J. D. McGaugh	4
D. Beatty - NPS	1	G. H. Minton	1
L. Chajson	1	N. R. Nelson	1
R. H. Chastain	4	C. P. Obermesser	1
I. H. Coen	1	S. S. Pawlicki	1
P. Cohen	1	C. G. Poncelet	1
R. J. Creagan	1	E. U. Powell	1
J. P. Cunningham	1	H. L. Russo	1
W. F. Davis	1	T. Stern	1
P. G. DeHuff	1	R. L. Stoker	1
R. J. French	1	G. R. Taylor	1
J. M. Gallagher	1	A. G. Thorp II	1
D. T. Galm	1	L. S. Tong	1
N. E. Gordon	1	H. J. von Hollen	1
H. W. Graves, Jr.	1	H. E. Walchli	1
P. B. Haga	1	J. H. Wright	1
D. F. Hanlen	1	T. F. Wyke	1
R. G. Hobson	1	J. M. Yadon	1
A. R. Jones	1	T. I. C.	3
A. S. Kitzes	1	TOTAL	69

EXTERNAL DISTRIBUTION

USAEC, Division of Reactor Development, Chief, Water Reactors Branch, Washington 25, D. C.: Attention - W. R. Voigt	20
USAEC, Division of Reactor Development, Reports and Statistics Branch, Washington 25, D. C.	1
USAEC, Division of Reactor Development, Water Reactors Branch, Washington 25, D. C.: Attention - D. E. Erb	1
USAEC, New York Operations Office, 376 Hudson Street, New York 14, New York: R. E. Behmer, Chief, Civilian Projects Branch	2
J. Wise, Reactor Division	4
USAEC, New York Patents Group, Brookhaven Office, Upton, Long Island, New York: Attention - Harmon Potter	1
Division of Technical Information, P. O. Box 62, Oak Ridge, Tennessee	4
Yankee Atomic Electric Company, 441 Stuart Street, Boston 16, Massachusetts: Attention - R. J. Coe	6
USAEC "Standard Distribution List" UC-80 per pages iv, v and vi	609
Total External Distribution	648

Standard Distribution (Category UC-80)
(TID-4500 - 17th Ed.)

No. of Copies	
4	Aberdeen Proving Ground
1	Aerojet-General Corporation
1	Aerojet-General Nucleonics
8	Aeronautical Systems Division
2	Air Force Special Weapons Center
1	Albuquerque Operations Office
1	Alco Products, Inc.
1	Allis-Chalmers Manufacturing Company
1	Allis-Chalmers Manufacturing Company, Washington
1	Allison Division - GMC
1	American Bosch Arma Corporation
10	Argonne National Laboratory
1	Armour Research Foundation
1	Army Ballistic Missile Agency
2	Army Chemical Center
1	Army Chemical Center (Taras)
1	Army Environmental Hygiene Agency
1	Army Signal Research and Development Laboratory
1	AEC Scientific Representative, Belgium
1	AEC Scientific Representative, France
1	AEC Scientific Representative, Japan
3	Atomic Energy Commission, Washington
4	Atomic Energy of Canada Limited
4	Atomics International
4	Babcock and Wilcox Company
2	Battelle Memorial Institute
1	Beryllium Corporation
4	Brookhaven National Laboratory
1	Bureau of Medicine and Surgery
1	Bureau of Ships (Code 1500)
1	Bureau of Yards and Docks
1	Chicago Patent Group
1	Combustion Engineering, Inc.
1	Combustion Engineering, Inc. (NRD)
2	Convair Division, Fort Worth
1	Defence Research Member
1	Denver Research Institute
1	Department of the Army
4	duPont Company, Aiken
1	duPont Company, Wilmington
1	Edgerton, Germeshausen and Grier, Inc., Las Vegas
1	Frankford Arsenal
1	Franklin Institute of Pennsylvania

Standard Distribution (Continued)

No. of Copies	
2	General Atomic Division
3	General Electric Company (ANPD)
6	General Electric Company, Richland
1	General Nuclear Engineering Corporation
1	Gibbs and Cox, Inc.
1	Glasstone, Samuel
1	Hughes Aircraft Company
2	Iowa State University
2	Jet Propulsion Laboratory
2	Knolls Atomic Power Laboratory
1	Lockheed Aircraft Corporation
4	Los Alamos Scientific Laboratory
1	Lowry Air Force Base
1	Maritime Administration
1	Martin Company
1	Massachusetts Institute of Technology (Hardy)
1	Massachusetts Institute of Technology (Thompson)
1	Monsanto Chemical Company
1	Mound Laboratory
1	NASA Lewis Research Center
1	National Bureau of Standards
1	National Bureau of Standards (Library)
1	National Lead Company of Ohio
1	Naval Medical Research Institute
2	Naval Ordnance Laboratory
1	Naval Postgraduate School
1	Naval Radiological Defense Laboratory
3	Naval Research Laboratory
1	New Brunswick Area Office
1	New York Operations Office
1	New York University (Richtmyer)
1	Nuclear Materials and Equipment Corporation
1	Nuclear Metals, Inc.
1	Oak Ridge Institute of Nuclear Studies
10	Office of Naval Research
1	Office of Naval Research (Code 422)
1	Office of the Chief of Naval Operations
1	Office of the Surgeon General
1	Ordnance Materials Research Office
1	Ordnance Tank-Automotive Command
1	Patent Branch, Washington
1	Pennsylvania State University
6	Phillips Petroleum Company (NRTS)
1	Picatinny Arsenal
1	Power Reactor Development Company
3	Pratt and Whitney Aircraft Division

No. of Copies	
2	Public Health Service
1	Puerto Rico Water Resources Authority
1	Purdue University
1	RAND Corporation
1	Rensselaer Polytechnic Institute
1	Republic Aviation Corporation
1	Research Analysis Corporation
1	Sandia Corporation, Albuquerque
1	Schenectady Naval Reactors Operations Office
1	Space Technology Laboratories (PRL)
1	States Marine Lines, Inc.
1	Stevens Institute of Technology
1	Surgeon General
1	Sylvania Electric Products, Inc.
1	Technical Research Group
1	Tennessee Valley Authority
1	Texas Nuclear Corporation
2	Union Carbide Nuclear Company (ORGDP)
8	Union Carbide Nuclear Company (ORNL)
1	United Nuclear Corporation (NDA)
1	U. S. Geological Survey, Denver
1	U. S. Patent Office
1	University of California, Berkeley
2	University of California, Livermore
1	University of Puerto Rico
1	University of Rochester
2	University of Rochester (Marshak)
1	Walter Reed Army Medical Center
1	Watertown Arsenal
4	Westinghouse Bettis Atomic Power Laboratory
2	Westinghouse Electric Corporation
1	Yankee Atomic Electric Company
325	Division of Technical Information Extension
75	Office of Technical Services, Washington
609	TOTAL

TABLE OF CONTENTS

TABLE OF CONTENTS (Continued)

TABLE OF CONTENTS (Continued)

LIST OF FIGURES

LIST OF FIGURES (Continued)

LIST OF FIGURES (Continued)

LIST OF TABLES

LIST OF TABLES (Continued)

ABSTRACT

The reactivity characteristics of the operating Yankee Core I are analyzed. Calculations of kinetic parameters, kinetic coefficients, control rod and boron worth, core lifetime and burnup rate, and fission product poisoning, are described. A large amount of experimental data obtained during Core I operation is included and comparisons are made between prediction and experiments.

1.0 INTRODUCTION

The Yankee Core Follow Program, supported jointly by the Westinghouse Electric Corporation and the Yankee Atomic Electric Company, was a program to gather, analyze, and interpret experimental data from the Yankee plant to ascertain the nuclear behavior of the first core. The information was expected to be of value to both Westinghouse as the nuclear designer and to Yankee as the owner and operator.

This report describes the analytical work which was performed as an integral part of the Yankee Core Follow Program on the reactivity characteristics and behavior of the first core. A companion report[1] describes the power distribution analyses performed under the same program. An attempt has been made to include a large amount of experimental data whenever comparisons of calculations and experiments were possible. This report was prepared and edited under the Yankee Core I Evaluation Program, sponsored by the USAEC. As such it constitutes the first of a series of technical reports on the evaluation of the Yankee Core I.

The Yankee reactor is of the pressurized light water type, with rod shaped fuel elements of slightly enriched UO_2 (3.4 w/o in U-235) contained in stainless steel. A description of the nuclear core and the associated plant can be found in reference 2. Core loading was initiated in July 1960 and initial criticality was achieved in August 1960. This was followed by an extensive test program which terminated in January 1961 when the plant attained the Core I design thermal output (392 MWt). A description of the experimental data which was obtained during this period can be found in reference 3. A description of the analytical physics work which supported this series of experiments can be found in reference 4. The Yankee Core Follow Program was a logical extension of the initial research and development design programs and the startup experiment program.

From January 1961 until June 1961 the first core operated at its design thermal output of 392 MWt or 110 MWe of net electrical power for a total burnup of approximately 3500 EFPH* or 2700 MWD/Tonne. In June 1961 an increase in power level from 392 MWt to 485 MWt (150 MWe) was authorized. End of core lifetime at 392 MWt and rated conditions (514°F, 2000 psig) occurred in January 1962 at an average burnup of 8000 EFPH or 6270 MWD/Tonne. At this

*EFPH = equivalent full power hours referenced at 392 MWt. This definition of EFPH will be used throughout the context of this report.

time all control rods had been removed from the core. This was followed by a core lifetime extension period where power and main coolant temperature were continuously lowered to balance the loss of reactivity due to burnup. Final shutdown occurred on May 18, 1962 at a power level of 270 MWt, main coolant temperature 431°F and a total average burnup of 10,680 EFPH or 8360 MWD/Tonne.

As part of its license agreement, Yankee was required to shut down the reactor at intervals of about 2000 EFPH to perform measurements of the kinetic coefficients of the core. The purpose of the tests was to obtain information on the effect of Pu buildup on the kinetic characteristics of the core. In addition to data on kinetic coefficients, Yankee has obtained a large amount of experimental data on control rod worth, boron worth, Xe-135 poisoning and fuel depletion rate, in addition to the power distribution data [1]. This information, obtained in a large utility reactor, under conditions of actual operation, is felt to be of great value to the industry as a whole.

The excellent operating characteristics of the core have verified the technical feasibility and economic potential of this type of reactor. The predicted performance of the core [4], confirmed by the initial startup experiment program [3] was further substantiated by actual operation of the core at power during a period of 17 months. The agreement between calculations and measurements of the core reactivity characteristics was very good. In general the core behaved as predicted. However anomalies in the detailed reactivity behavior of the operating core were observed which were not predicted by standard reactivity calculations. These anomalies in no way interfered with the safe operation of the reactor. Instead they served as a basis for detailed analytical studies which have led to a better understanding of the physics of pressurized water, UO_2 fueled reactors.

Section 2.0 of this report describes the operation history of the first core, in terms of power, EFPH, control rod motion and reactivity behavior. Section 3.0 describes the physics calculations pertaining to the reactivity characteristics of the first core and compares the calculational results to experiments.

2.0 OPERATION HISTORY OF THE YANKEE CORE I

2.1 Power and EFPH History

Figure 2.1 shows the power and EFPH history of Core I in terms of daily average load in gross MWe and accumulated full power hours referenced to 392 MWt. Figure 2.1 shows six major shutdowns. These are listed in Table 2.1.

Table 2.1

Major Shutdowns in Yankee Core I

Date of Shutdown	Length of Shutdown	Purpose of Shutdown
2/19/61	92 hours	Valve maintenance inside vapor container
4/1/61	185 hours	Low power physics testing (1900 EFPH)
5/2/61	39 hours	Vapor container inspection, pressurizer instrument connection repair and turbine control valve repairs
6/24/61	41 hours	Plant protective system changes and vapor container inspection
7/10/61	326 hours	Low power physics testing (4000 EFPH)
11/3/61	109 hours	Low power physics testing (6400 EFPH)

The control rods were completely withdrawn from the core on December 22, 1961. Reactivity losses due to burnup were then compensated by decreasing main coolant temperature and power level. Final plant shutdown occurred on May 18, 1962.

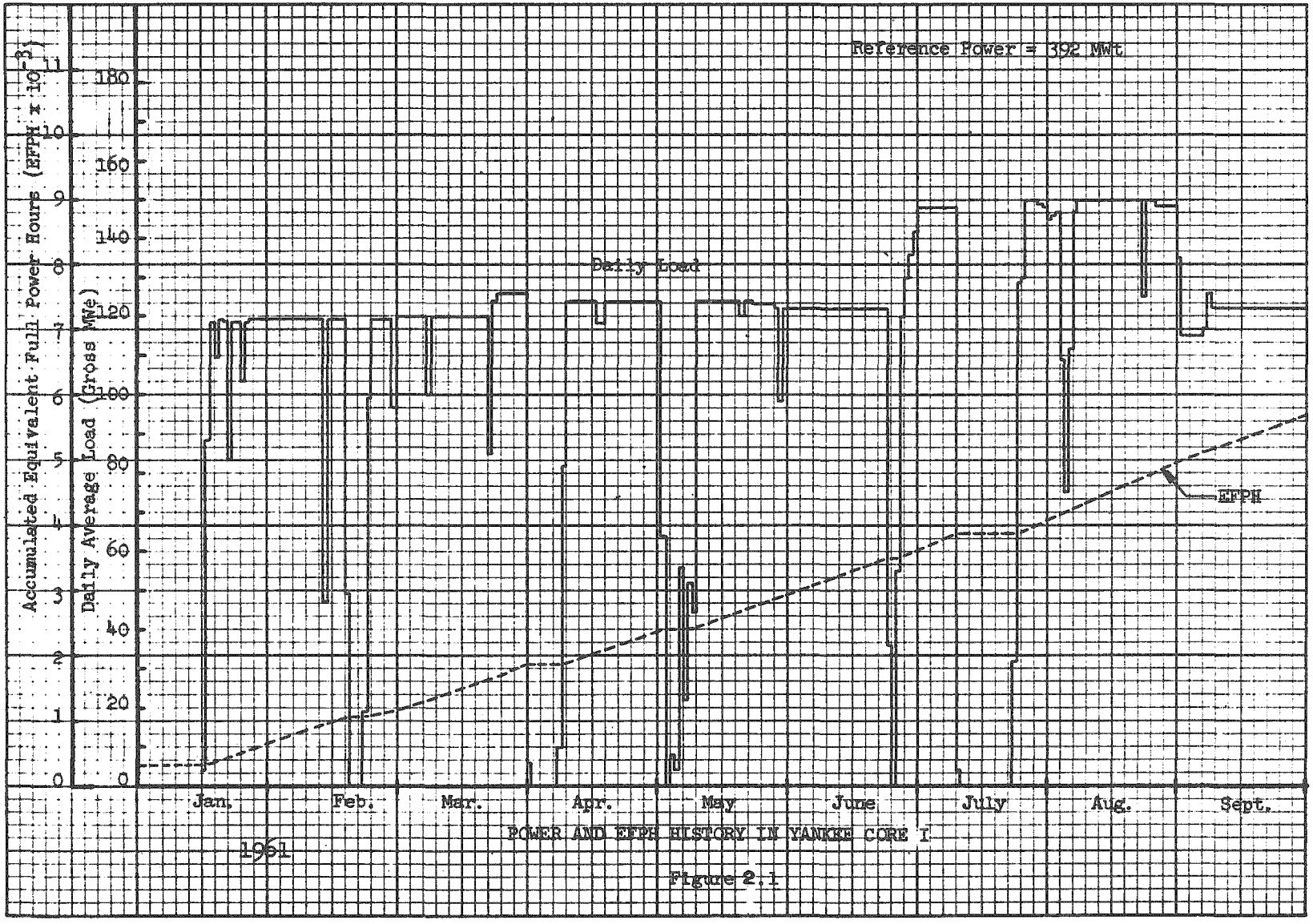

POWER AND EFPH HISTORY IN YANKEE CORE I

Figure 2.1

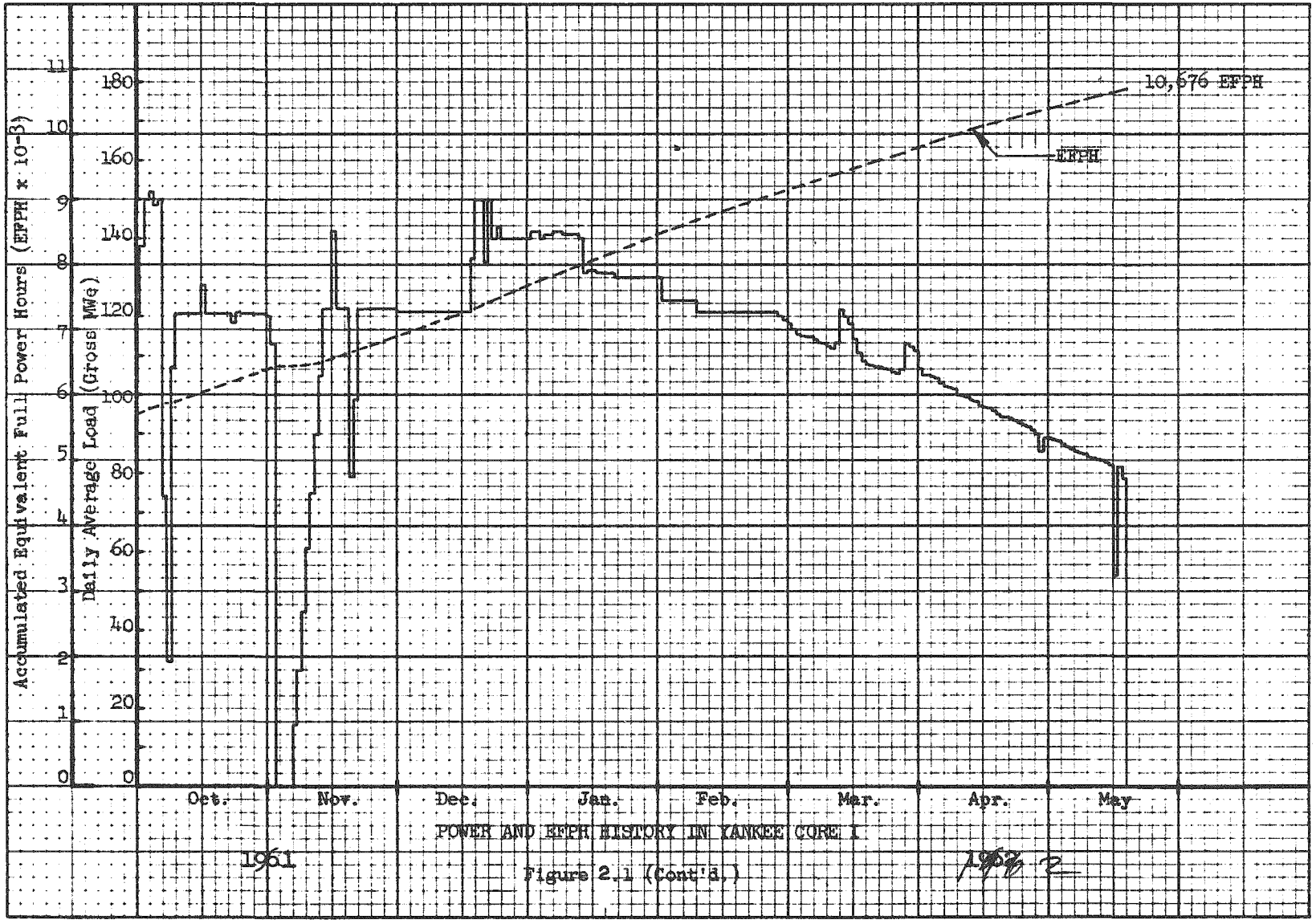

POWER AND EFPH HISTORY IN YANKEE CORE I

Figure 2.1 (Cont'd.)

2.2 Control Rod Motion History

Figure 2.2 shows the controlling rod group heights as a function of EFPH for the reference withdrawal sequence (6 4 2 3 5 1).* A description of the control rod group locations and identification can be found in reference 4. Anomalous behavior of the data, as evidenced by motion of rod groups 5 and 1 results either from changes in power level (see Figure 2.1), from anomalous reactivity variations (see Figure 2.3), or from scheduled physics testing.

2.3 Reactivity History

It is possible to obtain a history of the reactivity behavior in Yankee by observing the motion of the control rods and the variation of main coolant pressure, temperature and boron concentration from a given reference point in time. A continuous record of rod position, and primary coolant pressure and temperature is available at the control panel. A history of accumulated reactivity change is obtained by using measured control rod worth, boron worth and pressure and temperature coefficients. An analytical reactivity model which predicts reactivity variations with time is based on a calculation of the variation of the reactivity tied up in the Doppler effect, the fission products xenon and samarium, and of the reactivity loss in fuel depletion. Each of these effects can be separately verified by experiments. The adequacy and completeness of this analytical model can be evaluated by a comparison of the predicted reactivity behavior with the measured reactivity behavior. However, any discrepancy between the measured and predicted reactivity history does not necessarily reflect a fault in the analytical model. That is, the accuracy of the measured reactivity history depends on the availability and accuracy of control rod worth, boron worth, and reactivity coefficient data. In this report the term "anomalous reactivity variation" will refer to the difference between the measured and predicted reactivity variation.

---

*The normal control rod withdrawal pattern in Yankee is 642351; i.e., group 6 is withdrawn first, followed by the withdrawal of group 4, etc. To obtain a more uniform distribution of burnup, control rod groups at equivalent radii were interchanged periodically. At the time of an interchange, groups 1 and 2 and groups 3 and 4 were interchanged.

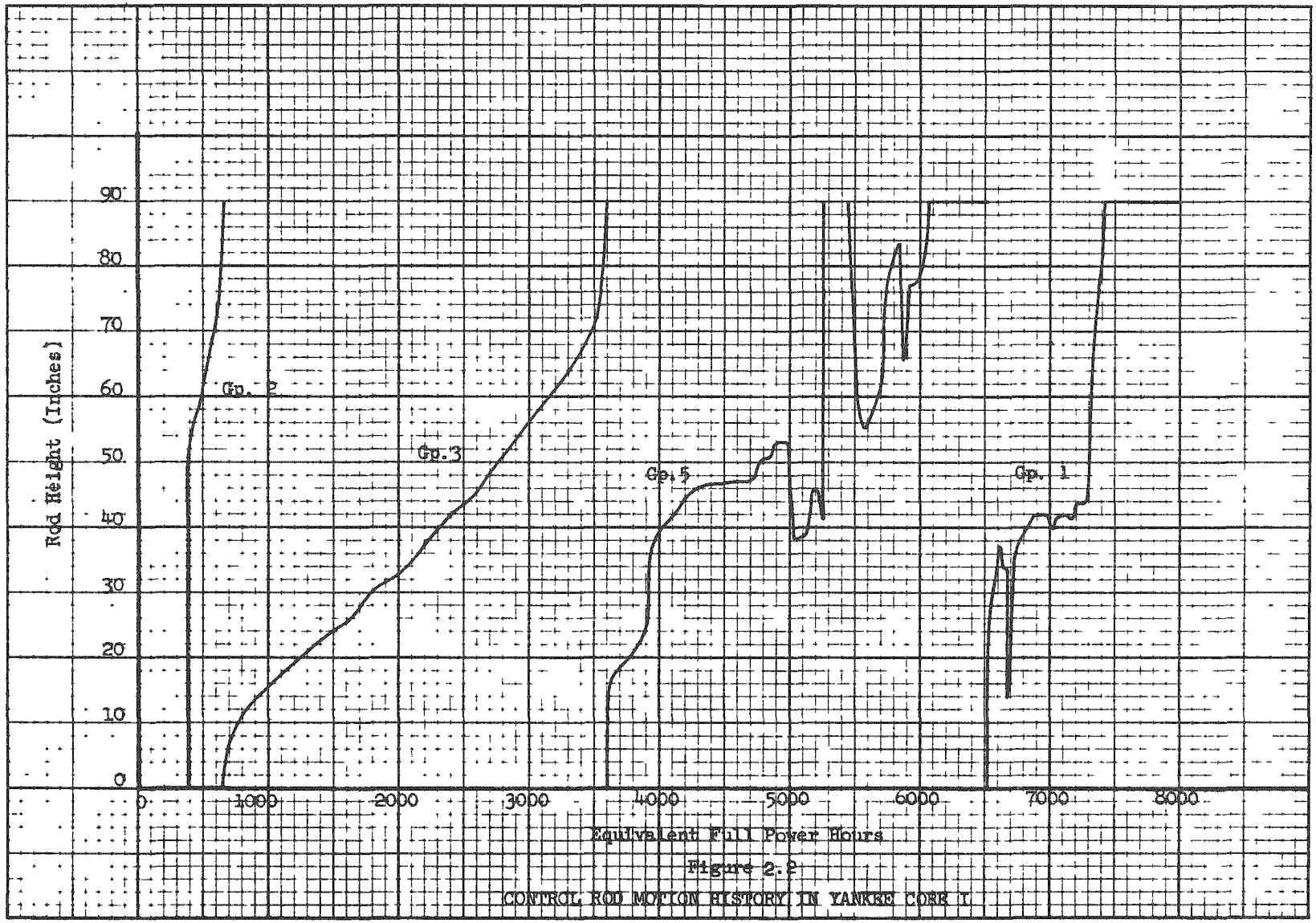

Figure 2.2

CONTROL ROD MOTION HISTORY IN YANKEE CORE I

2.3.1 Reference Conditions for the Analysis of Core Reactivity Behavior

No large anomalous reactivity variation was observed before the 4000 EFPH shutdown. The first occurrence of a significant anomalous reactivity variation took place during startup to power after the 4000 EFPH shutdown. The anomalous variation was based on a comparison of the control rod position at power before the shutdown with that after steady state conditions were reached after returning to power. A detailed study of the reactivity history was subsequently initiated and carried out to the final shutdown on May 18, 1962. The reference point chosen was that for the hot, zero-power core immediately preceding startup at 4000 EFPH.

The reference main coolant temperature and pressure were chosen at 514°F and 2050 psig, respectively. The reference position for the control rods was 12 in. on group 2, with groups 6 and 4 removed and groups 3, 5, 1 inserted, which is the zero-power rod position before startup. Based on this rod position, the rod position at power before shutdown, measured rod worth data, and the measured power coefficient and Xe-135 poisoning before the shutdown, a loss in reactivity of 0.14% ρ is obtained, with the reactor at zero power. This loss may be explained by the calculated increase in Sm-149 poisoning (- .18%), the calculated increase in fission product poisoning (- .05%) and the calculated increase in reactivity due to Pu-239 buildup during the shutdown (+ .1%)(Section 3.0).

2.3.2 Calculation of Anomalous Reactivity Variations

The measured reactivity variation is obtained from

$$\rho^{\text{measured}} = \rho(\text{control rods}) + (T - 514)\frac{\partial \rho}{\partial T}$$

$$+ (P - 2050)\frac{\partial \rho}{\partial P} + C_B \frac{\partial \rho}{\partial C_B} \qquad (2.1)$$

A record of rod position, temperature and pressure, and boron concentration with time was obtained from data transmitted to Westinghouse from the plant, supplemented by the plant log sheets. The zero power rod worth and boron worth data obtained during the 4000 EFPH shutdown were used in equation (2.1) for the total range of reactivity history. This was necessitated because a complete set of rod worth and boron worth data was obtained only during the 4000 EFPH shutdown. Corrections for moderator temperature and pressure variations were done by using temperature and pressure coefficients measured during the 4000 and 6400 EFPH shutdown.

The calculated reactivity variation is obtained from

$$\rho^{\text{calculated}} = \rho^{\text{Xe}} + \rho^{\text{Sm}} + \rho^{\text{Doppler}} + \rho^{\text{depletion}} - \rho^{\text{Sm}}_{\text{startup}} \qquad (2.2)$$

The Sm-149 poisoning at time of startup ($\rho^{\text{Sm}}_{\text{startup}}$) was - 0.865% (section 3.9). Xe-135 and Sm-149 poisoning in equation (2.2) were calculated by means of the HISTORIAN code (section 3.8). The power defect was based on the calculated power coefficient shown in Figure 3.7 (section 3.4). The calculation of reactivity loss in fuel depletion was based on a calculated burnup coefficient of 0.92×10^{-5}/EFPH (section 3.7).

The anomalous reactivity variation is defined as the difference between the measured reactivity variation and the calculated reactivity variation as obtained by equations (2.1) and (2.2),

$$\rho^{\text{anomalous}} = \rho^{\text{measured}} - \rho^{\text{calculated}} \qquad (2.3)$$

Figure 2.3 shows the anomalous reactivity behavior between July 23, 1961 (4000 EFPH) and May 18, 1962 (10,700 EFPH). A positive anomalous reactivity variation corresponds to a gain in reactivity while a negative anomalous reactivity corresponds to a loss in reactivity. Figure 2.3 should be studied together with the power history of Figure 2.1 and the control rod motion history of Figure 2.2.

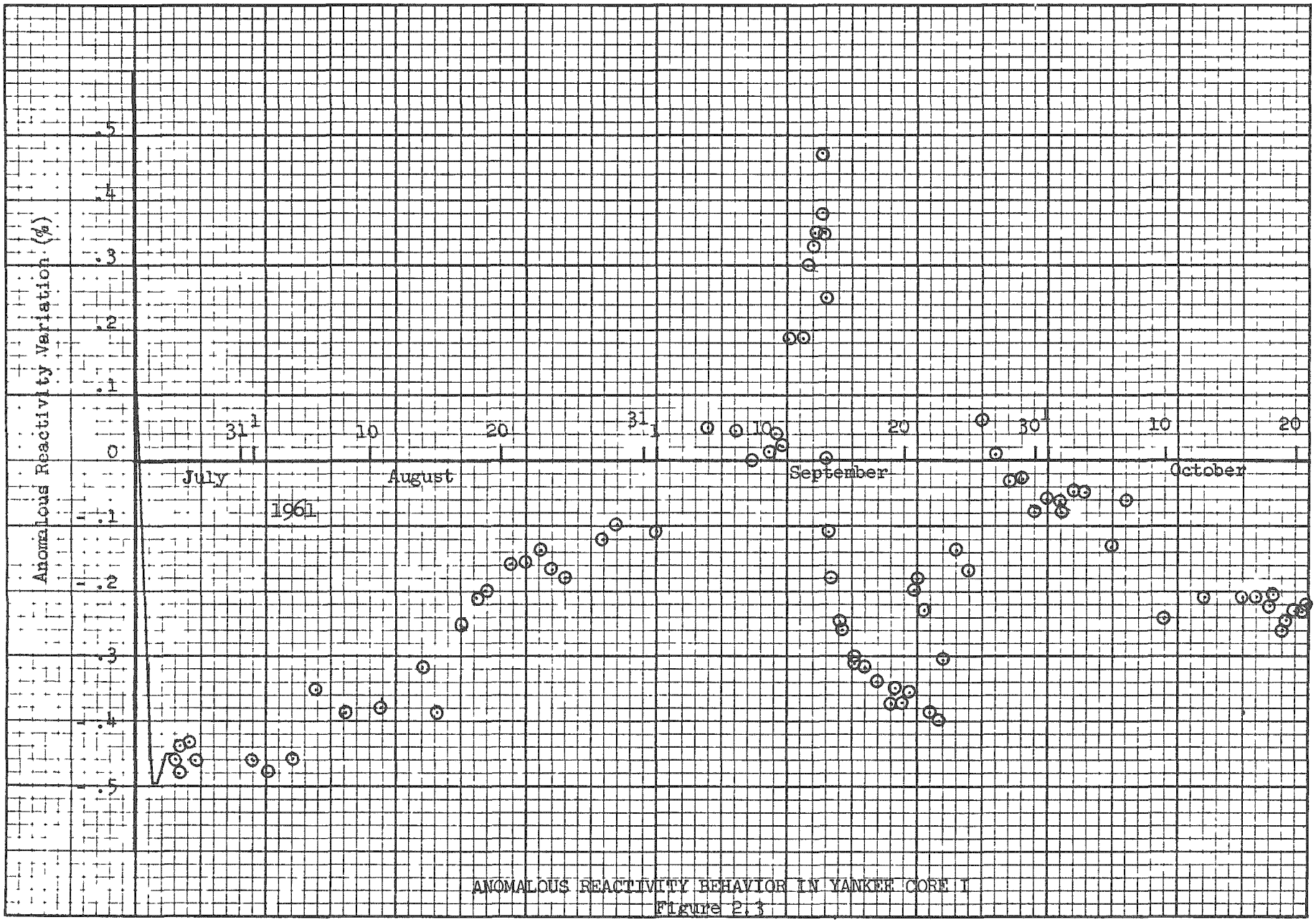

ANOMALOUS REACTIVITY BEHAVIOR IN YANKEE CORE I
Figure 2.3

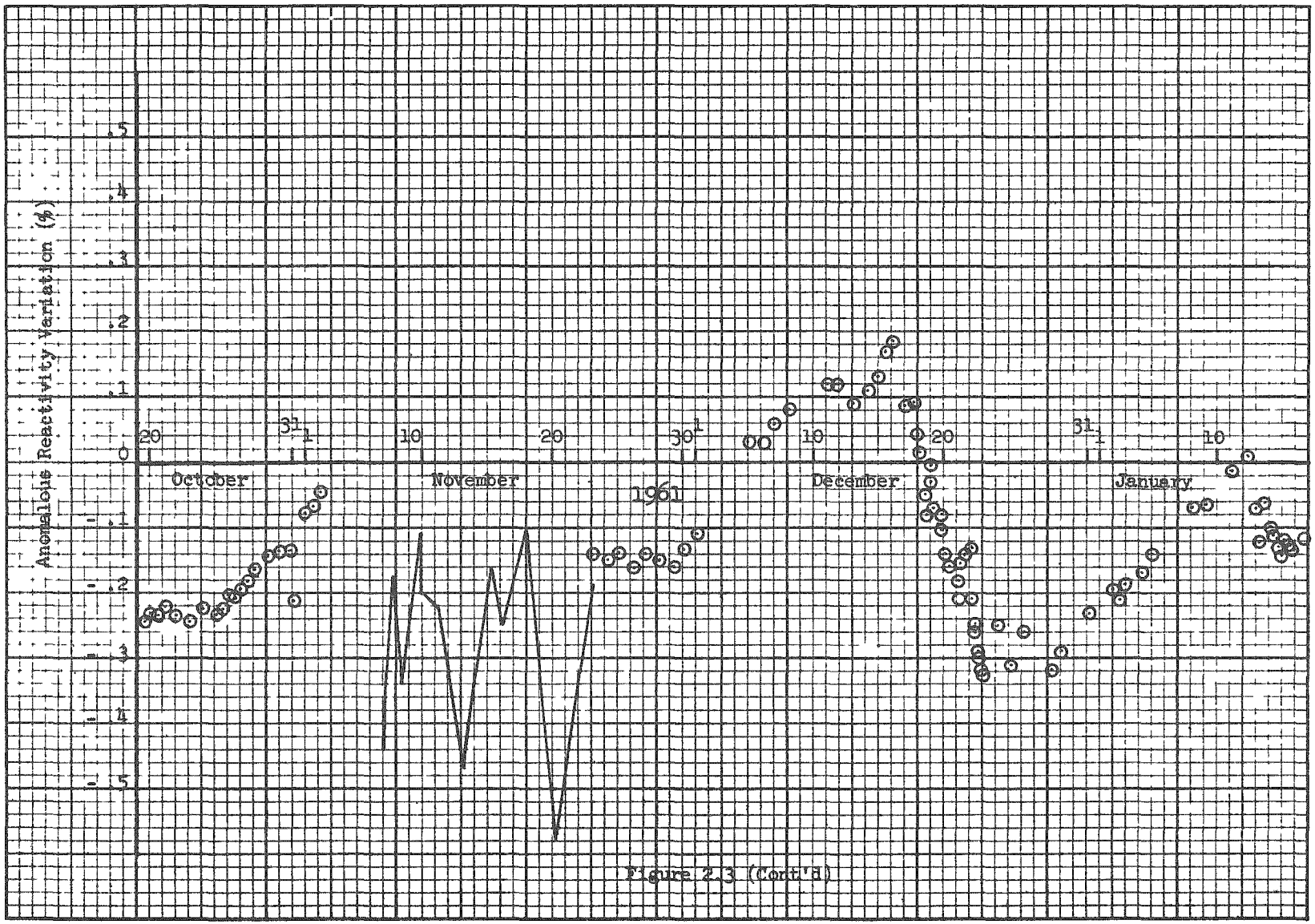

Figure 2.3 (Cont'd)

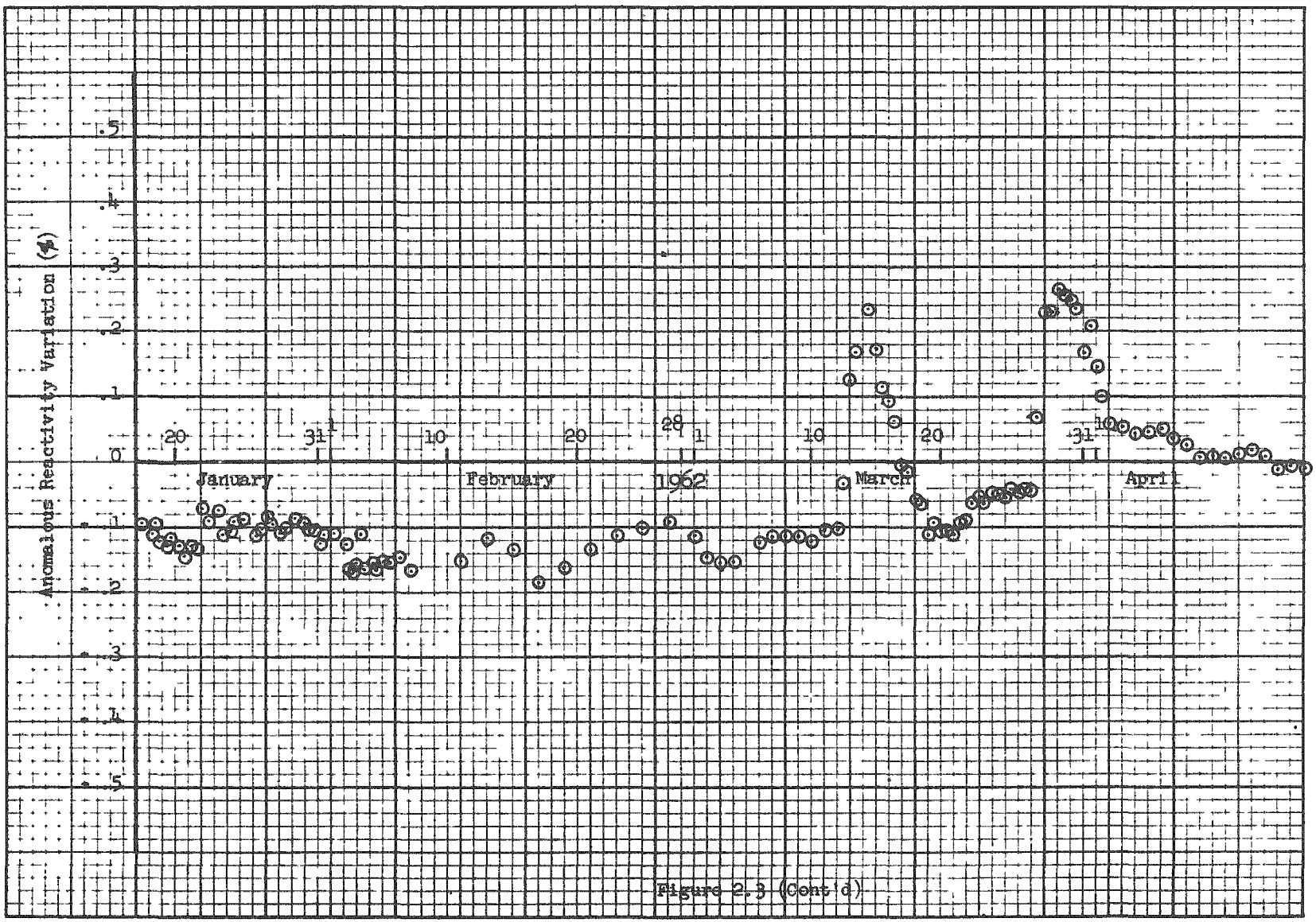

Figure 2.3 (Cont'd)

Figure 2.3 (Cont'd)

The initial loss of reactivity which occurred upon returning to power after the 4000 EFPH shutdown is clearly evident. The events which took place during the boron test at power on September 13, 1961 are of importance since the main purpose of the test was to confirm the feasibility of chemical shim operation at power. On September 12, 24 hours before the boron test, an unexplained reactivity gain occurred. Boration took place on September 13. The reactivity gain (~ 0.4%) continued until the core was borated to 390 ppm with rod group 1 at 59 in. and all other rod groups withdrawn. The only change in plant conditions noted on September 12 was an increase in the coolant pH from 7.0 to 9.2 with an increase in ammonia concentration to about 3 ppm. After boration a loss in reactivity (~ 0.8%) occurred first at a fast rate, then at a slower rate after all rods were completely withdrawn. After dilution there was a gain in reactivity (~ 0.5%) at a rate roughly similar to the rate of loss during the test.

2.3.3 Analysis of Anomalous Reactivity Variations

There are three sources from which it is possible to draw explanations for the anomalous reactivity behavior of Figure 2.3. These are:

1. Errors in the calculation of $\rho^{measured}$. These include the use of incorrect control rod worth data, temperature and pressure coefficients, and boron worth.

2. Errors in the calculation of $\rho^{calculated}$. These may include

   a) discrepancy in the models used for Xe and Sm poisoning, Doppler effect and depletion rate;

   b) the omission of reactivity mechanisms in the calculation of $\rho^{calculated}$.

The reactivity calculations described in section 3.0 have disclosed reactivity mechanisms in Yankee which can explain most of the anomalous reactivity behavior of Figure 2.3. It is difficult to associate a definite explanation to each anomalous reactivity variation, since the variations are small, of the order of a few tenths of a percent in reactivity. However, an attempt has been made to explain the gross reactivity behavior of Figure 2.3.

1. The initial rapid loss in reactivity (~ .5%) upon returning to power on July 23, 1961 after the 4000 EFPH shutdown with the subsequent slow gain (~ .5%) over a period of about 40 days, is explained in section 3.4.3 as a power coefficient effect resulting from changes in the pellet-clad gap geometry.

2. The gain in reactivity (~ .4%) which occurred on September 12, 1961 can be empirically attributed to chemistry effects. On March 13, 1962 and on March 27, 1962, hydrazine was purposely added to the main coolant to raise the ammonia concentration of the coolant to about 4 ppm. These tests were performed in an attempt to duplicate the coolant chemistry conditions of September 12, 1961. Coolant pH increased from about 7 to about 9. A reactivity gain of about 0.3% was noticed during both of the tests. The reactivity was lost after the ammonia concentration had been reduced to pre-test levels. Although it appears possible that a highly absorbing poison was removed from core surfaces during the test and subsequently redeposited on the core surfaces, no definite conclusion on the processes involved has been reached as of the present time.

3. Approximately 0.8% in reactivity was lost after boration of the core at power on September 13, 1961 which includes the gain of 0.4% that occurred the previous day, as noted below. Although it is not possible to conclude with certainty that boron plate-out on core surfaces is not the cause for the anomalous reactivity loss, it is nevertheless possible to explain the reactivity loss on the basis of mechanisms other than boron plate-out*. Based on the calculations of section 3.0, several possible causes for the reactivity loss during the boron test at power have been combined:

	Reactivity Variation
Coolant chemistry - Completion of the transient which was initiated on September 12, 1961	- 0.4%
Increase in the statistical weight factor on the power defect (section 3.4.3)	- 0.2%
Redistribution of main coolant temperature in the core (section 3.12)	- 0.1%
Error in the worth of control rod groups 1 and 5 (section 3.5.2)	- 0.1%
Boron depletion during test (section 3.6.3)	+ 0.1%
	- 0.7%

It should also be pointed out that a 10% error in boron worth corresponds to a reactivity of about 0.25%.

---

*Examinations of the Yankee spent fuel assemblies after the final shutdown in May 1962 have revealed minimal levels of crud deposited on surfaces. However it cannot be concluded that the same conditions necessarily existed during power operation.

4. The anomalous reactivity behavior which followed the 6400 EFPH shutdown from November 7 to November 23, 1961 occurred during an extended period of power coefficient measurements. The power level was raised in small increments over a period of 2 weeks. The anomalous reactivity behavior can be explained on the basis of the use of incorrect control rod worth data during the Xe-135 transients which occurred during the tests. As mentioned previously, the zero power rod worth data measured during the 4000 EFPH were used to calculate $\rho^{measured}$. In section 3.5.2 it is shown that control rod worth can be significantly different during Xe-135 transients.

5. The slow reactivity variations (~ 0.3%) which occurred during October, late November and between December 16 and January 12 all showed the same trend: a loss in reactivity followed by a slow gain of reactivity at a rate roughly equivalent to the burnup rate. Two possible explanations can be suggested. First, it is suggested that the anomalous reactivity variations are not real and result from the use of incorrect control rod worth data. The differential worth of groups 1 and 5 have been shown to be significantly affected by burnup and power (section 3.5.2). However this mechanism does not explain the reactivity gain which followed the complete withdrawal of control rods from the core. Second, it is suggested that the anomalous reactivity variations are real and correspond to variations in the power coefficient. Control rod motion can shift the power distribution into regions of previously low fuel temperature and therefore relatively large pellet-clad gap and high power coefficient. This will lead to a reduction in core reactivity. However, the subsequent expansion, possible cracking of the pellets, and redistribution of UO_2

within the fuel rods will result in a reduction of the power coefficient and a gain in reactivity. This explanation is reinforced by the fact that the reactivity variations mentioned above bear resemblances to the reactivity variation which followed the startup on July 23, 1961, when a variation in the power coefficient was actually measured.

3.0 CALCULATIONAL AND EXPERIMENTAL PHYSICS RESULTS

Before describing the reactivity calculations, it is important to point out the definition and concept of reactivity as used in the calculations. In the calculations the reactor is always maintained in a static condition by introducing an eigenvalue ν/ν_o which multiplies the total fission source such that the rate of change of the neutron population with time is zero [5] ($\nu/\nu_o = 1$ for a critical reactor). The fluxes obtained with this technique are the static fluxes and the criticality factor, defined as $k_s = \nu_o/\nu$, is the static criticality factor. In calculating the reactivity effect of a perturbation, such as control rods, Xe-135, etc., it is not always possible to maintain the reactor critical in the calculations. The technique used is to calculate the eigenvalue ν/ν_o which maintains the unperturbed reactor in steady state. The reactor is then perturbed and a new eigenvalue ν'/ν_o is obtained. The reactivity effect of the perturbation is then defined as

$$\rho_s = \frac{\nu' - \nu}{\nu_o} \qquad (3.1)$$

ρ_s is a static reactivity. Equation (3.1) is consistent with the definition of reactivity given by Henry [5]. Comparison of calculated results obtained with equation (3.1) and experiment is made valid by using an effective delayed neutron fraction in the conversion from a measured period to reactivity [6]

3.1 Period-To-Reactivity Conversion

Reactivity determinations in the Yankee Reactor are based on measurements of the stable periods obtained after given changes in a core parameter which affect the neutron economy of the reactor*. The reactivity is inferred from the period measurement through the inhour equation. As was mentioned above, the calculated reactivity is the static reactivity ρ_s. To allow a valid comparison between calculations

*For the sake of simplicity reactivity is sometimes determined indirectly by measuring the compensating variation in moderator temperature which maintains the reactor critical after a change in a core parameter has been performed, and making use of the directly measured moderator temperature coefficient.

and experiments, the reactivity inferred from period measurements must be the static reactivity. This may be accomplished by writing the inhour equation in terms of effective delayed neutron fractions[6] :

$$\rho_s = \frac{\Lambda}{T} + \sum_i \frac{\beta_{i_{eff}}}{1 + \lambda_i T} \tag{3.2}$$

where Λ is the neutron generation time, $\beta_{i_{eff}}$ is the effective delayed neutron fraction of the ith delayed neutron group, λ_i is the decay constant of the ith group precursor, and T is the reactor period. The neutron generation time in Yankee is of the order of 2×10^{-5} sec^{-1} such that, for the range of periods encountered in measurement, the term $\frac{\Lambda}{T}$ in equation (3.2) may be neglected.

The effective delayed neutron fraction can be defined as

$$\beta_{i_{eff}} = \bar{I}\,\bar{\beta}_i \tag{3.3}$$

where $\bar{\beta}_i$ is an average delayed neutron fraction for the core and $\bar{I}$ is the importance function of delayed neutrons which accounts for the different effectiveness of prompt and delayed neutrons in contributing to the neutron cycle. The approximations are made that the same $\bar{I}$ applies to all delayed neutron groups and that $\bar{I}$ is independent of period. Calculations of $\bar{I}$ for different delayed neutron source energy spectra have shown that the first approximation is valid for the entire core lifetime. The dependence of $\bar{I}$ on period is negligible for periods of the order of seconds such as are encountered in Yankee. Diffusion theory with two energy groups was used to calculate $\bar{I}$ and $\bar{\beta}_i$ as a function of core lifetime. $\bar{\beta}_i$ is calculated from

$$\bar{\beta}_i = \frac{\int_v \sum_j \left[\phi_1(\bar{r})\, \nu_1^j\, {}^j_{f_1}(\bar{r}) + \phi_2(\bar{r})\, \nu_2^j\, \Sigma^j_{f_2}(\bar{r}) \right] \beta_i^j \, dV}{\int_v \sum_j \left[\phi_1(\bar{r})\, \nu_1^j\, {}^j_{f_1}(\bar{r}) + \phi_2(\bar{r})\, \nu_2^j\, \Sigma^j_{f_2}(\bar{r}) \right] dV} \tag{3.4}$$

where j includes all the fissionable isotopes present in the core.

$\bar{I}$ is calculated from

$$\bar{I} = \frac{\lambda_D}{\lambda_P} \tag{3.5}$$

where λ_P is the eigenvalue obtained with a prompt neutron fission spectrum and λ_D is the eigenvalue obtained with a delayed neutron spectrum and is defined as

$$\lambda_D \equiv \frac{\int_V \sum_j \left[\phi_1^D (\bar{r})\, \nu_1^j\, \Sigma_{f_1}^{jD} (\bar{r}) + \phi_2^D (\bar{r})\, \nu_2^j\, \Sigma_{f_2}^{jD} (\bar{r}) \right] dV}{\int_V \sum_j \left[\phi_1 (\bar{r})\, \nu_1^j\, \Sigma_{f_1} (\bar{r}) + \phi_2 (\bar{r})\, \nu_2^j\, \Sigma_{f_2}^j (\bar{r}) \right] \beta^j\, dV} \tag{3.6}$$

where $\phi^D (\bar{r})$ is the delayed neutron flux and the $\nu \Sigma_f^D$ are averages over the delayed neutron flux spectrum. The definition of $\beta_{i_{eff}}$ as expressed by equations (3.3) through (3.6) is consistent with the general definition given by Henry [5] and is consistent with the definition of reactivity used in the calculations.

Calculations were performed at beginning-of-life, at 1900, 4000 and 6400 EFPH* and at 10,500 EFPH (final shutdown) with the two-dimensional PDQ code [7], using experimental critical core configurations. At each value of burnup two calculations were performed. The first calculation used thermal constants from SOFOCATE [8] and fast constants obtained from MUFT-4 [9] with a prompt fission neutron spectrum. From this calculation the prompt eigenvalue λ_P was obtained together with the prompt fluxes $\phi_1 (\bar{r})$ and $\phi_2 (\bar{r})$ for use in equations (3.4) and (3.6). The delayed neutron fluxes were obtained from a similar calculation except for the following changes. The nu-fission cross sections which were input to the problem were defined as

$$\begin{aligned} \nu_1 \Sigma_{f_1} (\bar{r}) &= \sum_j \nu_1^j \Sigma_{f_1} (\bar{r})\, \beta^j \\ \nu_2 \Sigma_{f_2} (\bar{r}) &= \sum_j \nu_2^j \Sigma_{f_2}^j (\bar{r})\, \beta^j \end{aligned} \tag{3.7}$$

*These values of burnup correspond to shutdowns scheduled for physics experiments.

The converged pointwise flux distributions from the prompt calculation were input to the problem. These flux distributions when combined with the nu-fission cross sections defined in equation (3.7) yield the spatial delayed neutron source distribution. The fast constants (except $\nu_1\Sigma_{f_1}$ and $\nu_2\Sigma_{f_2}$ which were defined as in equation (3.7)) were obtained from MUFT-4 with a delayed neutron source spectrum. The thermal constants were the same as for the prompt problem. One outer iteration was specified. The output fluxes from this problem are the delayed neutron fluxes $\phi_1^D(\bar{r})$ and $\phi_2^D(\bar{r})$.

The non-uniform burnup distributions used in the calculations were obtained from in-core instrumentation data[1]. The core was represented in an R-Z model with 16 core regions. Group constants were input to each core region to correspond to the average burnup in each region. The control rods were homogenized[10] in given regions of the core to represent the critical configurations. The delayed neutron data of Keepin, Wimett and Zeigler[11] were used in the calculations. Fissions in U-235, U-238, Pu-239, Pu-240 and Pu-241 were considered.

The variations of $\bar{I}$ and β_{eff}* with core life are shown in Figures 3.1 and 3.2. β_{eff} decreases by 18% over the entire core lifetime. Most of the decrease is a result of the increasing number of Pu fissions with their relatively small fractional delayed neutron yields. It is noted that the delayed neutron importance function, $\bar{I}$, is less than unity at all times throughout core lifetime. This is explained by the fact that although delayed neutrons, being born at lower energies, have a smaller leakage probability than prompt neutrons, they do not cause fast fissions in U-238. Since leakage rates are relatively small in a large core such as Yankee, delayed neutrons are less effective than prompt neutrons in contributing to the neutron cycle.

---

* $\beta_{eff} = \sum_i \beta_{i_{eff}}$

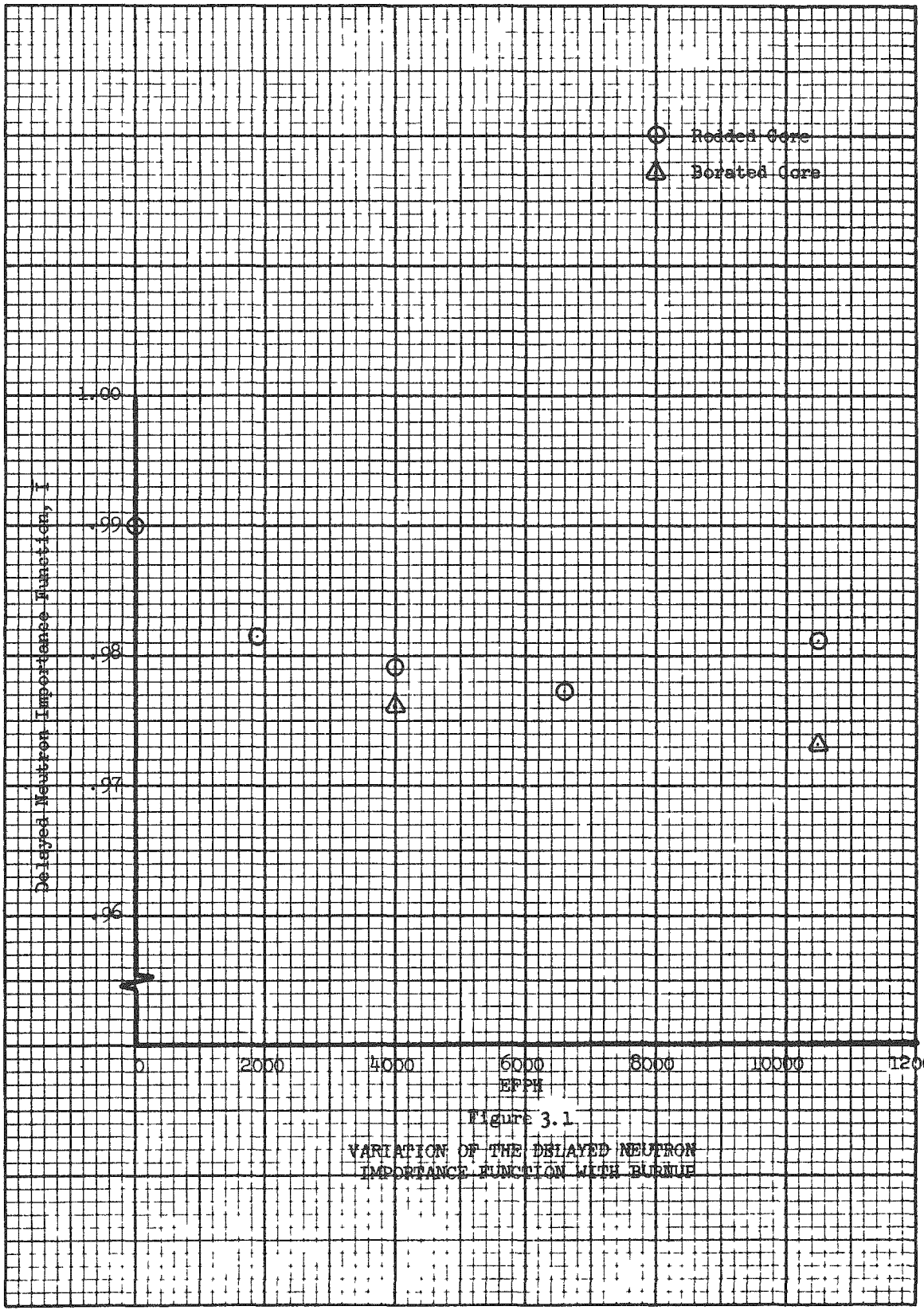

Figure 3.1

VARIATION OF THE DELAYED NEUTRON IMPORTANCE FUNCTION WITH BURNUP

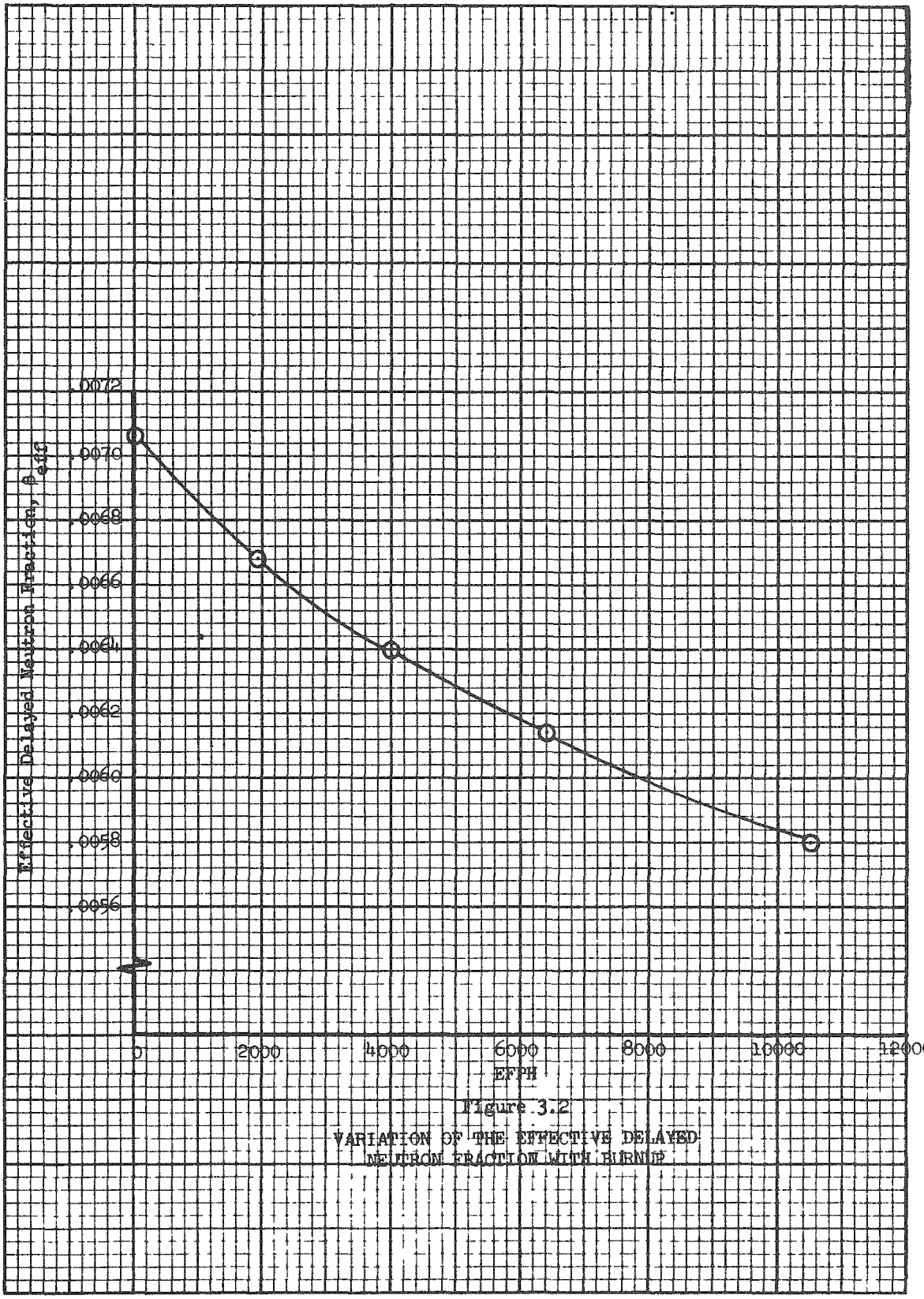

Figure 3.2

VARIATION OF THE EFFECTIVE DELAYED NEUTRON FRACTION WITH BURNUP

The delayed neutron importance function, $\bar{I}$, is relatively constant throughout core life. The increase in the value of $\bar{I}$ at 10,500 EFPH is due to the fact that the core had operated with all rods withdrawn for 3000 EFPH with a resulting flattening of the burnup and power distributions. Insertion of rod group 1 in the center of the core to maintain the zero power core critical at 10,500 EFPH resulted in a relatively large radial leakage from the core which increased the relative importance of the delayed neutrons.

The calculations of β_{eff} were performed for critical rodded cores. In order to ascertain the effects of a change in control rod position and of a change in thermal absorption rate on the values of $\bar{\beta}$ and $\bar{I}$, calculations were performed at 4000 EFPH and 10,500 EFPH with all control rods removed and with boron added to the coolant to maintain criticality. There was a negligible change in the value of $\bar{\beta}$ while the value of $\bar{I}$ decreased slightly. The values of $\bar{I}$ for the borated core are plotted in Figure 3.1. It should be noted that both the addition of boron and the decrease in leakage as the rods are removed tend to reduce $\bar{I}$. Based on these calculations, it is concluded that, in a depleted core β_{eff} is relatively insensitive to changes in the method of control and in the thermal absorption of the core.

3.2 Moderator Temperature Coefficient

The moderator temperature coefficient in Yankee is quite negative as a result of the rapid rate of change in moderator density with temperature for pressurized water at elevated temperatures [4]. Measurements made in the zero power core before power operation of the plant revealed that the moderator temperature coefficient was a sensitive function of the amount of boric acid dissolved in the coolant [3], the effect of the boron being to render the coefficient less negative. Because Yankee was the first large power reactor to use the combination of slightly enriched UO_2, stainless steel and light water together, no experimental data was available at the time of the effect of depletion

and Pu buildup on the moderator temperature coefficient. As a result, a series of tests was planned at intervals of about 2000 EFPH to measure the moderator temperature coefficient in the hot, zero power core. The measurements showed very little change in the moderator temperature coefficient throughout the core life.

One-dimensional, two-group diffusion theory calculations of the moderator temperature coefficient in the hot, zero power, clean initial core showed excellent agreement with experiment [4], as can be seen in Table 3.1. These calculations also revealed that the moderator temperature coefficient was a sensitive function of the amount of control in the form of control rods in the core. A model for the temperature coefficient in the depleted core has been defined as a summation of terms:

$$\frac{\partial \rho}{\partial T} = \frac{\partial \rho}{\partial T}\Big)_0 + (B \times R) + C \qquad (3.8)$$

where $\partial\rho/\partial T)_0$ is the temperature coefficient in the unrodded, undepleted core, R is the percent reactivity controlled by control rods, B is a function of temperature, and C is a correction to the coefficient to account for burnup.

A series of cell calculations with the AIM-5 diffusion theory code [12] was performed to calculate the function B. A homogenized symmetric cell in slab geometry was chosen with a symmetry flux boundary condition at one boundary and a control rod boundary condition α [10] (ratio of current to flux at the rod boundary) at the other boundary. The width of the cell was varied to simulate changes in control rod worth. For each value of control rod worth, k_{eff} was calculated at each of five different moderator temperatures and the moderator temperature coefficient was obtained from a plot of k_{eff} versus temperature. The function B was then obtained from the calculated coefficients for the unrodded core and the rodded core, and the calculated rod worths. Figure 3.3 shows the results of the calculations. Two calculated curves are shown. One was obtained by fitting the curve of k_{eff} versus temperature

to a second degree equation while the other was obtained by fitting the curve of k_{eff} versus temperature to a fourth degree equation. The calculated curves are compared in Figure 3.3 to a curve obtained by fitting experimental data obtained during the first 4000 EFPH to an expression similar to that of equation (3.8) [13]. The agreement between calculation and experiment is good in that both predict an effect of control rods on the moderator coefficient of about the same magnitude. Since no calculations were made of the effect of burnup on the function B, it is possible that burnup may explain some of the difference between calculation and experiment.

A calculation of the effect of burnup on the hot moderator temperature coefficient was made by calculating the coefficient at various stages of burnup in an uncontrolled core. The calculation was based on a uniform burnup model. The calculated change in moderator temperature coefficient as a result of burnup is shown in Figure 3.4. The calculations predict a positive effect of burnup on the coefficient, although at high burnup the effect tends to be in the opposite direction.

Table 3.1 shows a comparison of the measured moderator temperature coefficient and the coefficient calculated by equation (3.8).

Table 3.1

Measured and Calculated Moderator Temperature Coefficient in the Hot, Zero Power, Xenon-Free Core

EFPH	$\partial\rho/\partial T$ (Calculated) ($\times 10^{-4}$/°F)	$\partial\rho/\partial T$ (Measured) ($\times 10^{-4}$/°F)
0	- 3.16	- 3.10 ± .07
1900	- 2.75	- 2.91 ± .03
4000	- 2.48	- 2.91 ± .02
6400	- 2.25	- 2.84 ± .05
10700	- 1.91	- 2.84 ± .04

The data of Table 3.1 are plotted in Figure 3.5. The calculations predict a decrease in the absolute magnitude of the coefficient while measurements showed little change in the coefficient with burnup. Since the effect of

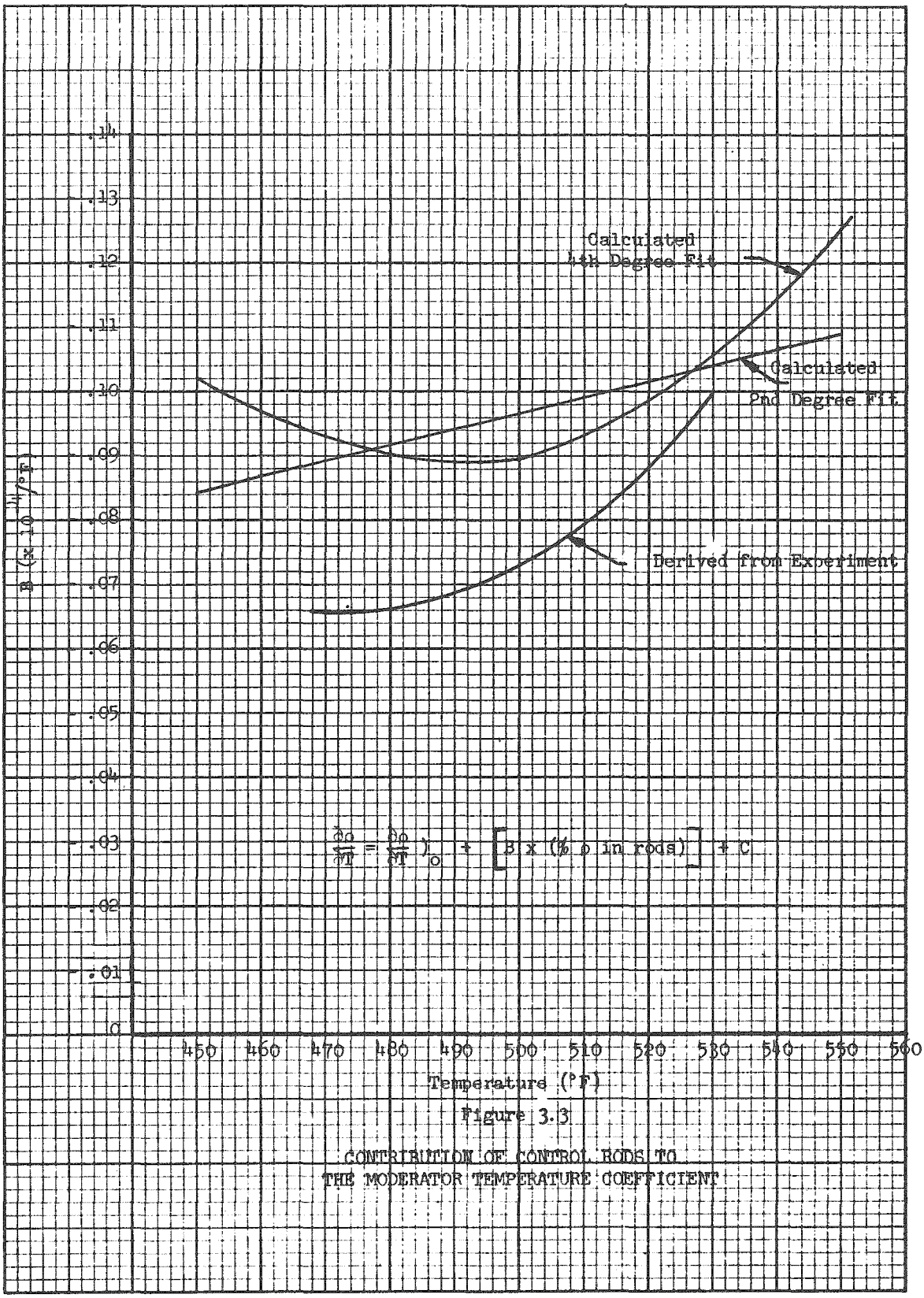

Figure 3.3

CONTRIBUTION OF CONTROL RODS TO
THE MODERATOR TEMPERATURE COEFFICIENT

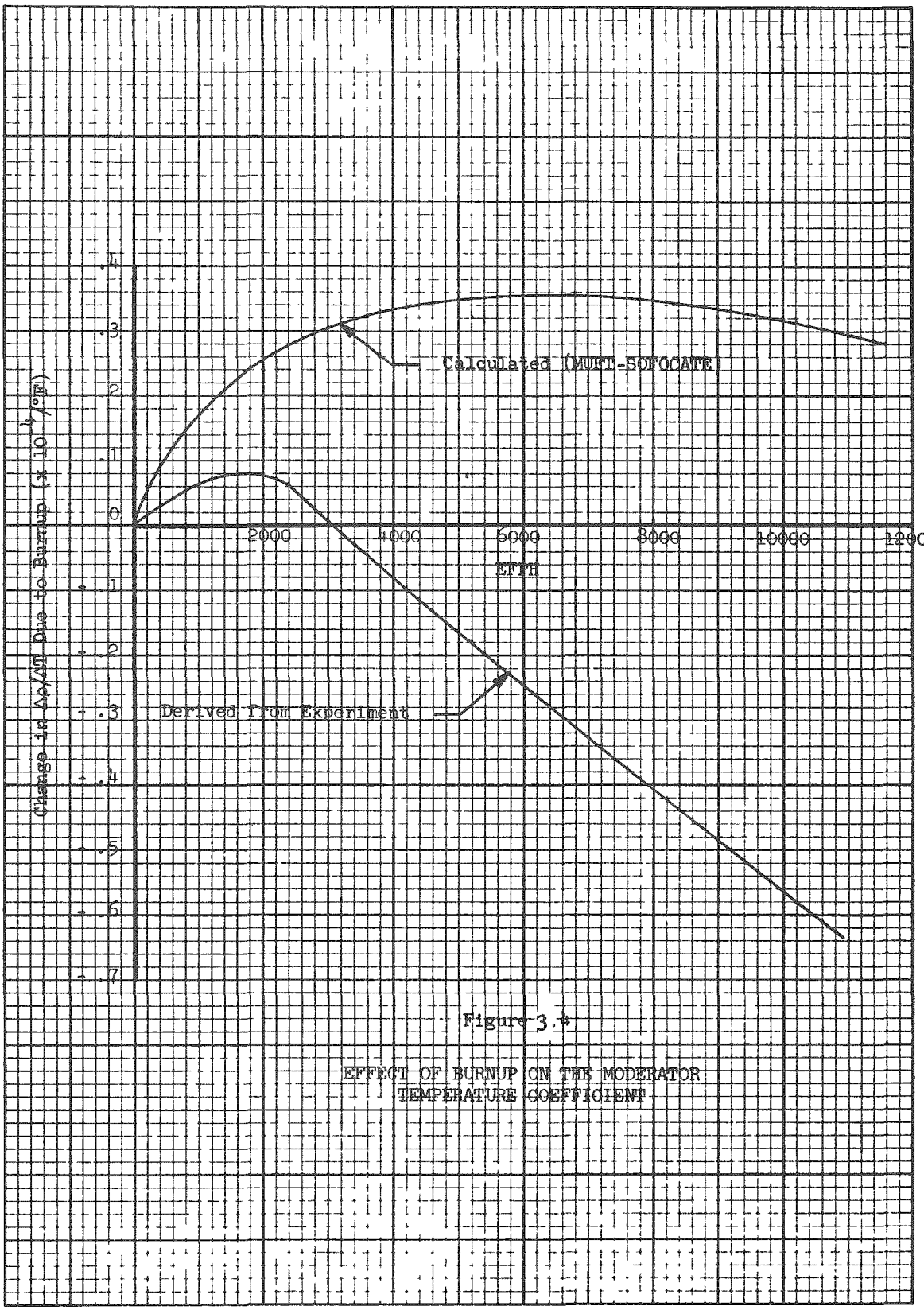

Figure 3.4

EFFECT OF BURNUP ON THE MODERATOR TEMPERATURE COEFFICIENT

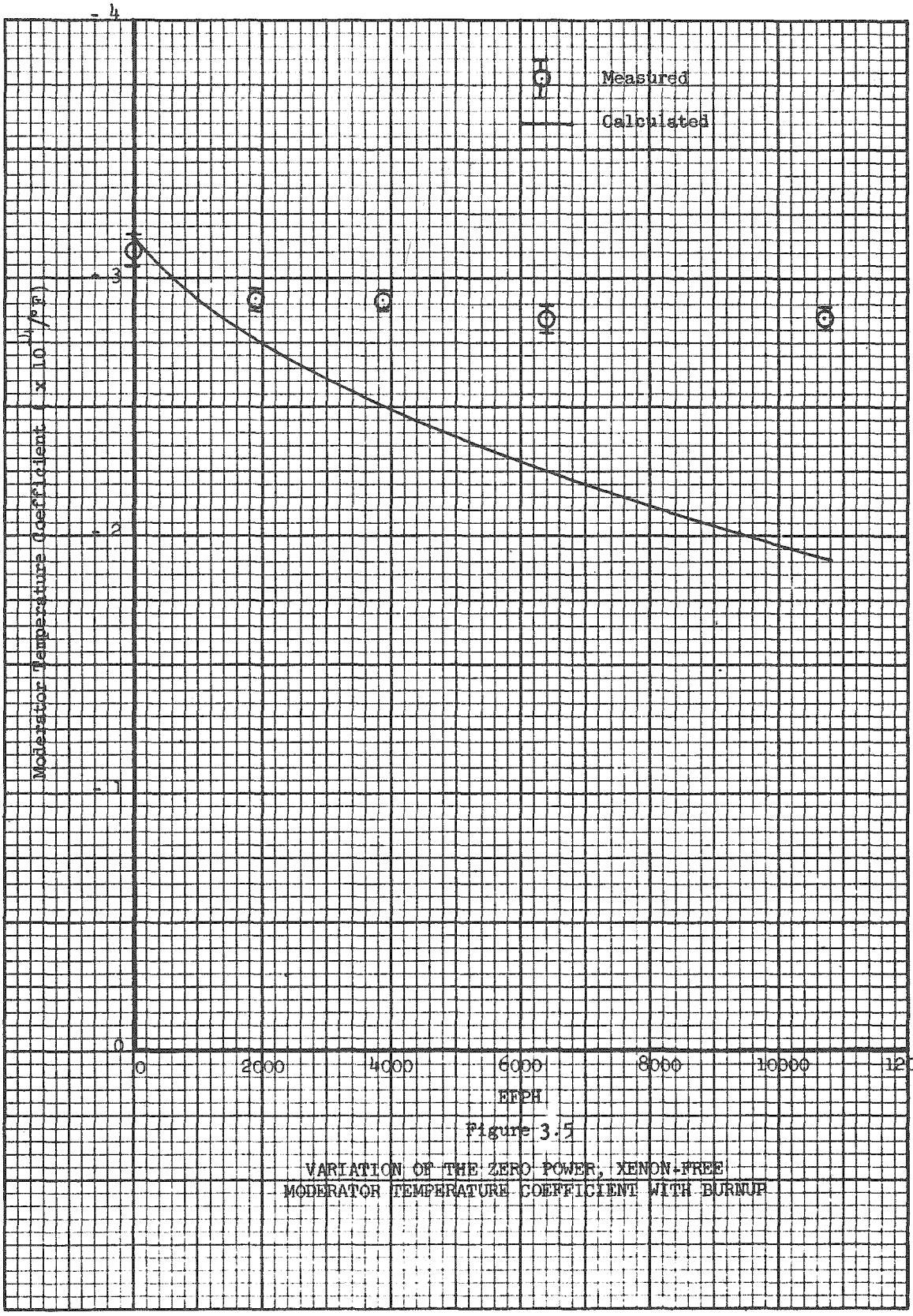

Figure 3.5

VARIATION OF THE ZERO POWER, XENON-FREE MODERATOR TEMPERATURE COEFFICIENT WITH BURNUP

control rods appears to be fairly well represented (Figure 3.3), it is believed that the discrepancy between measurements and calculations comes from the treatment of the effect of burnup on the coefficient. By using the calculated value of B at 514°F and the measured value of the temperature coefficient, the effect of burnup on the "measured" coefficient was deduced and plotted on Figure 3.4. The curve predicts a positive contribution during the first 3000 EFPH and a negative contribution for higher burnups. The reasons for the discrepancy between this curve and the calculated curve are not clear. One reason for the discrepancy is probably the assumption of uniform burnup in the calculations. However, it is felt that the discrepancy can be attributed in large part to the microscopic treatment of the absorption in plutonium and fission products, since Doppler broadening and self-shielding effects for plutonium and fission products are not included in the homogenized MUFT calculations.

3.3 Pressure Coefficient

The pressure coefficient in Yankee is a small, positive coefficient of reactivity which results from the increase in water density with increasing pressure. Since the core is undermoderated, an increase in moderator density corresponds to an increase in core reactivity. Consistent with the calculation of the moderator temperature coefficient, a model for the pressure coefficient was defined as in equation (3.8) for the temperature coefficient. Table 3.2 shows a comparison of calculated and measured moderator pressure coefficients.

The agreement between calculations and experiment is good. The effect of burnup on the pressure coefficient was calculated to be very small (a maximum of about 2% of the beginning-of-life coefficient), with a negative effect for the first 5000 EFPH and a positive effect afterwards. The decrease in the coefficient with life is therefore due to the withdrawal of control rods. Since burnup has little effect on the water density coefficient of reactivity, it may be argued that the calculated positive effect of burnup on the moderator temperature coefficient (Figure 3.4) is a spectrum effect. This corroborates the statement made earlier that the discrepancy between calculated and measured moderator temperature coefficient in the depleted core can be attributed to spectrum effects.

Table 3.2

Measured and Calculated Moderator Pressure Coefficient in the Hot, Zero-Power, Xenon-Free Core

EFPH	$\partial\rho/\partial$ Pr (Calculated) ($\times 10^{-6}$/psig)	$\partial\rho/\partial$ Pr (Measured) ($\times 10^{-6}$/psig)
0	3.17	2.98 ± .30
8	3.14	2.87 ± .03
132	3.11	2.80 ± .02
1900	2.93	2.47 ± .04
4000	2.77	2.45 ± .06
6400	2.62	2.71 ± .10
10,700	2.26	2.65 ± .09

3.4 Power Coefficient

The power coefficient of reactivity relates the change in reactivity which results from Doppler broadening of U-238 resonances to a change in power. It is an important parameter for accident analyses and power capability analyses in a Yankee type reactor since it is the predominant shutdown mechanism in the event of a fast power transient. However the reactivity loss (or power defect) in going to rated power constitutes a direct loss in lifetime capability. In Core I, the power defect amounts to roughly 25% of the total reactivity available for fuel depletion.

The power coefficient depends primarily on three factors; the fuel pellet temperature, which determines the extent of the Doppler broadening of the U-238 resonances; the pellet to coolant heat transfer coefficient, which determines the variation of pellet temperature with power; and the power distribution in the core, which determines the

distribution of fuel temperatures in the core and therefore the statistical weight factor on the power coefficient. This may be expressed as

$$\frac{\partial \rho}{\partial P} = \frac{\partial \rho}{\partial T_{eff}} \times \frac{\partial T_{eff}}{\partial P} \times W \qquad (3.9)$$

where P is the average core power, T_{eff} is an effective fuel temperature and W is a statistical weight factor.

3.4.1 Variation of Reactivity with Fuel Temperature - the Doppler Effect

The first term on the right of equation (3.9) is the Doppler coefficient. The Doppler coefficient for Yankee has been calculated [4] by application of the Monte Carlo method [14]. A parabolic temperature distribution was assumed in the pellets. An effective fuel temperature is defined as

$$T_{eff} = T_S + 0.35 (T_{max} - T_S) \qquad (3.10)$$

where T_S is the pellet surface temperature and T_{max} is the center of pellet temperature. T_{eff} is a single temperature value which gives the same Doppler effect as the actual parabolic distribution of temperatures in the pellet.

The assumption is made that a change in fuel temperature does not directly affect absorption in the U-235 resonances. That is, Doppler broadening of U-235 resonances is neglected. However, because of the competition for absorption in the U-235 and U-238 resonances, a change in fuel temperature and in the resonance absorption in U-238 will indirectly affect the absorption rate in U-235 resonances. Consistent with this and the definition of reactivity given in Section 3.0 the Doppler coefficient is defined as

$$\frac{\partial \rho}{\partial T_{eff}} = \left(\frac{1 + M^2 B^2}{\eta f \epsilon p}\right) \cdot \left(\frac{1}{p_{28}} \frac{\partial \rho_{28}}{\partial T_{eff}}\right) \qquad (3.11)$$

where p is the total resonance escape probability. For Core I the first factor on the right of equation (3.11) is 1.12 and varies by only 1% over the total range of power levels.

Figure 3.6 shows the Doppler coefficient as a function of the effective fuel temperature. Two coolant temperatures are shown to demonstrate the effect of the coolant temperature. At operating temperature and power, the rate of change of the Doppler coefficient with effective fuel temperature is about $.55 \times 10^{-8}/°F$, or a 3% change in Doppler coefficient for a 100°F change in effective fuel temperature. Other things being constant, this would correspond to a change of about 0.05% in reactivity at power. Since what is actually measured is a power coefficient, and because of the large uncertainties in the calculations of the heat transfer characteristics of the fuel rod and their effect on the power coefficient, it is difficult to estimate the accuracy of the Doppler coefficient calculations. However, a comparison of the method with recent measurements by Hellstrand [15] of the U-238 resonance integral temperature coefficients in oxide fuels has shown agreement to within 5%.

3.4.2 Pellet to Coolant Heat Transfer

Equation (3.9) shows that the power coefficient is directly proportional to the rate of change of the effective fuel temperature with power. This is strongly dependent on the pellet-to-coolant conductance. This is an area where little is known and where in-pile experimental data on high burnup, high temperature fuel are not readily available.

During fabrication of the Yankee fuel rods, a pellet-clad gap is formed. The cold diametral gap is 4 mil. This gap is reduced to about 3 mil at average operating power because of the differential expansion of the pellet and clad. Table 3.3 shows the variation of the diametrical gap with local power density. These gaps are based on expansion of an uncracked pellet assuming the gap to be filled with air at one atmosphere pressure.

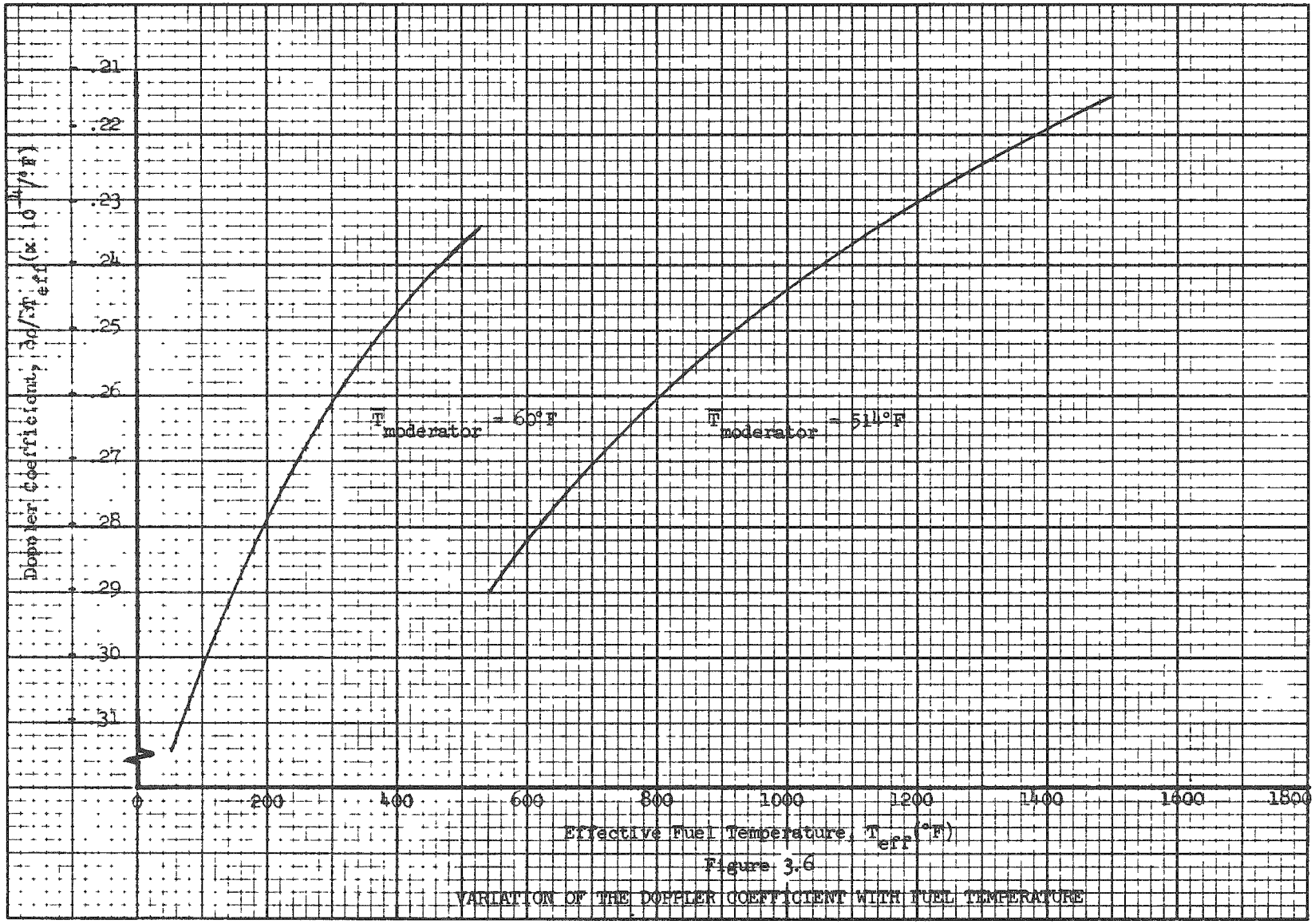

Figure 3.6

VARIATION OF THE DOPPLER COEFFICIENT WITH FUEL TEMPERATURE

Table 3.3

Variation of the Diametrical Pellet-Clad Gap with Power Density for an Uncracked Pellet

Coolant Temperature (°F)	Power (MWt)	Power Density (KW/ft)	Diametrical Gap (mil)
68	0	0	4.00
514	0	0	4.54
514	100	0.56	4.15
514	200	1.13	3.83
514	300	1.69	3.55
514	400	2.25	3.29
514	500	2.82	3.05
514	600	3.38	2.83
514	700	3.95	2.62
514	800	4.51	2.42

These calculations would indicate that pellet-clad contact occurs only at very high power densities. However, considerable amount of pellet cracking may occur, and for pellets which are located in higher than average power densities, the pellet and clad may come in contact. The heat transfer characteristics of the fuel rod are extremely sensitive to the gap characteristics. Little usable data are available on gap conductance and contact resistance. Since the actual conditions of the pellets and the gap during operation at power are not known, it is difficult to predict the heat transfer characteristics of the fuel rod and therefore the power coefficient to any desired accuracy. Furthermore, these heat transfer characteristics probably vary during the lifetime of a reactor operation because of mechanical changes of the fuel pellets, the high irradiation of the pellet and clad, and the buildup and release of gaseous fission products. Prediction of the power coefficient and its variation in time is therefore, at least for the present, a difficult area.

It is nevertheless possible to obtain some idea of the importance of the fuel rod heat transfer characteristics in determining the power coefficient. The following analysis represents such an attempt. It has been necessary to make simplifying assumptions and to work with an idealized model. However, the conclusions deduced from such an analysis and the extent of the agreement with experimental data are useful in reaching an understanding of the phenomena involved.

In the following calculations, the pellet has been assumed uncracked. Average values for the thermal coefficients of linear expansion for SS and UO_2 have been used. The calculations have been performed for an "average" pellet, that is, a pellet in a location of average core power density. The method consists essentially in computing the effective fuel temperature T_{eff} at various power levels P and differentiating the resulting curve to obtain $\partial T_{eff}/\partial P$ as a function of P. The effective fuel temperature is calculated according to equation (3.10). The temperature rise in the average pellet is determined from

$$(T_{max} - T_S) = \frac{q_v r_u^2}{4K_u} \tag{3.12}$$

where q_v is the fuel specific power in Btu/hr-ft^3, r_u is the pellet radius and K_u is the thermal conductivity of UO_2. Equation (3.12) assumes uniform heat generation and negligible flux depression. The pellet surface temperature is obtained from:

$$T_S = T_b + \Delta T_f + \Delta T_c + \Delta T_g \tag{3.13}$$

where T_b is the coolant bulk temperature, ΔT_f is the coolant film temperature drop, ΔT_c is the temperature drop in the clad and ΔT_g is the temperature drop in the gap. If one assumes heat transfer

by conduction only, equation (3.13) can be written

$$T_S = 514°F + \frac{q'}{2\pi}\left[\frac{1}{h_f r_o} + \frac{\ln(r_i/r_o)}{K_c} + \frac{\ln(r_i/r_u)}{K_g}\right] \qquad (3.14)$$

where q' is the average heat per unit length, r_o is the outside radius of the clad, r_i is the inside radius of the clad, h_f is the film conductance, K_c is the thermal conductivity of the clad and K_g is the thermal conductivity of the gap. Equations (3.10), (3.12) and (3.14) may be combined to obtain an expression relating T_{eff} to power. It should be noted that the thermal conductivities and radii are functions of temperature such that an explicit expression for T_{eff} as a function of power cannot be written, and some type of iterative procedure must be used.

Typical values for the temperature drops in a fuel rod with average power density in equations (3.13) and (3.14) at full power are: ΔT_f, 15°F; ΔT_c, 15°F; ΔT_g, 400-500°F; $T_{max} - T_S$, 300-400°F. Most of the temperature drop between pellet and coolant occurs therefore in the gap, and one would suspect a strong dependence of the power coefficient on the gap heat transfer characteristics. The gas content of the gap will exert a strong influence on the gap conductance. As a result of the methods of fuel rod fabrication, one would expect that the gap gas content be hydrogen and the components of air. However, tests conducted after the fuel rods were brazed showed that the gap contained mostly hydrogen and argon at very low pressures [16]. This would indicate that after a relatively short period of operation, most of the gas content would consist of Xe and Kr fission gases released from the pellets.

From the above considerations one would expect a dependence of the power coefficient on power level and on time of operation. In the calculations described below, several gap compositions have been used -- air, fission gases, hydrogen. Variation of the thermal

conductivity of these gases with temperature has been taken from reference 16. It is of interest to compare the thermal conductivities of these gases at a given temperature. This is shown in Table 3.4.

Table 3.4

Thermal Conductivity of Various Gases at One Atmosphere and 800°F

Gas	Thermal Conductivity (Btu/hr-ft-°F)
H_2	0.20
Air	0.032
Kr	0.012
0.85 Xe + 0.15 Kr	0.0089
Xe	0.0079

The thermal conductivity of UO_2 decreases with temperature in the range of interest to this study [17]. The variation with temperature was obtained from a fit to experimental data.

Effect of the Heat Transfer Characteristics on the Power Coefficient

The power coefficient was calculated at 392 MWt and 485 MWt for several gap gas contents at one atmosphere. Table 3.5 shows the results in terms of a percent difference, with the power coefficient based on an air gap as reference. In Table 3.5 the positive % difference means an increase in the absolute magnitude of the power coefficient. The table indicates the strong dependence of the power coefficient on gap composition.

In order to estimate the relative effects of the pellet thermal conductivity and the gap thermal conductivity on the power coefficient, calculations were performed of the power coefficient at 485 MWt where the thermal conductivities were varied over a range of 20%. The results are given in Table 3.6.

Table 3.5

Variation of the Power Coefficient with Gap Composition

Gap Composition	% Difference 392 MWt	485 MWt
Air	0	0
75% Air 25% Xe	+ 4	-
Fission gases (85% Xe, 15% Kr)	+ 58	+ 43
99% Fission gases, 1% Hydrogen	-	+ 23

Table 3.6

Effect of a Change in Thermal Conductivity on the Power Coefficient

% Change in Thermal Conductivity K	Condition*	% Change in $\Delta\rho/\Delta P$ at 485 MWt
+ 5% in K_g	Fission gases at 1 ATM in gap	- 4%
+ 20% in K_g	Fission gases at 1 ATM in gap	- 14%
+ 20% in K_u	Air at 1 ATM in gap	- 7%
+ 20% in K_u	Pellet-clad-contact h_g = 1000 Btu/in-ft^2-°F	- 10%
+150% in h_g	Pellet-clad contact h_g = 1000 Btu/in-ft^2-°F	- 22%

*These calculations assumed uncracked pellets; however, the results probably also apply qualitatively to cracked pellets.

The calculations indicate that the power coefficient is quite sensitive to the thermal conductivity of the gap medium and that it is much less sensitive to the thermal conductivity of the pellet. However the thermal conductivity of the pellet becomes more important in the event of pellet-clad contact. With the pellet and clad in contact, the power coefficient is relatively insensitive to the contact conductance.

All the calculations above have used gas conductivities for a gas pressure of 1 atmosphere. The effect of gap pressure on the power coefficient is probably very small since the pressure effect on thermal conductivity is small and diminishes as the temperature increases. For a temperature of 940°F, the percent increase in thermal conductivity between 1 atmosphere and 1285 psi is 8.5% for fission gases and 4.8% for air [16].

From the foregoing analyses it may be concluded that

1) the power coefficient is very sensitive to the gas composition of the pellet-clad gap,

2) for a given gas composition, the power coefficient is relatively insensitive to the gap pressure. If it is assumed that the gap is filled with fission gases after a relatively short period of power operation, changes in fission gas release will not affect the power coefficient,

3) with a gap between pellet and clad, the power coefficient is relatively insensitive to changes in the pellet thermal conductivity. With pellet and clad in contact, the sensitivity is increased,

4) with pellet and clad in contact, the power coefficient is relatively insensitive to the contact pressure.

These conclusions are somewhat restricted, since they are based on analyses which assume no cracking of the pellet. In this case, and if it is assumed that the gas gap composition is unaltered during operation, the power coefficient at a given power level should remain constant under extended power operation, except

for changes in the statistical weight factor and for small changes due to variations in pellet conductivity. However, in the event of pellet cracking, significant changes in the power coefficient may occur as a result of changes in the gap geometry.

Fission Gases Buildup and Release

Calculations [16] based on the quantity of fission gases released and the initial mixture present in the gap indicate that the pellet-clad gap becomes predominantly fission gases early in core life. To estimate the relative abundance of the various fission gases a calculation was made of the total concentration of fission gases produced in the fuel pellets after 4000 hours of operation. The calculation consisted in solving the differential equations describing the production of the isotopes of the fission products Xe and Kr. Total Xe and Kr concentration after 4000 hours was calculated as 7.6×10^{18} atoms per cc of core. Of this amount, 87% was Xe and 13% was Kr. The fission gas content is made up mostly of stable isotopes, except for small amounts of 10.3y half life Kr^{85} and 5.22d half life Xe^{133}. Table 3.7 shows the breakdown of the fission gases.

Table 3.7

Total Fission Gas Content after 4000 Hours at 392 MWt

Isotope	% Abundance	
Kr^{83}	1.8	13.1%
Kr^{84}	3.4	
Kr^{85}	1.0	
Kr^{86}	6.9	
Xe^{131}	8.9	86.9%
Xe^{132}	14.6	
Xe^{133}	1.0	
Xe^{134}	27.6	
Xe^{136}	34.8	

This calculated fission gas composition agrees well with the (0.85 Xe, 0.15 Kr) gap mixture which was used in the calculation of the power coefficient. This assumes that the diffusion and release rates are similar for Xe and Kr isotopes.

Variation of the Power Coefficient with Power

The power coefficient was calculated as a function of power level assuming the pellet-clad-gap to be filled with air at one atmosphere. The calculation was repeated at high power assuming pellet and clad contact. In the event of pellet-clad contact, the third term in parentheses on the right of equation (3.14) becomes $(1/r_i\ h_g)$ where h_g is the contact conductance. A constant value of 1000 Btu/hr-ft^2-°F [16] was used to calculate the power coefficient. The results of these calculations are plotted in Figure 3.7, assuming a unity statistical weight factor. The calculations are compared to experimental data obtained during the return to power after the 6400 EFPH shut-downs. These measurements were performed by compensating for reactivity variation due to a power change by a change in moderator temperature maintaining a fixed control rod position. It should be noted that the errors shown in the figure do not reflect any uncertainties in the moderator temperature coefficient. The calculated variation of the power coefficient with power agrees very well with experiment. However the agreement in the magnitude of the power coefficient is probably fortuitous. In the next section it will be shown that a statistical weight factor between 1.2 and 1.3 should be applied to the calculated power coefficient. Furthermore, if it is assumed that the gap composition is fission gases and not air, Table 3.5 indicates an increase of 40 to 60% in the calculated power coefficient, although the presence of hydrogen in the gap would limit this increase*

*The presence of some hydrogen in the gap may result from adsorption of water vapor by the UO_2 during fabrication. It has been found that for O/U ratios less than stoichiometric, the water vapor reacts with uranium metal to produce hydrogen. [18]

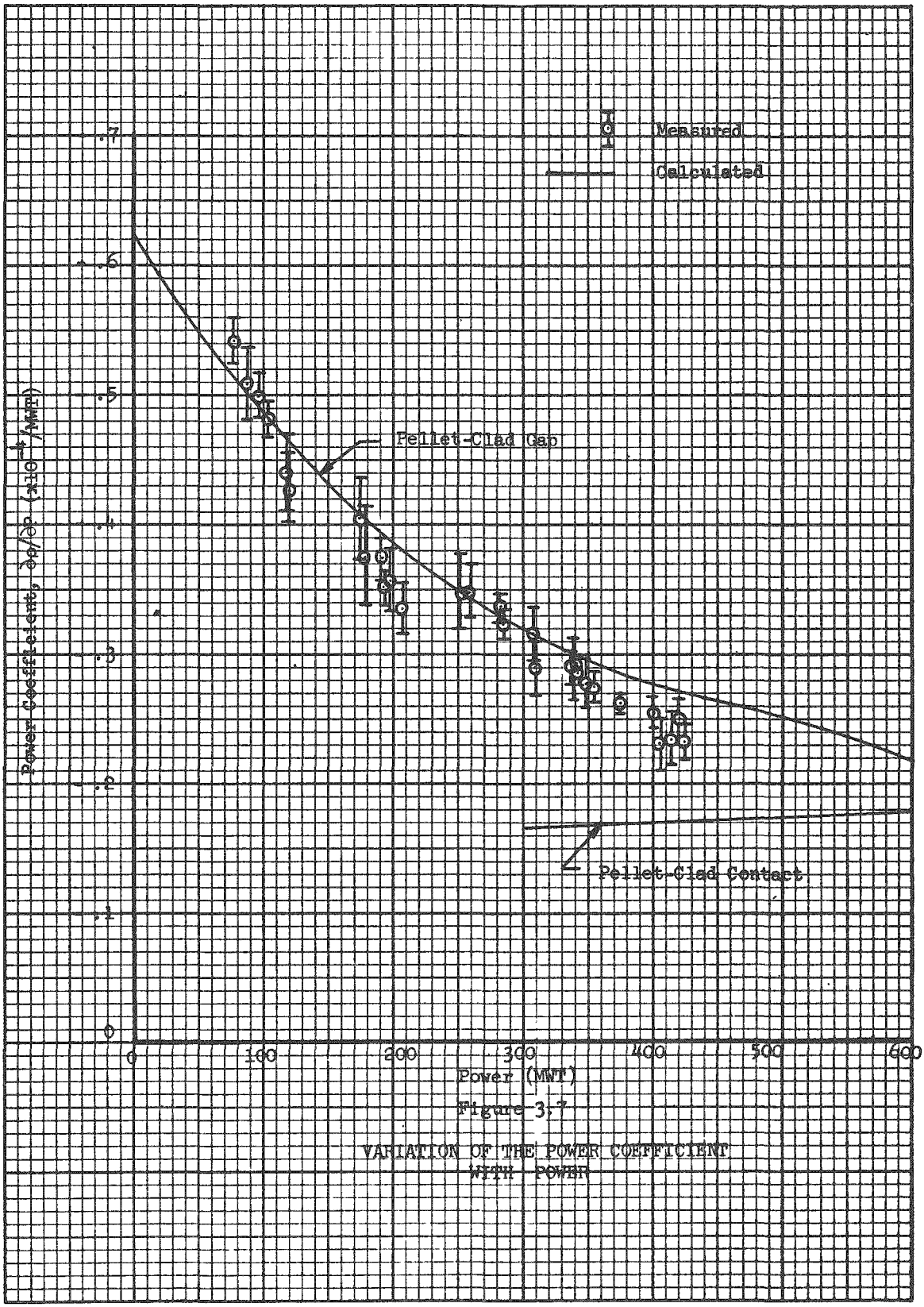

Figure 3.7

VARIATION OF THE POWER COEFFICIENT WITH POWER

Thus it would seem that the calculations, based on uncracked pellets and a gap composition of fission gases, overestimates the power coefficients by 50% or more. However any amount of pellet cracking will reduce the thermal barrier associated with the pellet-clad gap and therefore the power coefficient. Thus it appears that the overestimate of the power coefficient in the calculations results from the assumption of uncracked pellets and the uncertainty as to the actual composition of the gas in the gap.

Figure 3.7 indicates that the variation of the power coefficient with power is well predicted at low power by a model which assumes a gap between pellet and clad which decreases as fuel temperature increases in a manner consistent with the relative expansion coefficients of UO_2 and stainless steel. However, at high power the experimental data indicate a trend toward the calculated coefficient based on pellet-clad contact. This model is applicable at very high power where contact has occurred for most fuel rods. The transition between the two models may be explained on the basis of the distribution of fuel temperatures in the core. There is a range of local power density and therefore fuel temperatures in the core such that some pellets are in contact while the others are not. The transition region between the two calculational models correspond to a combination of the models which account for the distribution of pellet temperatures in the core. From Figure 3.7 this transition region for Yankee is probably from 1.96 KW/ft to 3.08 KW/ft. At an average power density of 1.96 KW/ft, the peak power density in the core may be roughly 5.6 KW/ft. However, Table 3.3 which gives the variation in diametrical gap as a function of power assuming uncracked pellets and an air medium, indicates that there is a definite gap at this high value of power of about 2 mils. For contact to occur at some location in the core at an average power density of 1.96 KW/ft, considerable pellet cracking must have occurred, with a resulting decrease in the diametrical gap between pellet and clad. This in effect corroborates the statement made above that pellet cracking is the reason for the overestimate in the calculated power coefficient.

3.4.3 Statistical Weight Factor on the Power Coefficient

The non-uniform fuel temperature distribution in the core affects the total power coefficient in that a high fuel temperature in a region of high neutron importance causes a greater reduction in reactivity than a high fuel temperature in a region of lesser neutron importance. A familiar technique is to calculate the power coefficient assuming a uniform distribution of the average power and to apply statistical weight factors to account for non-uniform power distributions.

Two-group perturbation theory was used to compute statistical weight factors on the power defect based on in-core instrumentation data obtained throughout core life [1]. In this context, the statistical weight factor is defined as the ratio of reactivity worth calculated with a non-uniform perturbation in a non-uniform core, to the reactivity worth calculated with a uniform perturbation in a uniform core. The perturbation produced in going to power was assumed to consist of an equivalent change in the zero power fast energy absorption cross section of the core in the form

$$\delta \Sigma_{a_1}(\bar{r}) = \left[\Sigma_{a_1}(\bar{r}) + \Sigma_R(\bar{r}) \right] \alpha_p(\bar{r})\, P\, (\bar{r}) \qquad (3.15)$$

where $\alpha_p(\bar{r})$ is the value of the power coefficient at the power P at location $\bar{r}$ in the core. The unweighted power coefficient α_p which was used in the calculation was the calculated power coefficient based on a pellet-clad gap filled with air. The calculated variation of α_p with power is best given in the form of an exponential:

$$\alpha_p = C_0 + C_1 e^{-C_2 P} \qquad (3.16)$$

Since the in-core instrumentation yields an activation distribution, it was necessary to derive correlations between fast and thermal normal and adjoint fluxes and power, and the wire activation. Those

correlations are functions of burnup and therefore vary throughout the core. The derivation of the expression for the statistical weight factor on the power defect can be found in the Appendix.

Only the final equation is reproduced here. The statistical weight on the power defect is given by

$$W^{Dop} = \frac{\int (\Sigma_{a_1}(\bar{r}) + \Sigma_R(\bar{r}))(\frac{C_1}{C_2} + C_0 P_{Avg} I^N(\bar{r}) - \frac{C_1}{C_2} e^{- C_2 P_{Avg} I^N(\bar{r})}) I^{*2}(\bar{r}) \, dV}{\frac{(\bar{\Sigma}_{a_1} + \bar{\Sigma}_R)}{\bar{M}} (\frac{C_1}{C_2} + C_0 P_{Avg} - \frac{C_1}{C_2} e^{- C_2 P_{Avg}}) \int M(\bar{r}) I^{*2}(\bar{r}) \, dV} \tag{3.17}$$

where

$$I^N(\bar{r}) = \frac{\frac{I(\bar{r}) \beta(\bar{r})}{\sigma(\bar{r})}}{\frac{1}{V} \int \frac{I(\bar{r}) \beta(\bar{r})}{\sigma(\bar{r})} dV} \tag{3.18}$$

$$I^*(\bar{r}) = \frac{I(\bar{r})}{\sigma(\bar{r})} \tag{3.19}$$

$I(\bar{r})$ is the wire activation in arbitrary units. The parameters β, σ, and M are functions of burnup. The barred parameters correspond to the value of the parameters at the average burnup of the core.

The parameters Σ_{a_1}, Σ_R, β, σ, and M were calculated as a function of burnup and the results fitted to polynomials. The calculations implied by equation (3.17) were then programmed as an additional option in the YADAR [1] in-core instrumentation data

reducing code. The calculation requires as prerequisite the calculation of the burnup distribution. This burnup distribution is then used with the wire activation distribution in equation (3.17).

The statistical weight factors on the power defect are plotted in Figure 3.8 as a function of control rod removal for the programmed withdrawal sequence, for an average power level of 392 MWt. The statistical weight factor varies between a maximum of 1.38 and a minimum of 1.22 which implies a maximum of 12% variation in the power coefficient as a result of statistical weight effects. The flattening effect of the non-uniform burnup distribution on the power distribution is evident in that the variations of the statistical weight factor with control rod motion are reduced at high values of burnup. There is almost no change in the statistical weight factor during the entire withdrawal of group 5 and during half of group 1 withdrawal. Table 3.8 gives the statistical weight factors on the power defect during the core lifetime extension period after complete withdrawal of all control rods. The decrease in the statistical weight factor is a result of the flattening of the power distribution due to the non-uniform spatial burnup distribution in the core [1].

Table 3.8

Statistical Weight Factor on the Power Defect During Core Lifetime Extension Period

EFPH	P(MWt)	Statistical Weight Factor
7690	392	1.285
8100	392	1.273
8250	392	1.272
8560	392	1.259
8920	392	1.252

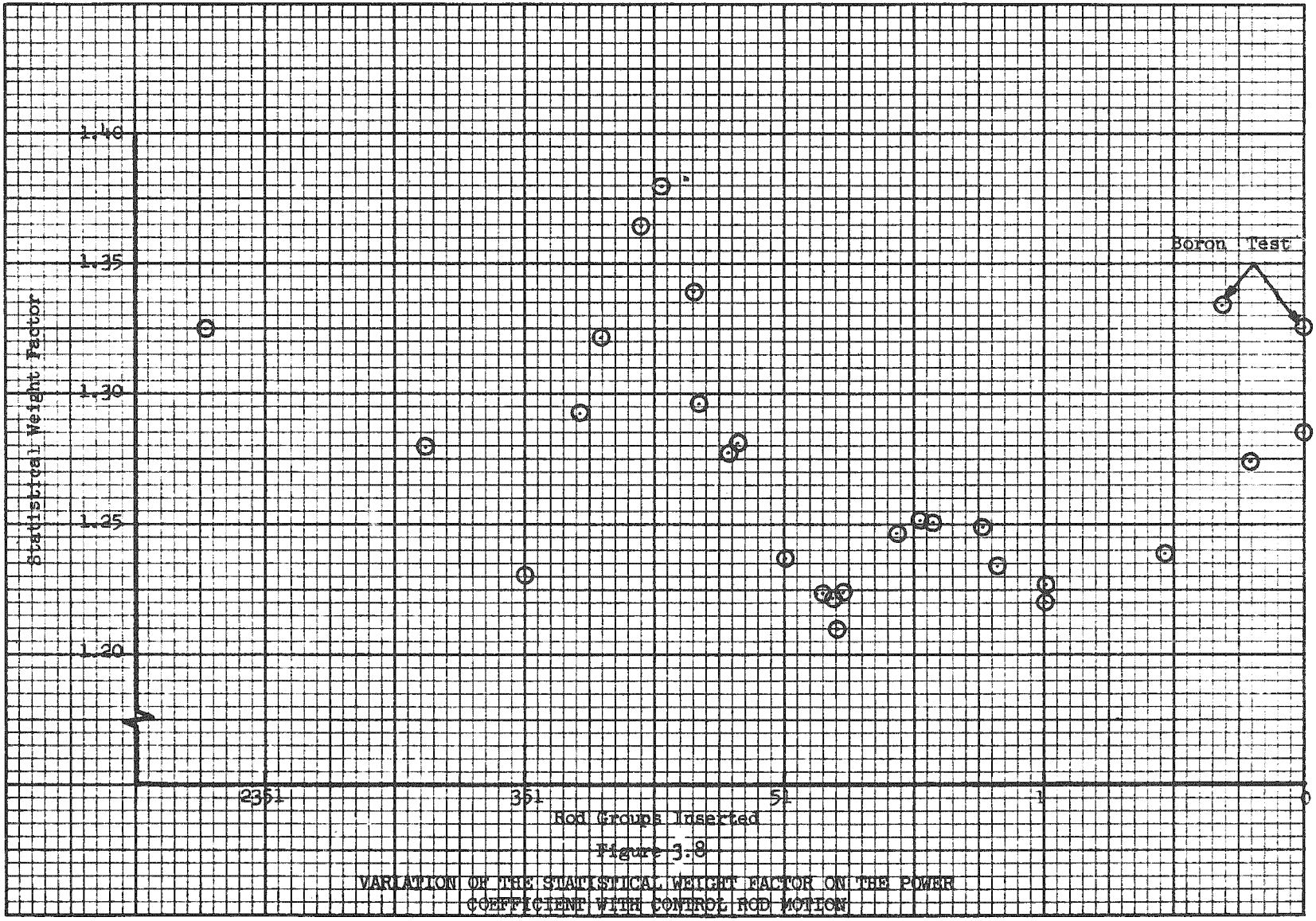

Figure 3.8

VARIATION OF THE STATISTICAL WEIGHT FACTOR ON THE POWER COEFFICIENT WITH CONTROL ROD MOTION

Equation (3.17) reveals that the statistical weight factor on the power defect is a function of the average core power (P_{Avg}). Figure 3.9 shows the variation of the statistical weight factor with average power level for three control rod configurations. The statistical weight factor decreases rapidly with power at low average power levels. However, the sensitivity of the statistical weight factors to the average power level decreases as the power is increased.

3.4.4 Power Coefficient at Various Times in Core Life

Figure 3.10 shows measurements of the power coefficient at 380 MWt made at various times in core life. There is no change in the coefficient during withdrawal of rod group 5 and initial withdrawal of rod group 1. This is consistent with the calculation of the statistical weight factors and with the statement of section 3.4.2 that the power coefficient should remain constant under extended power operation. However, the measurement made at 4000 EFPH yielded a coefficient approximately 45% larger in absolute magnitude than the later measurements. Figure 3.8 shows that about 7% of this increase can be attributed to statistical weight effects. The measurement was made upon returning to power after the scheduled 4000 EFPH shutdown. This shutdown lasted 2 weeks and the plant was brought to the cold condition. A possible explanation for the large power coefficient which was measured after the shutdown is that the large decrease in the pellet temperature during the shutdown, from operating temperature to almost room temperature, with the accompanying contraction of the pellet, resulted in an effective pellet-clad gap which was larger than during normal power operation. The subsequent expansion of the pellets upon returning to power and the return to an equilibrium geometrical configuration resulted in a decrease of the coefficient back to its equilibrium value. These considerations are consistent with the apparent loss in reactivity upon returning to power after the 4000 hour shutdown and the subsequent period of power operation with no control rod motion for about three weeks (see section 2.3).

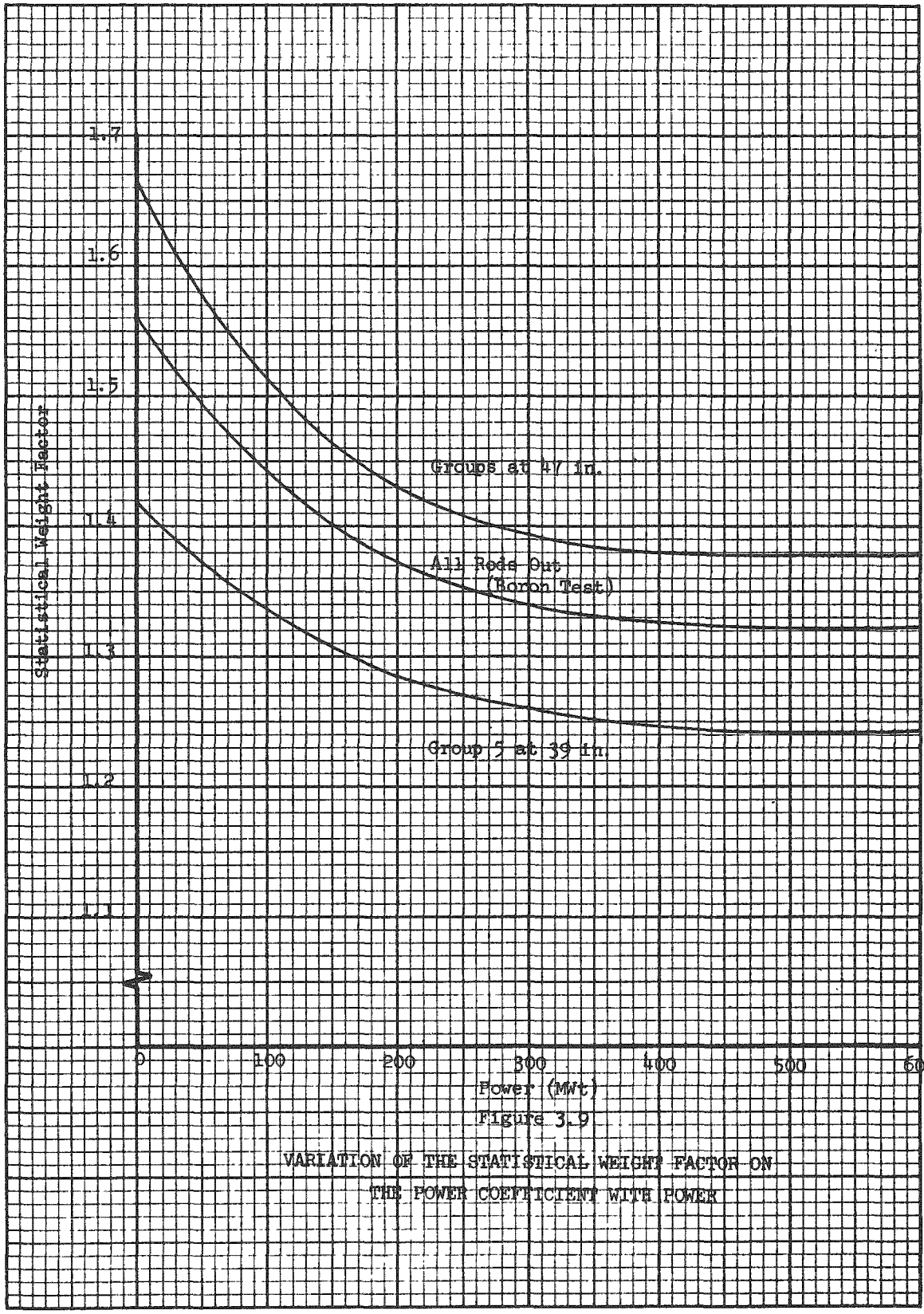

Figure 3.9

VARIATION OF THE STATISTICAL WEIGHT FACTOR ON THE POWER COEFFICIENT WITH POWER

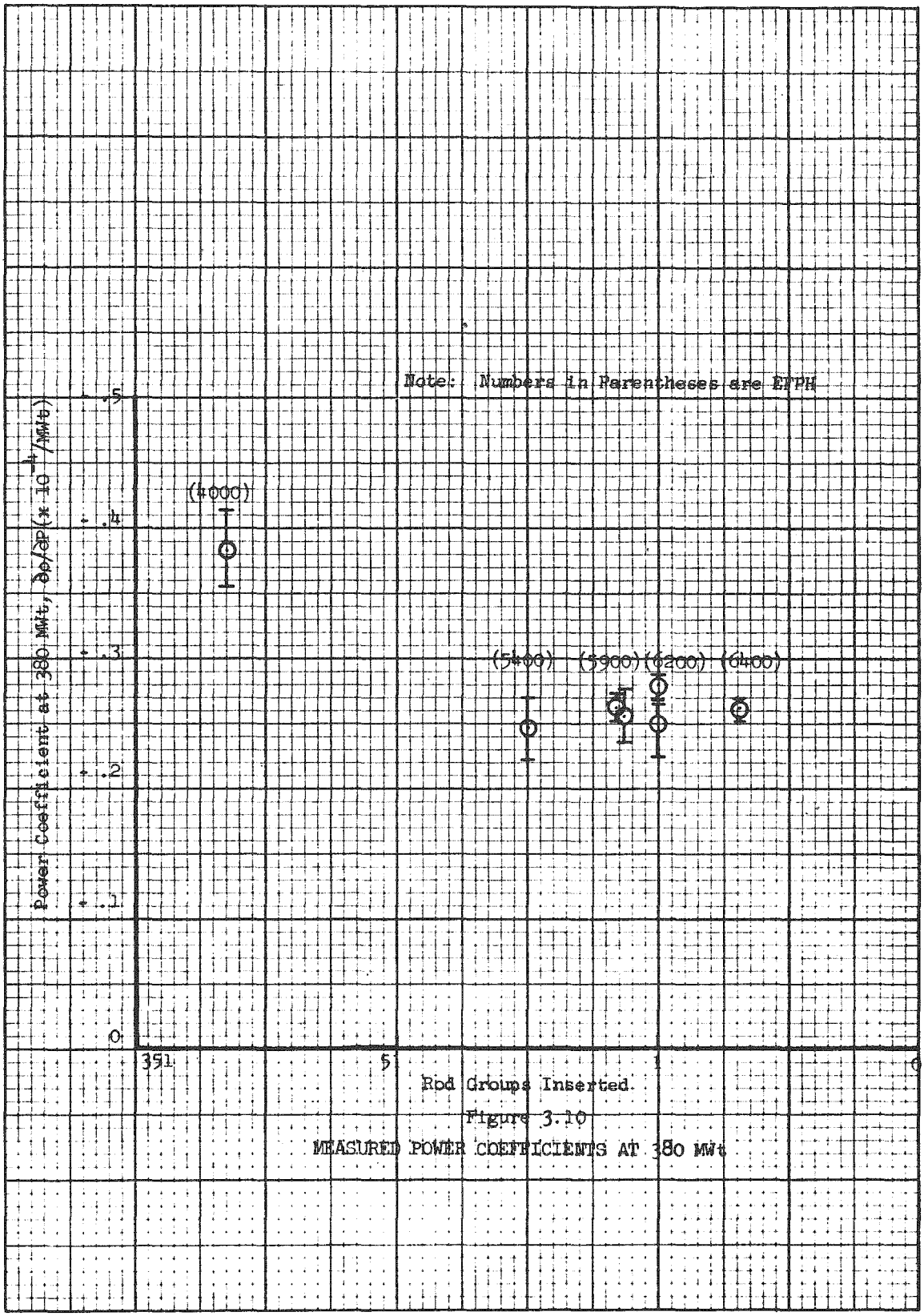

Figure 3.10

MEASURED POWER COEFFICIENTS AT 380 MWt

3.5 Control Rod Worth

During normal operation at power, reactivity changes due to power changes and fuel depletion are compensated for in Yankee by control rod motion. In the analysis of the reactivity behavior of the core during operation at power it is therefore important to know the behavior of control rod worth.

The differential worth of a control rod depends primarily on the local flux level in the neighborhood of the control rod, the diffusion properties of the surrounding medium and the competition for neutron absorption by other absorbers. One would therefore expect a strong dependence of the differential worth of a control rod on the burnup distribution, fuel temperature distribution, coolant temperature distribution and fission product (Xe) distribution in the core and on the control rod configuration in the core.

One-dimensional WANDA and two-dimensional RZ PDQ calculations were performed in an effort to obtain a quantitative evaluation of the effects discussed above. These include the effects of burnup, fuel temperature and coolant temperature distributions on integral control rod worth. It is possible to predict by WANDA or PDQ calculations the worth of individual control rod groups in the undepleted zero power core to within 10% of the measurements [3]. Nevertheless the results given below are more important in terms of the relative change in worth as a result of non-uniform distribution effects rather than in terms of absolute values.

3.5.1 Effect of Fuel Depletion on Control Rod Worth

Fuel depletion affects rod worth both because of its effects on flux distribution and because of the non-uniform increase in the core absorption cross section. Two-group, two-dimensional PDQ calculations with non-uniform burnup distributions were performed to obtain the change in integral rod worth with depletion. The calculations were done at zero power, and for the depleted cores with no Xe and peak Sm. These conditions correspond

to the conditions at the time of the control rod worth measurements. The results are plotted in Figure 3.11 for groups 1, 5, and 3. The calculated variation of integral worth with fuel depletion agrees reasonably well with experiments.

Figures 3.12 through 3.16 show measurements of differential rod worths at zero power, in the xenon-free, peak samarium core at various times in life, compared to the measurements at beginning-of-life. In all cases the differential worth in the lower half of the core is reduced, and the differential worth in the upper half of the core increased, as depletion proceeds. This is a consequence of the fact that depletion in the lower part of the core is greater than in the upper part of the core. The effect of the non-uniform burnup distribution on differential worth is quite pronounced and these measurements illustrate the fallacy of using rod worth data obtained before power operation to obtain reactivity worth data*.

3.5.2 Effect of Non-Uniform Fuel and Moderator Temperature and Fission Product Distribution on Control Rod Worth

The zero power measurements described above are performed under the condition of essentially uniform fuel and coolant temperature distributions. During operation at power, there are non-uniform distributions of fuel temperature and coolant density. These distributions depend on the control rod configuration and fuel depletion distribution in the core. One-dimensional radial WANDA calculations of the effect on integral rod worth in the programmed withdrawal sequence were performed by using different fuel and coolant temperatures in each of several core regions. The temperature distributions were computed on the basis of the zero power distribution for several control rod configurations. The calculations were done for the undepleted core. Table 3.9 shows the results for groups 1, 5, and 3.

---

*This statement does not imply that differential control rod worth measurements at zero power are not useful since such measurements usually serve to verify calculations and are useful in determining such important parameters as excess core reactivity.

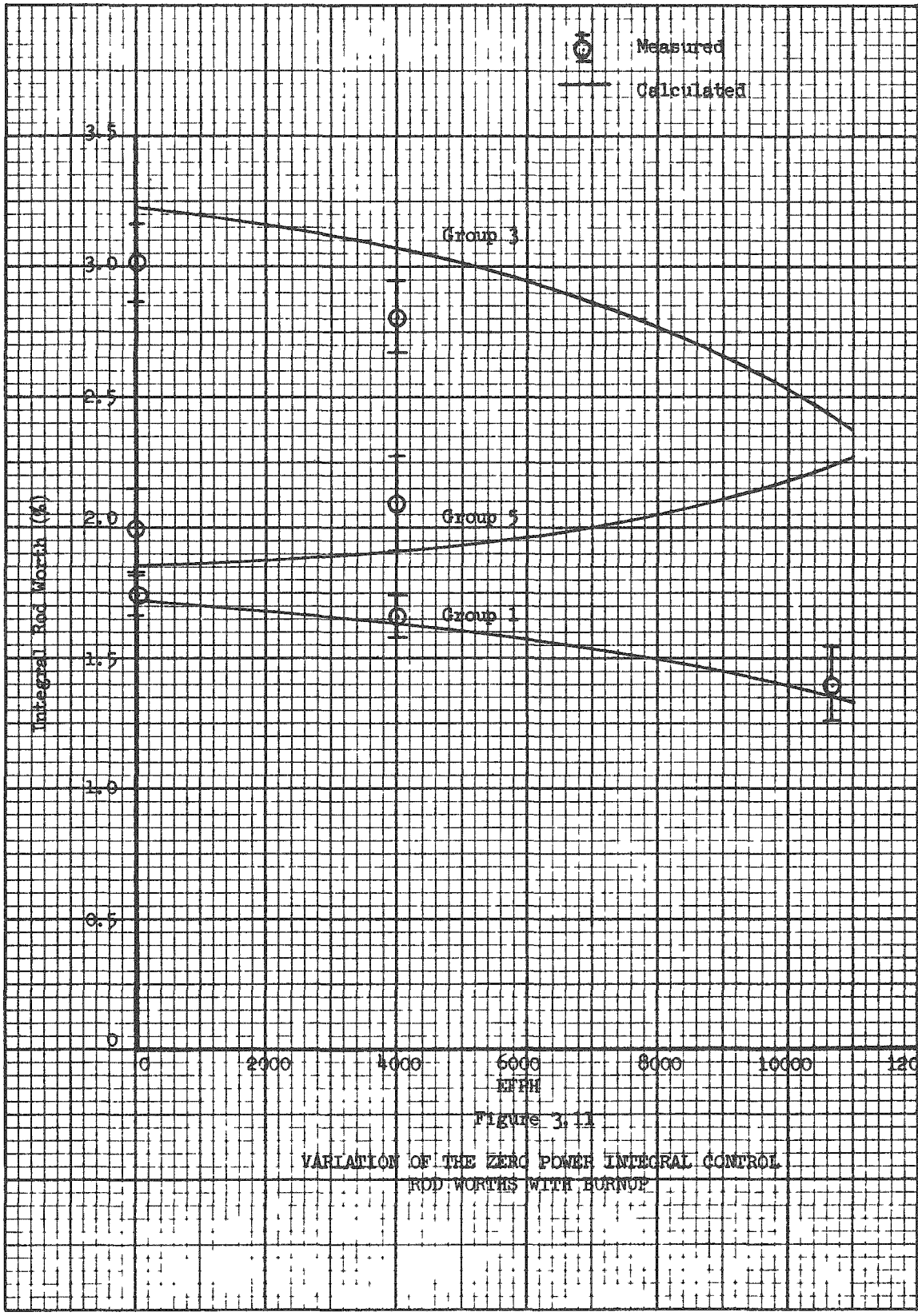

Figure 3.11

VARIATION OF THE ZERO POWER INTEGRAL CONTROL ROD WORTHS WITH BURNUP

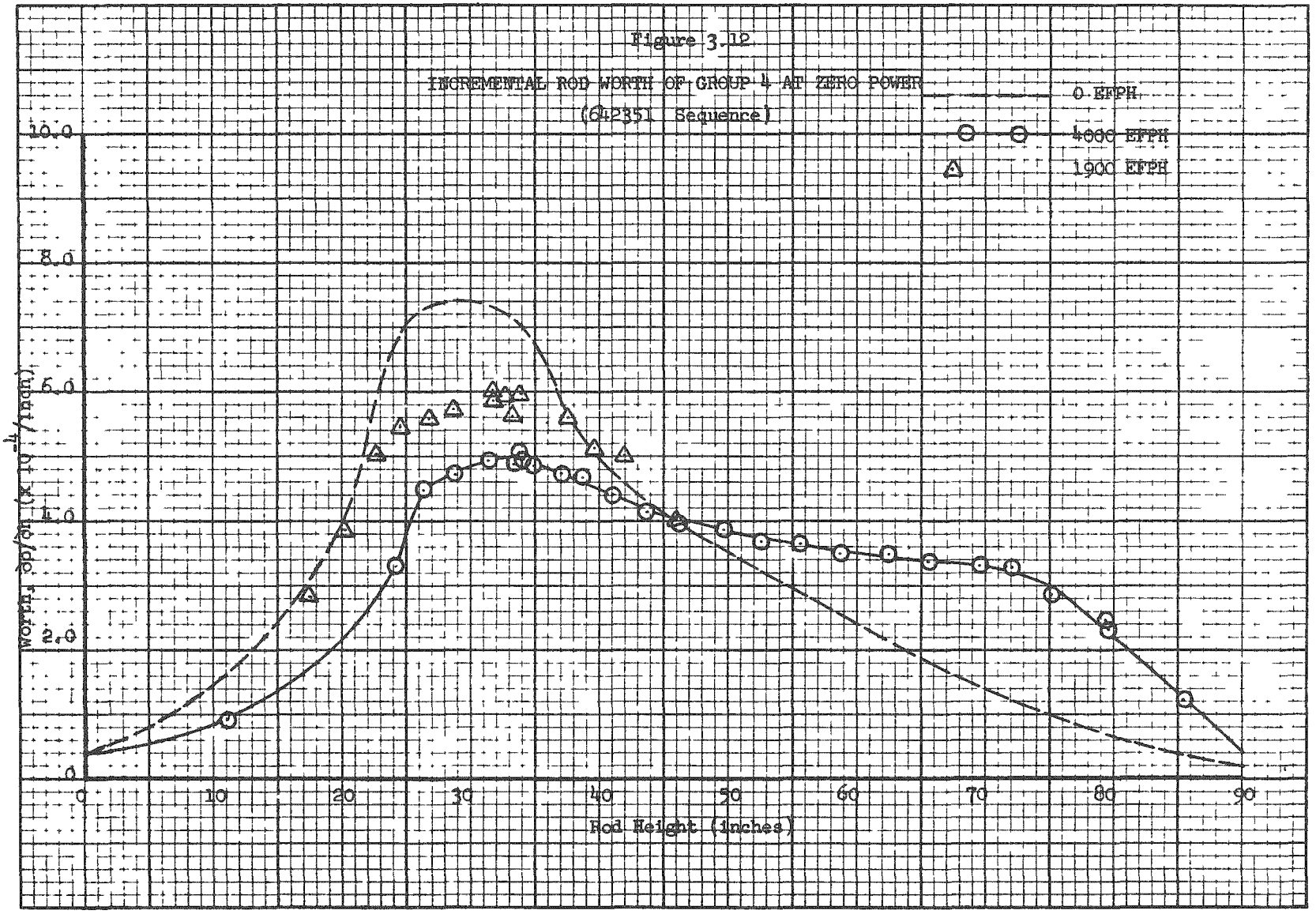
Figure 3.12
INCREMENTAL ROD WORTH OF GROUP 4 AT ZERO POWER
(042351 Sequence)
0 EFPH
4000 EFPH
1900 EFPH
10.0
8.0
6.0
4.0
2.0
0
Δk/k x 10⁻⁴/inch
0
10
20
30
40
50
60
70
80
90
Rod Height (inches)

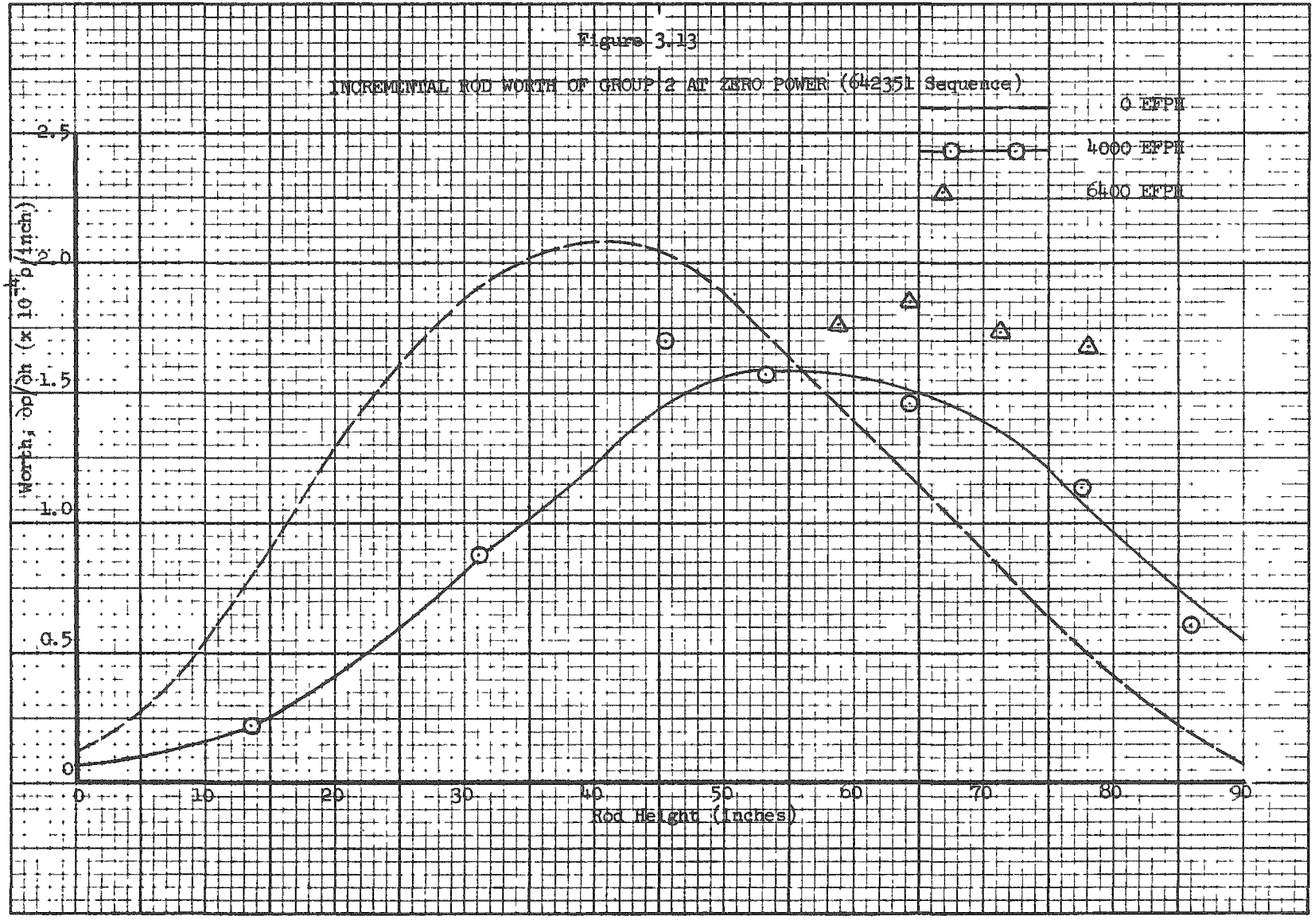
Figure 3.13
INCREMENTAL ROD WORTH OF GROUP 2 AT ZERO POWER (642351 Sequence)
0 EFPH
4000 EFPH
6400 EFPH
Worth, ∂ρ/∂h (x 10⁻⁴ Δρ/inch)
2.5
2.0
1.5
1.0
0.5
0
0
10
20
30
40
50
60
70
80
90
Rod Height (Inches)

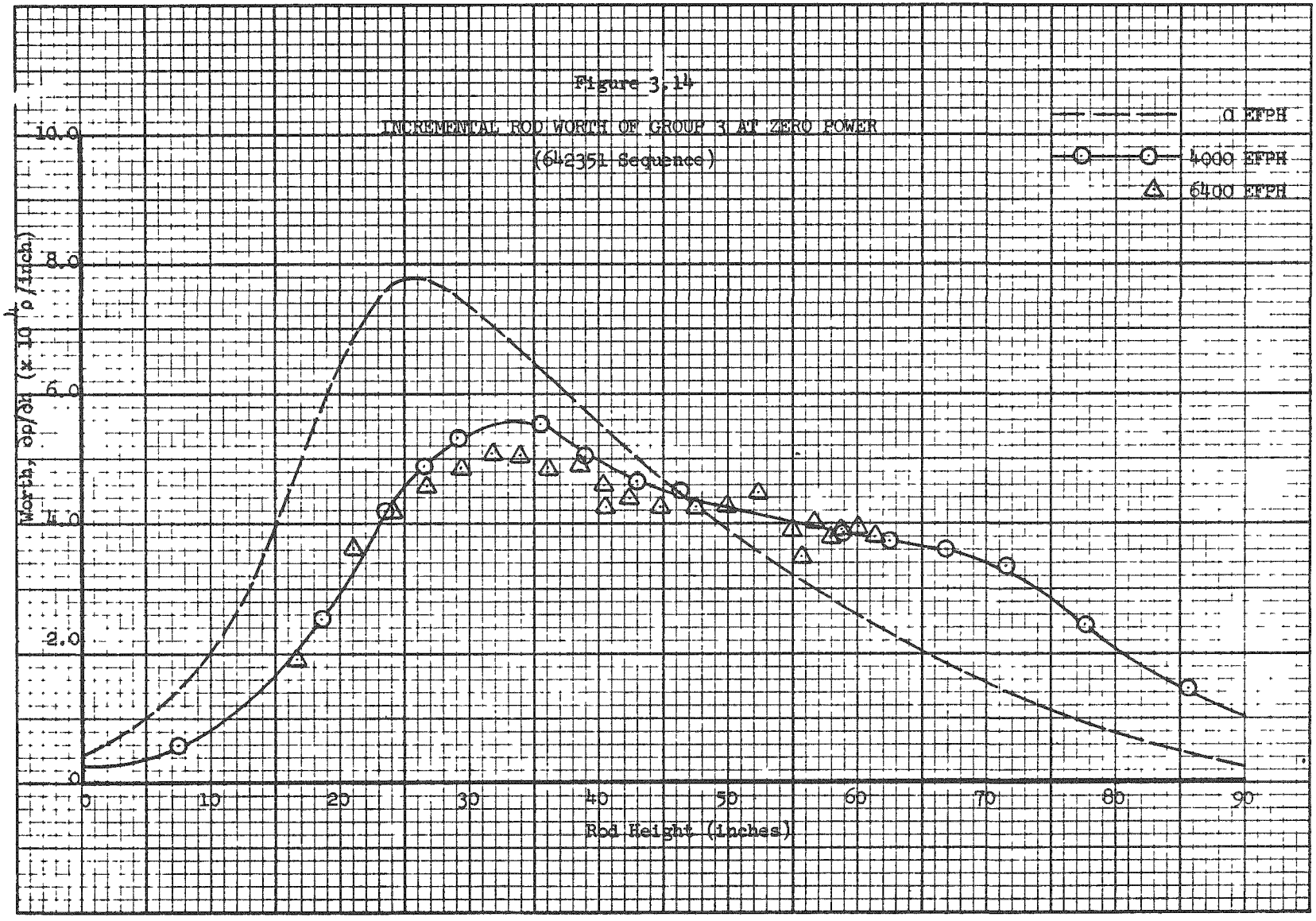
Figure 3.14
INCREMENTAL ROD WORTH OF GROUP 3 AT ZERO POWER
(64235A Sequence)
0 EFPH
4000 EFPH
6400 EFPH
Worth, dρ/dk (x 10⁴ /inch)
10.0
8.0
6.0
4.0
2.0
0
0
10
20
30
40
50
60
70
80
90
Rod Height (inches)

Figure 3.15
INCREMENTAL ROD WORTH OF GROUP 5 AT ZERO POWER
(542351 Sequence)

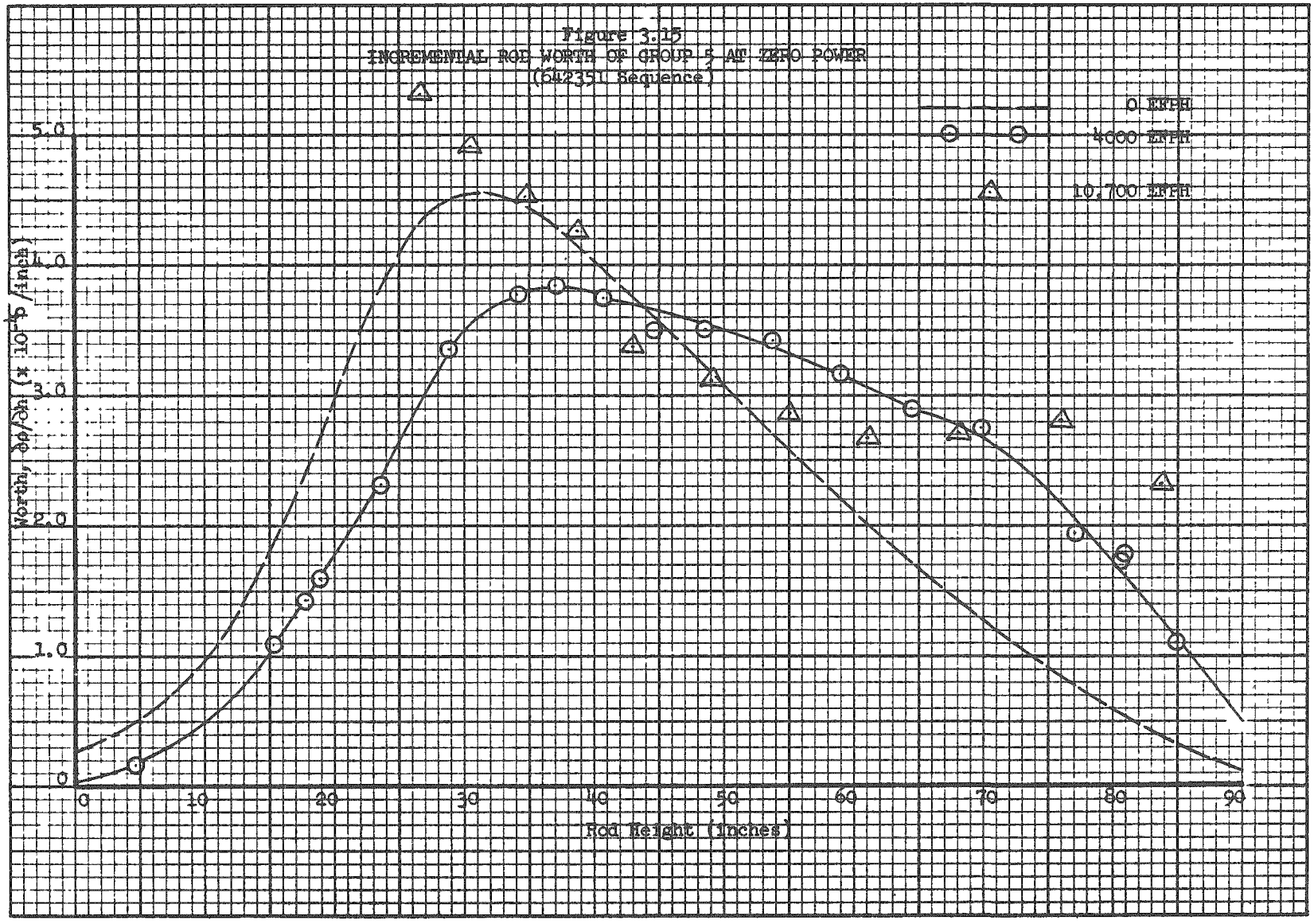

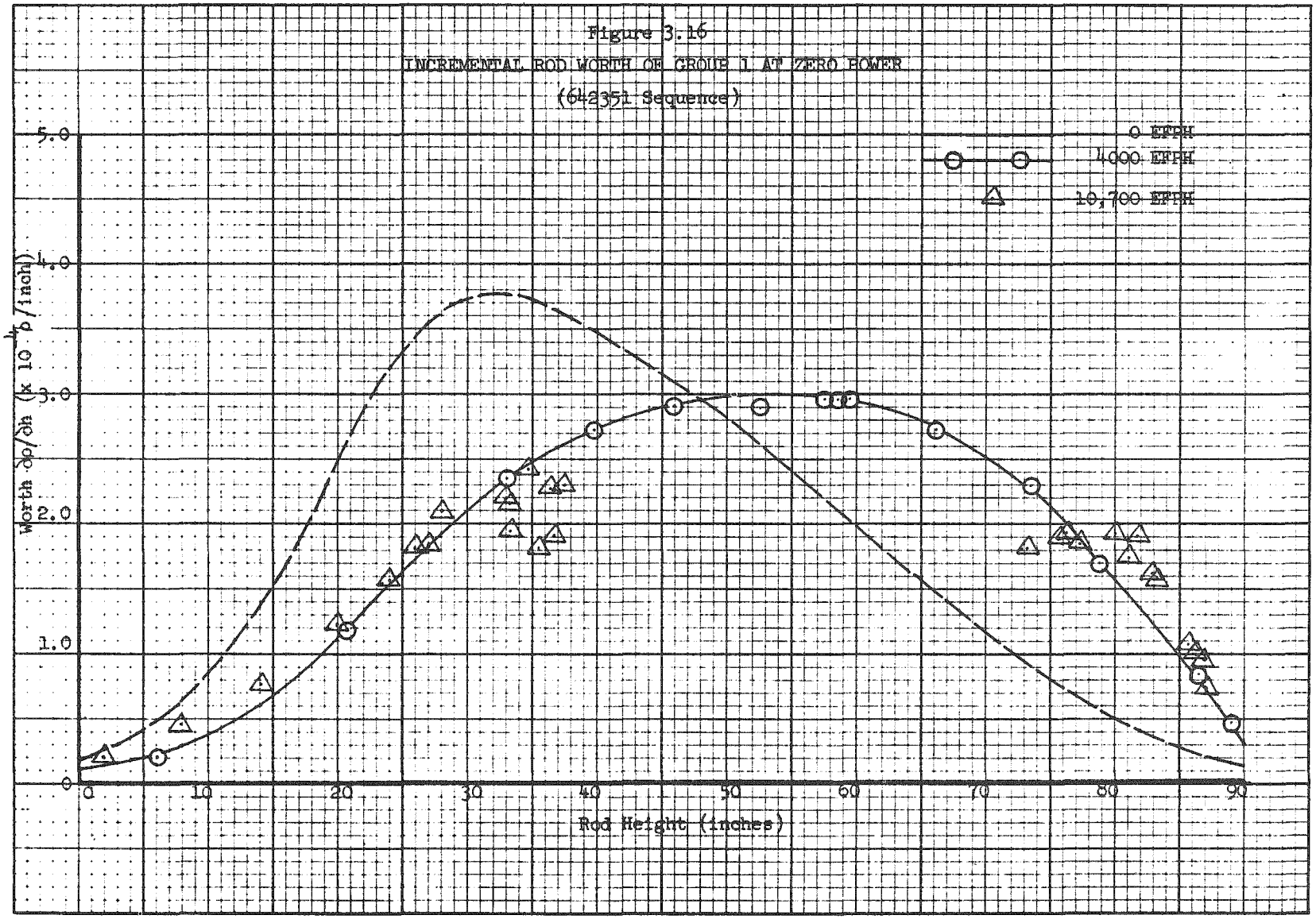
Figure 3.16
INCREMENTAL ROD WORTH OF GROUP 1 AT ZERO POWER
(642351 Sequence)
0 EFPH
4000 EFPH
10,700 EFPH
Worth ∂ρ/∂h (x 10⁻⁴ Δρ/inch)
5.0
4.0
3.0
2.0
1.0
0
0
10
20
30
40
50
60
70
80
90
Rod Height (inches)

Table 3.9

Effect of Non-Uniform Temperature Distributions
On Integral Rod Worths

Condition	Rod Worth (%) Group 1	Group 5	Group 3
0 Power, uniform T_{H_2O}	1.72	1.85	3.22
0 Power, non-uniform T_{H_2O}	1.64	--	--
392 MWt, uniform T_{H_2O} and T_{fuel}	1.73	--	--
392 MWt, non-uniform T_{H_2O} and T_{fuel}	1.44	2.12	2.79

The effect of the non-uniform radial fuel and coolant temperature distribution is to reduce the worth of group 1 by 16%, to increase the worth of group 5 by 15% and to reduce the worth of group 3 by 13%. Table 3.9 also shows that the effect of the non-uniform radial coolant density distribution alone is to reduce group 1 worth by 5%.

A calculation was also performed at an average core burnup of 5100 EFPH, of the effect of the non-uniform water density distribution on the worth of group 1 fully inserted with group 5 at 50 in. The calculation used the PDQ code in RZ geometry with a non-uniform burnup distribution. The worth was obtained with a uniform and with a non-uniform water density distribution. The results were a total worth of 2.54% with the uniform distribution and a total worth of 2.43% with the non-uniform distribution, or a difference of 0.1% $\Delta\rho$.

It should be noted that the above calculations of rod worth are based on a comparison of the core reactivity with and without a given rod group inserted. The resulting rod worth therefore includes any change in moderator temperature defect and fuel temperature defect due to statistical weight effects. However, this is consistent with the rod worth measurements which do not differentiate between reactivity changes due to withdrawal of a rod group and reactivity changes due to changes in statistical weight factors.

Differential rod worth during operation at power will differ from that at zero power. The various phenomena involved may be summarized as follows:

1. The non-uniform fuel depletion will cause a change in differential rod worth with time.

2. The low coolant temperature in the lower region of the core and the high coolant temperature in the upper region of the core will affect the differential rod worth since the effectiveness of a rod increases with decreasing water density.

3. Because of the non-uniform Doppler effect in the core, the flux distribution is different at power and at zero power. The epithermal differential rod worth may also decrease because of competition with resonance absorption in U-238.

4. The non-uniform distribution of xenon in the core will affect differential rod worth. This results both from the effects of xenon on flux distribution and the non-uniform competition for neutron absorption by xenon.

Figures 3.17 through 3.19 show measurements of the differential rod worth of groups 3, 5, and 1 at power under equilibrium xenon conditions. Differential control rod worths at power are obtained by measuring the compensating change in moderator temperature which maintains the reactor critical after a given change in control rod position. The measurements at power are compared to measurements made at zero power. The measurements at power cover the range from 850 EFPH to 3800 EFPH on group 3, 3800 EFPH to 6000 EFPH on group 5, and 6000 EFPH to 7600 EFPH on group 1. The measurements show a decrease in groups 3 and 1 worth at power consistent with the calculations of Table 3.9. The measured integral worth of group 1 at power is 1.20% $\Delta\rho$. This same value of rod worth is obtained from Table 3.9 by including the calculated variation of integral rod worth with fuel depletion of Figure 3.11.

Figures 3.20 through 3.22 show measurements of differential rod worth taken during xenon decay after reactor shutdowns. These data are compared with measurements obtained at zero power in the xenon-free core. It is noted that the rod worth data obtained during xenon decay differ from those at zero power and also from those obtained during power operation. The effect of the xenon transient on the differential rod worth is different for the different shutdowns. This is because the effect of the xenon transient on the differential rod worth depends on the power distribution and therefore the xenon distribution in the core prior to the shutdown. The axial power prior to the shutdown at 350 EFPH followed roughly a cosine distribution, and the axial power distribution prior to the 4000 EFPH shutdown was relatively flat, such that the data obtained following these shutdowns are roughly similar to the zero power data. Prior to the 1900 EFPH shutdown, the power distribution was peaked in the bottom of the core, so that more xenon was present in the bottom of the core than in the top of the core. The differential rod worth curve obtained during the xenon decay is therefore much distorted from the zero power curve.

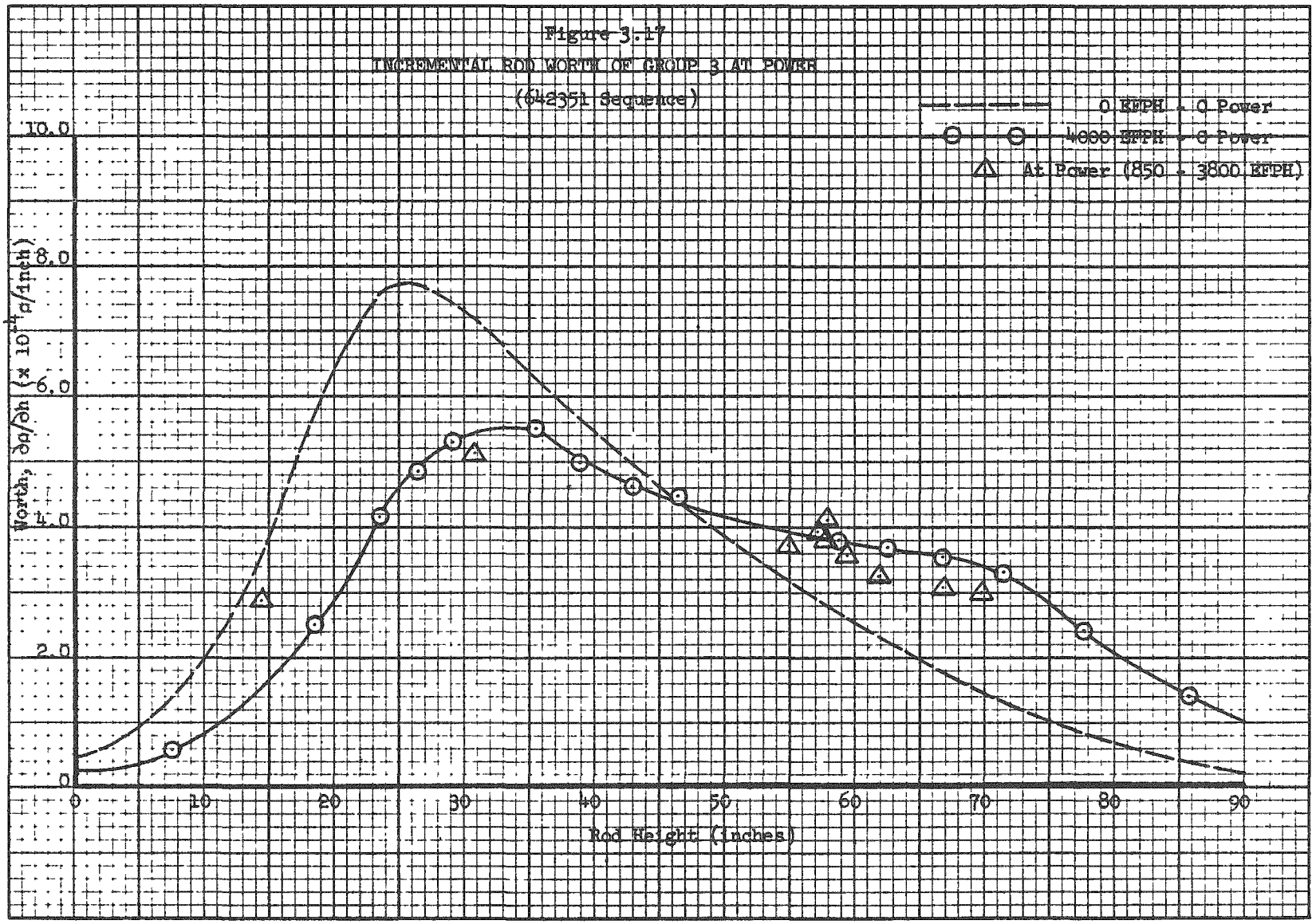
Figure 3.17
INCREMENTAL ROD WORTH OF GROUP 3 AT POWER
(42351 Sequence)
0 MWD - 0 Power
4000 MWD - 0 Power
At Power (850 - 3800 MWD)
Worth, dρ/dh (× 10⁻⁴ Δ/inch)
10.0
8.0
6.0
4.0
2.0
0
0
10
20
30
40
50
60
70
80
90
Rod Height (inches)

Figure 3.18
INCREMENTAL ROD WORTH OF GROUP 5 AT POWER
(642351 Sequence)

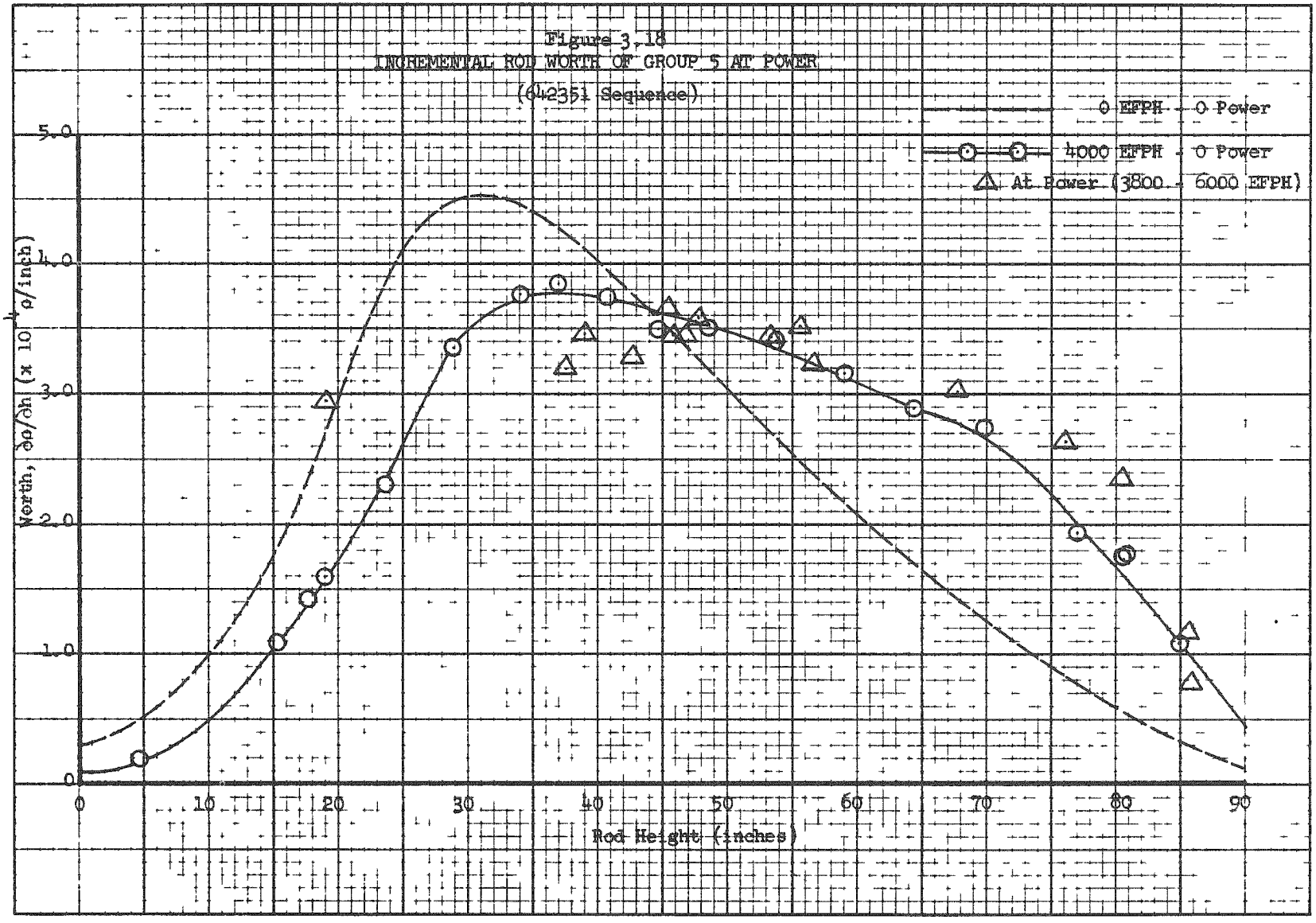

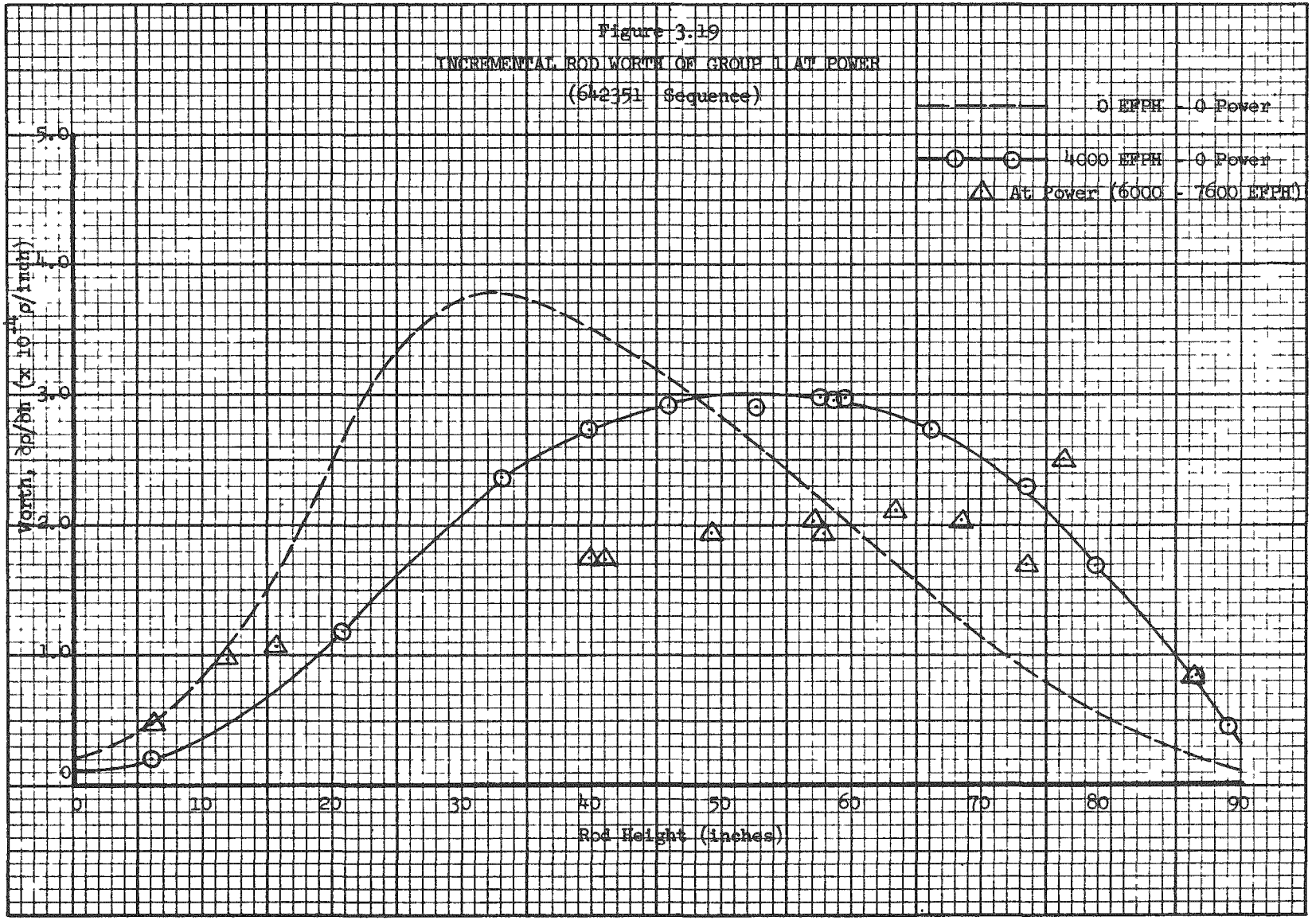
Figure 3.19
INCREMENTAL ROD WORTH OF GROUP 1 AT POWER
(642351 Sequence)
0 EFPH - 0 Power
4000 EFPH - 0 Power
At Power (6000 - 7600 EFPH)
Worth, ∂ρ/∂h (x 10⁻⁴ ρ/inch)
5.0
4.0
3.0
2.0
1.0
0
0
10
20
30
40
50
60
70
80
90
Rod Height (inches)

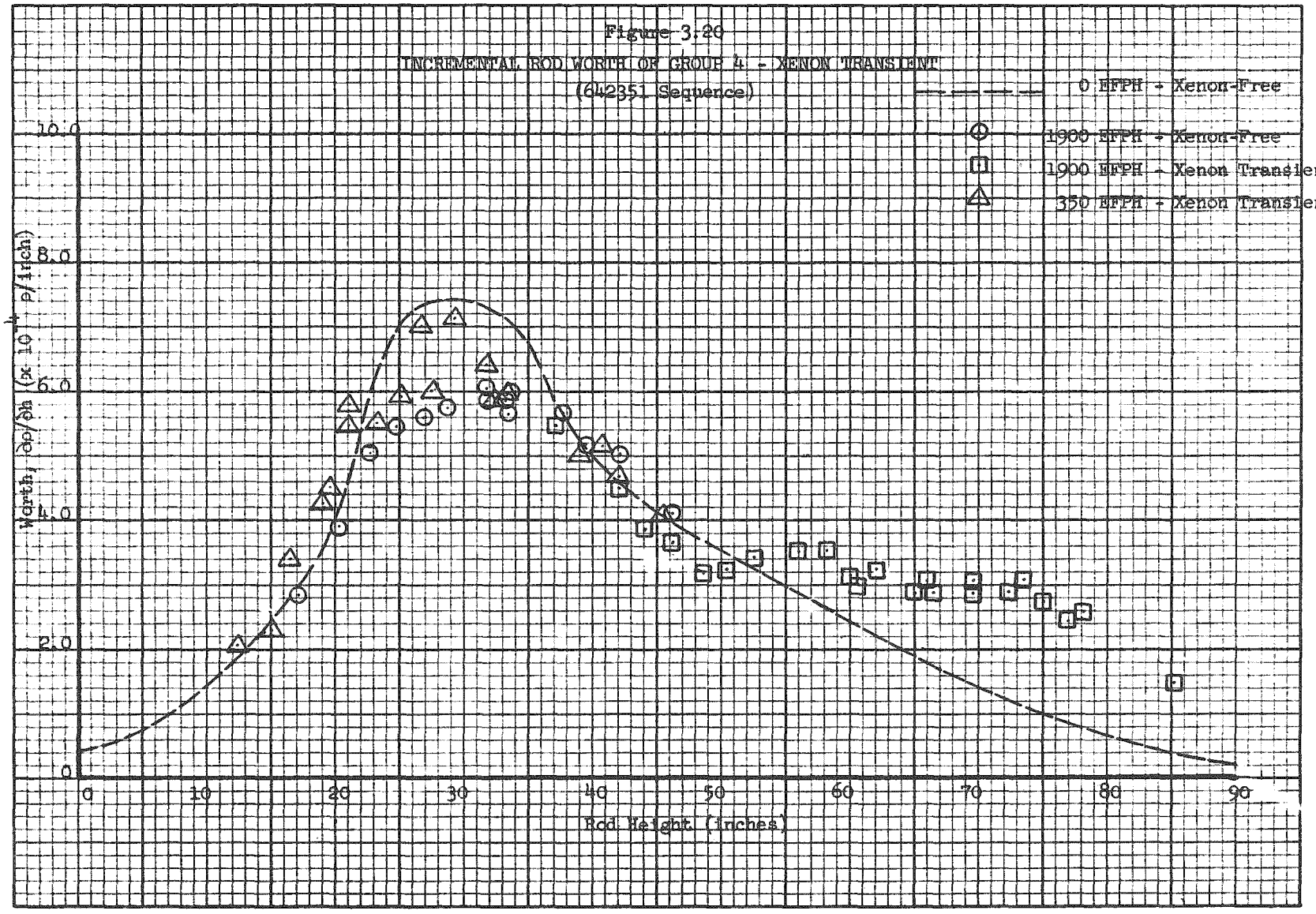
Figure 3.20
INCREMENTAL ROD WORTH OF GROUP 4 - XENON TRANSIENT
(642351 Sequence)
0 EFPH - Xenon-Free
1900 EFPH - Xenon-Free
1900 EFPH - Xenon Transient
350 EFPH - Xenon Transient
Worth, dρ/dh (x 10⁻⁴ ρ/inch)
10.0
8.0
6.0
4.0
2.0
0
0
10
20
30
40
50
60
70
80
90
Rod Height (inches)

Figure 3.21

INCREMENTAL ROD WORTH OF GROUP 2 - XENON TRANSIENT

(6-2351 Sequence)

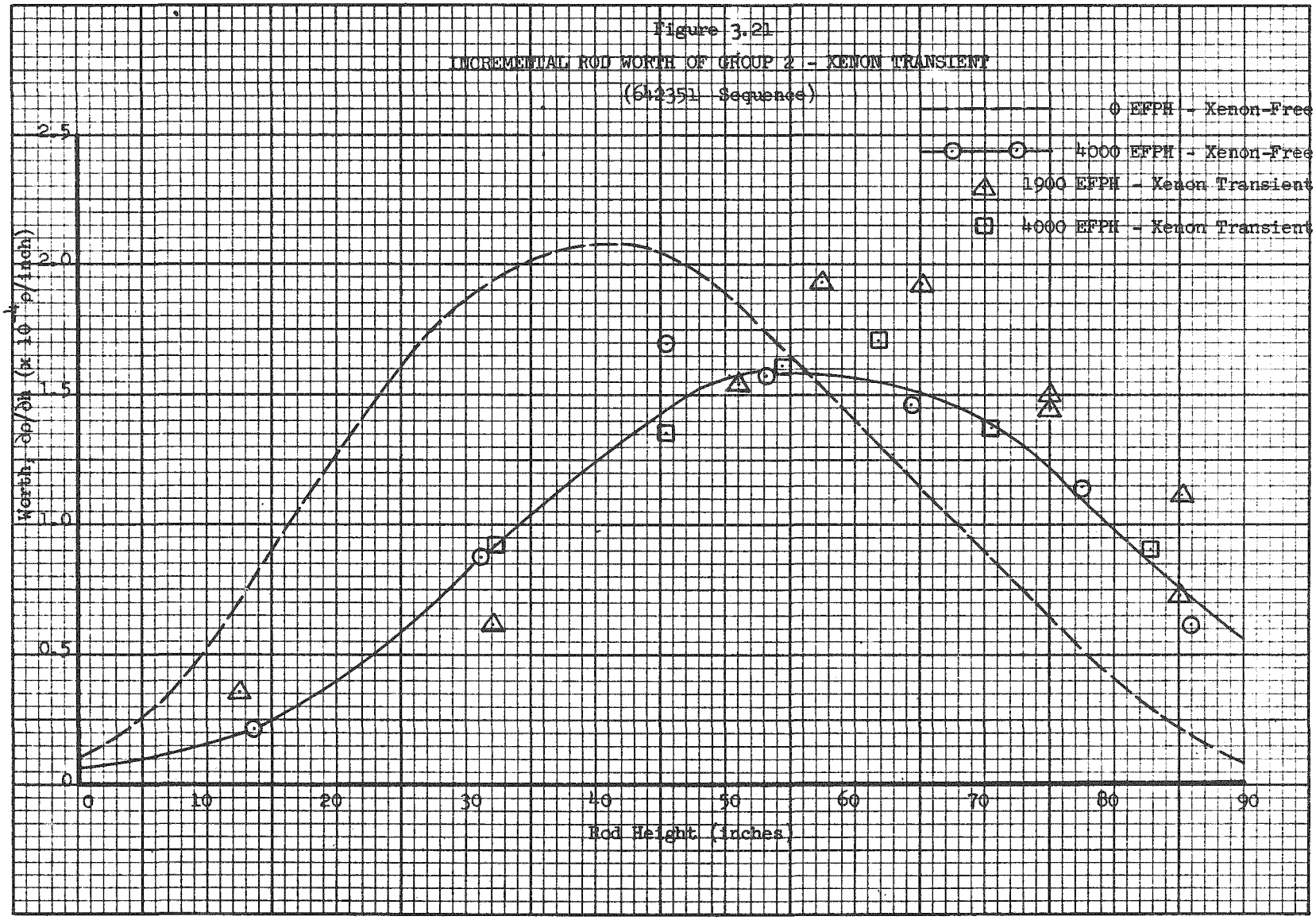

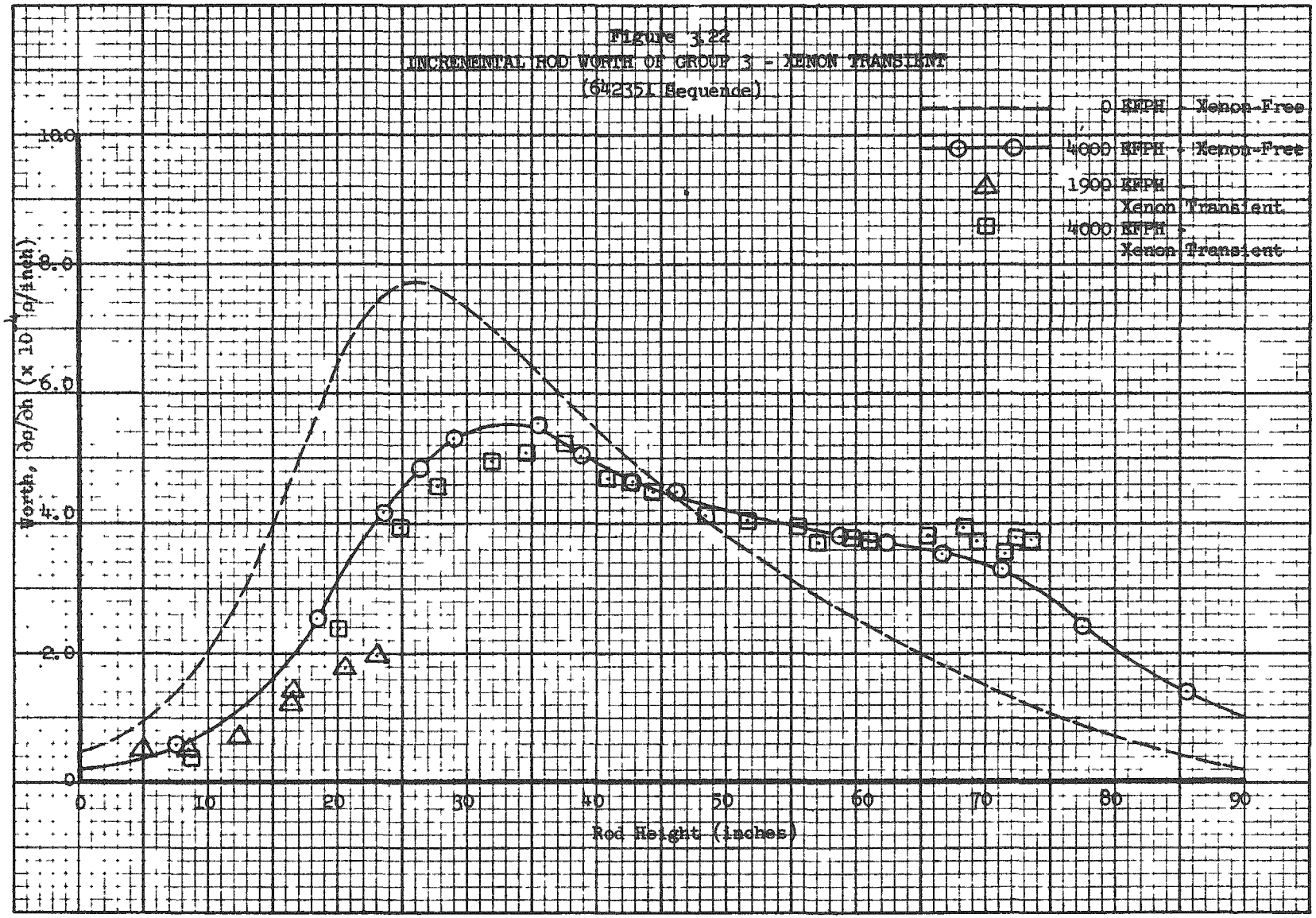
Figure 3.22
INCREMENTAL ROD WORTH OF GROUP 3 - XENON TRANSIENT
(64231 Sequence)
0 MWPH - Xenon-Free
4000 MWPH - Xenon-Free
1900 MWPH - Xenon Transient
4000 MWPH - Xenon Transient
Worth, dρ/dh (x 10⁴ Δρ/Inch)
10.0
8.0
6.0
4.0
2.0
0
0
10
20
30
40
50
60
70
80
90
Rod Height (inches)

3.6 Boron Worth

Boron, in the form of boric acid dissolved in the main coolant, is used by Yankee to provide cold shutdown of the reactor. Concentration is varied by means of both a bleed and feed system and an ion exchange system. Because the boron is uniformly distributed in the zero power core, it has proven extremely useful as a reactivity control system during the zero power physics experiments [3].

On September 13, 1961 Yankee initiated a boron test at power with the aim of obtaining information on operation at power with chemical shim. 400 ppm of boric acid, worth about 2.5% in reactivity, were injected into the coolant with the reactor operating at 380 MWt. A detailed description of the purpose of the test, the events, and the experimental information obtained during the test was submitted to the Atomic Energy Commission by the Yankee Atomic Electric Company [19]. A description and analysis of the reactivity history during the boron test was given in section 2.3 of this report. The experimental and calculational results pertaining to the reactivity worth of boron are given below.

3.6.1 Variation of Boron Worth with Burnup

Boron worths were measured during the startup experiment program [3] and during the 4000 EFPH shutdown. Figure 3.23 summarizes these measurements*. Figure 3.23 contains three lines, all of which were fitted by the method of least squares to experimental data. Boron worth decreases between 0 and 4000 EFPH. The marked difference in the slope of the curves between beginning-of-life and 4000 EFPH measurements is felt to be due to the non-uniform distribution of both fissionable and absorption material in the core, combined with the variation in power distribution over the range of boron concentration due to the motion of the control rods. From these data

---

*A measurement of boron worth was performed in the fully depleted core (10,700 EFPH) and yielded a value of $-(.733 \pm .026) \times 10^{-4}$/ppm over the range 0-40 ppm.

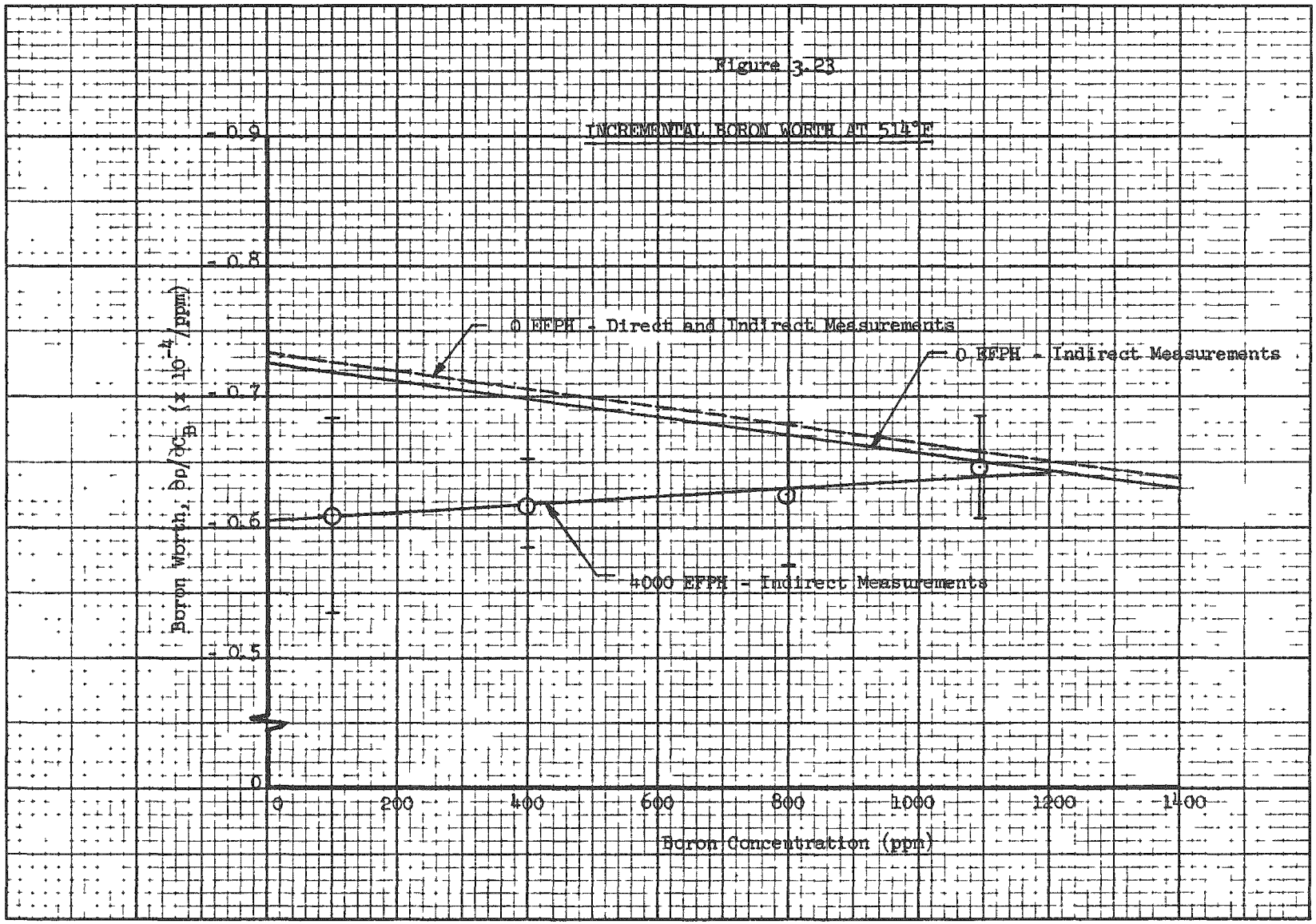
INCREMENTAL BORON WORTH AT 514°F
0 EFPH - Direct and Indirect Measurements
0 EFPH - Indirect Measurements
4000 EFPH - Indirect Measurements
Boron Worth, $\partial\rho/\partial C_B$ ($\times 10^{-4}$/ppm)
Boron Concentration (ppm)
0.9
0.8
0.7
0.6
0.5
0
0
200
400
600
800
1000
1200
1400

Figure 3.23

it can therefore be inferred that boron worth depends on boron concentration, the power distribution in the core, and the fuel depletion distribution.

A calculation of the boron worth was performed at an average burnup of 5100 EFPH at 392 MWt operation. The PDQ code was used in RZ geometry with a non-uniform burnup distribution, and with all control rods withdrawn. The calculated worth was -0.55×10^{-4}/ppm at an average boron concentration of 200 ppm. Based on the data of Figure 3.23, this calculation probably underestimated boron worth somewhat. This is consistent with the underestimate in the calculated boron worth at beginning-of-life [3]. The most likely source of the discrepancy is the assumption, made in the calculations, that the spectrum of neutrons to which the fuel and moderator are exposed is the same.

3.6.2 Non-Uniform Distribution Effects

The beginning-of-life and the 4000 EFPH measurements were done at zero power with a uniform coolant density and boron concentration distribution. This is not the case for operation at power. A calculation was performed to ascertain the magnitude of this effect. The worth of 420 ppm boron was calculated in the unrodded core at 392 MWt, 5100 EFPH. The PDQ code was used in RZ geometry with a non-uniform burnup distribution. In one calculation the water density was assumed uniform over the core. In a second calculation the water density and boron concentration were non-uniformly distributed over the core. In both calculations a uniform fuel temperature was assumed. The power distribution from the uniform problem was used to calculate the enthalpy in each of 16 core regions, and hence the water density in each region. The worth of the 420 ppm boron was 2.29% $\Delta\rho$ with a uniform density distribution and 2.27% $\Delta\rho$ with a non-uniform density distribution. The non-uniform boron distribution causes less than 1% decrease in boron worth.

3.6.3 Boron Depletion During the Boron Test at Power

Absorption of neutrons by B-10 at power will cause a decrease in the coolant boron concentration. The equation which describes this effect is simply

$$\frac{d\,N^{B\text{-}10}}{dt} = -N^{B\text{-}10}\left(\phi_1 \sigma_{a1}^{B\text{-}10} + \phi_2 \sigma_{a2}^{B\text{-}10}\right) \qquad (3.20)$$

with solution

$$N^{B\text{-}10}(t) = N^{B\text{-}10}(0)e^{-(\phi_1 \sigma_{a1}^{B\text{-}10} + \phi_2 \sigma_{a2}^{B\text{-}10})t} \qquad (3.21)$$

Before using equation (3.21) a correction factor must be applied to the thermal cross section to account for the peaking of the thermal flux in the moderator regions. The time constant in equation (3.21) was found to be 4.78×10^{-8} sec^{-1} corresponding to a half life of 4030 hours for operation at 392 MWt. For a 7-day period, equation (3.21) predicts a 2.9% decrease in boron concentration because of neutron absorption. This is equivalent to a gain of about 0.07% $\Delta\rho$.

3.7 Reactivity Loss Rate

3.7.1 Core Life Estimates

The ability to predict core lifetime depends primarily on the ability of the method used to calculate the excess reactivity of the undepleted core, the poisoning effect of the fission products xenon and samarium, and the reactivity loss rate due to fuel depletion. This last factor is a function of Pu-239 production (capture in U-238), capture and fission rates in Pu-239, Pu-240 and Pu-241, and capture rates in lumped fission products (all fission products except Xe-135 and Sm-149, which are treated explicitly). The measured Yankee core lifetime at 392 MWt and rated conditions (514°F, 2000 psig) is 8000 hours, or 6270 MWD/Tonne.

Table 3.10 lists core lifetimes calculated with one-dimensional (CANDLE) [20] and two-dimensional (TURBO) [21] models.

Table 3.10

Predictions of Core Lifetime

Method	$p_{r_3}^{28}$	$\sigma_{a_{th}}^{FP}$[1] ($\frac{\text{barns}}{\text{fission}}$)	$\sigma_{a_{epith}}^{FP}$ (barns/fission)	Initial Excess ρ(%) at 392 MWt	Core Life (MWD/T)
Experiment	--	--	--	9.85 ± .73	6270
CANDLE	.7587	64	0	8.52	6840
TURBO	.7587	64	0	8.52	6660
CANDLE	.7575	26.4	34	8.78	5700
CANDLE	.7575	80.2	24.2	8.78	5120
CANDLE	.7575	29.0	23.1	8.78	6240

[1] Hardened cross section

$p_{r_3}^{28}$ is the U-238 resonance escape probability in the third group of a four energy group scheme. In both the CANDLE and the TURBO calculations the group microscopic cross sections were constant throughout core lifetime. The cross sections corresponded to the undepleted core energy spectrum. The assumption of irradiation-independent microscopic cross sections is not a bad assumption in Yankee as was indicated by MUFT and SOFOCATE calculations at various irradiation times. The exceptions are Pu-239 and Pu-240 where the increased self-shielding effect causes a reduction in the absorption cross section with irradiation time [22].

The first CANDLE calculation and the TURBO calculation in Table 3.10 are the design calculations [23]. A hardened lumped fission product thermal cross section of 64 barns with no epithermal component was used. Core life is overestimated somewhat even though the initial excess reactivity is underestimated by about 1.3%. The underestimate in the reactivity loss rate is in large part due to the use of too low a fission product cross section. The last three CANDLE calculations in Table 3.10 make use of recently published values for lumped fission product cross sections. These calculations differ in another respect from the design calculations in that a revised fast group cross section library, consistent with recent MUFT calculations, has been used. This fact accounts for the different $p_{r_3}^{28}$ and the somewhat higher initial excess reactivity. The 26.4 barns (hardened), 34 barns cross sections were obtained from calculations at Bettis in 1960 [24]. These cross sections were calculated for fissions in U-235 and correspond to averages over an irradiation time approximately equivalent to that in Yankee. The 80.2 barns (hardened), 24.2 barns cross sections were taken from the compilation of fission product capture cross sections by Garrison and Ross [25]. These values are for U-235 fissions and neglect the effect of saturation due to burnout and decay. The 29.0 barns (hardened), 23.1 barns cross section correspond to the measured values of lumped fission product cross sections published by Gunst from Bettis in 1962 [26]. These cross sections were obtained from measurement in the Reactivity Measurement Facility (RMF) for enriched fuel taken to 64% U-235 depletion. Excellent agreement on core life is achieved with the use of the later cross section set. However the underestimate in initial reactivity (about 1%) indicates that this set of fission product cross sections probably underestimates core reactivity loss rate.

Based on end-of-life reaction rates, the last three sets of lumped fission product cross sections of Table 3.10 are equivalent to effective thermal cross sections of 129 barns,

153 barns, and 99 barns respectively. As noted above, these three sets of cross sections correspond to fissions in U-235 only. Because of the shift in the fission product yield curve, lumped fission product cross sections for fissions in Pu-239 are significantly different than for fissions in U-235. The compilation of Garrison and Ross yields lumped fission product cross sections of 269 barns (hardened) thermal and 33.9 barns epithermal for fissions in Pu-239.

3.7.2 Burnup Rate

Figure 3.24 shows calculated reactivity loss rates compared to the measured reactivity loss rate for the three sets of fission product cross sections of Table 3.10. The measured reactivity loss rate was obtained from measurements of the excess reactivity of the core at various times in core life. Therefore the data represent average depletion rate over relatively long periods rather than instantaneous reactivity loss rates. The calculated rate is sensitive to the value of the fission product cross section used in the calculations. The one-dimensional calculations predict the variation of reactivity loss rate with burnup quite well. This is encouraging in view of the fact that in the CANDLE calculations (radial geometry), criticality is maintained throughout core life by varying a poison homogenized uniformly in the core. The agreement between the measured variation of reactivity loss rate with burnup and the radial CANDLE calculations indicate that the programmed control rod withdrawal sequence followed in Core I resulted in a uniform axial burnup. Based on Figure 3.24, the Gunst 1962 data result in an underestimate in depletion rate. It would seem that the agreement with measured depletion rate would be achieved with fission product cross sections somewhere in between the data of Garrison and Ross and that of Bettis, 1960; that is, an effective thermal cross section of about 140 barns. Table 3.11 shows a comparison between measured and calculated (CANDLE) average reactivity loss rate in Core I. The averages are taken over the entire core lifetime.

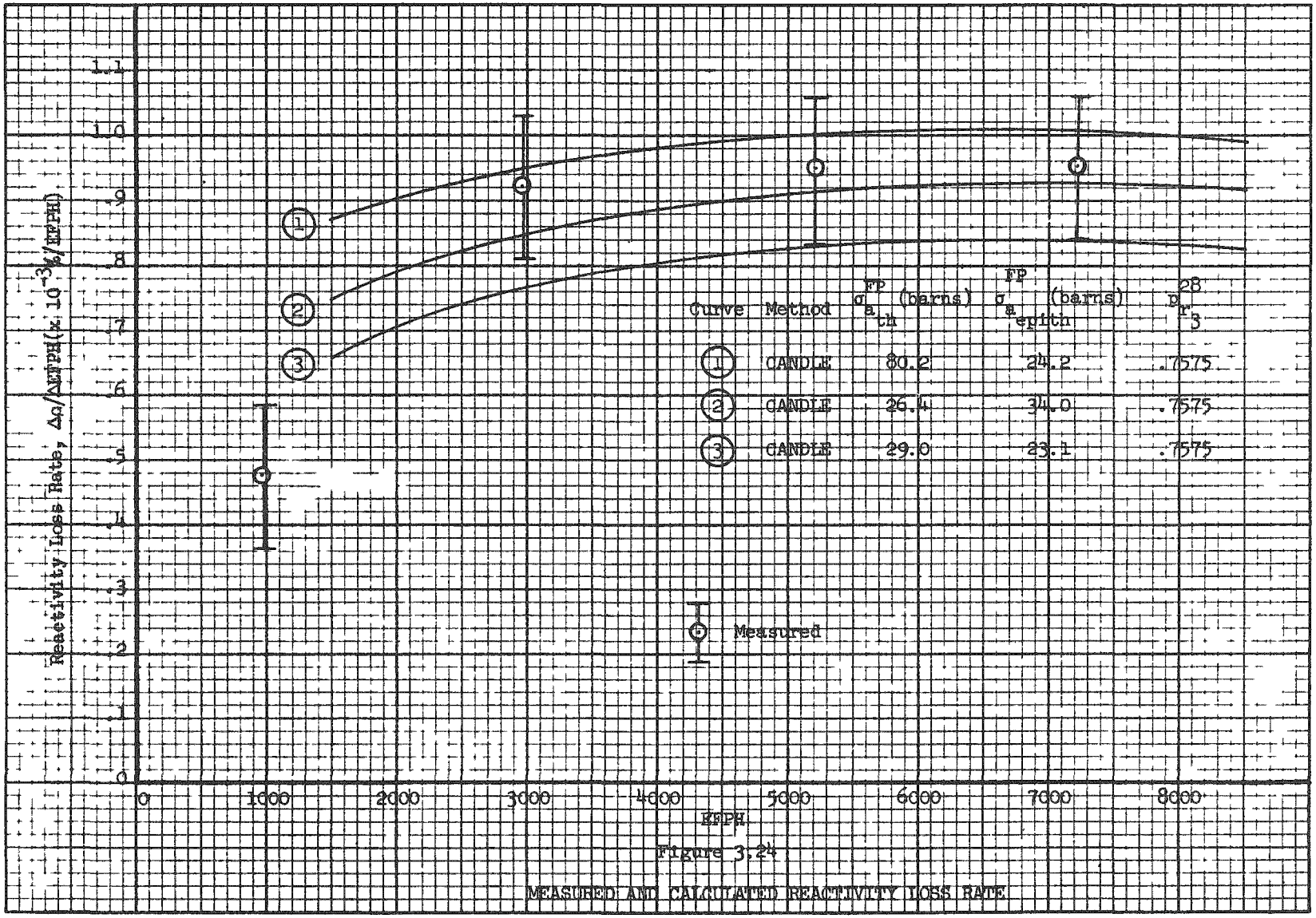

Figure 3.24

MEASURED AND CALCULATED REACTIVITY LOSS RATE

Table 3.11

Measured and Calculated Average Reactivity Loss Rates in Core I

	$\sigma_{a_{th}}^{FP}$ (barns)	$\sigma_{a_{epith}}^{FP}$ (barns)	$p_{r_3}^{28}$	$(\Delta\rho/\Delta EFPH)_{Avg}$ ($\times 10^{-3}$%/EFPH)
Experiment	--	--	--	- .83 ± .10
CANDLE	64	0	.7587	- .666
CANDLE	26.4	34	.7575	- .835
CANDLE	80.2	24.2	.7575	- .930
CANDLE	29.0	23.1	.7575	- .764
CANDLE	26.4	34	.7196	- .678

The agreement is quite good for the CANDLE problem with fission product cross sections of 34 b epithermal and 26.4 b thermal. As was mentioned above, the Garrison and Ross data yields an overestimate in depletion rate while the Gunst data yields an underestimate in depletion rate. It should be noted however that the choice of a best value for fission product cross sections to yield agreement with the measured reactivity loss rate is not necessarily warranted. That is, Table 3.11 shows that a factor of two change in effective thermal fission product cross section causes about a 20% change in reactivity loss rate, while only a 5% change in the value of $p_{r_3}^{28}$ causes a 19% change in reactivity loss rate. It should also be remembered that both fuel and fission product cross sections are not constant throughout core life, as is assumed in the CANDLE calculations.

The burnup distributions obtained from the in-core instrumentation during the Core I lifetime extension period after the removal of all control rods were used in RZ PDQ calculations, maintaining a constant power of 392 MWt and an average coolant temperature of 514°F. Reactivity loss rates were obtained from the calculated criticality factors at various EFPH. The results are shown in Table 3.12. An effective thermal fission product cross section of 90 barns was used in the calculations.

Table 3.12

PDQ Calculated Reactivity Loss Rates During Core Lifetime Extension Period

EFPH	$\Delta\rho/\Delta$EFPH ($\times 10^{-3}$ %/EFPH)
8050	- .770
8300	- .667
8750	- .640
9150	- .635

The calculations predict a decrease in reactivity loss rate of 18% between 8000 and 9300 EFPH. This decrease in burnup rate is probably due to the change in power density distribution due to the non-uniform burnup in the core [1].

3.7.3 Calculations of Critical Configurations

Two-dimensional (RZ PDQ), two-group diffusion theory calculations of experimental critical configurations were performed at various times in life. The calculations used a thermal absorption cross section of 90 barns for the lumped fission products. The burnup distributions used in these calculations were obtained from YADAR and the control rods were represented by fast and thermal

absorption cross sections homogenized in given regions of the core [10]. Equilibrium xenon and samarium poisonings were assumed in the depleted cores. Power effects and xenon poisoning effects were included on the basis of uniform power density throughout the core. The results are given in Table 3.13.

Table 3.13

Two-Dimensional Diffusion Theory Calculations of Critical Core Configurations

EFPH	Power (MWt)	Critical Rod Group Position	PDQ k_{eff}	k_{eff} corrected for rod position
0	0	42351 at 0", 5 at 51"	.9886	.9894
1900	392	51 at 0", 3 at 26"	.9947	.9925
2700	392	51 at 0", 3 at 47"	.9999	.9988
4000	485	1 at 0", 5 at 24"	1.0021	1.0001
5100	392	1 at 0", 5 at 53"	1.0041	1.0052
6300	485	1 at 0", 5 at 90"	.9992	1.0024
8000	392	OUT	1.0088	1.0088

Because of mesh spacing restrictions it was not always possible to locate the controlling rod group in the calculations exactly at the critical position. The k_{eff} values obtained from PDQ were therefore corrected to the critical controlling rod group height by using a measured differential control rod worth. The corrected k_{eff} values are also shown in Table 3.13. These values of k_{eff} are plotted in Figure 3.25 as a function of MWD/Tonne. The agreement is good over the entire range of rod removal. The underestimate in the calculated excess reactivity of the hot, zero power undepleted core is evident. The underestimate in the calculated reactivity loss rate with burnup,

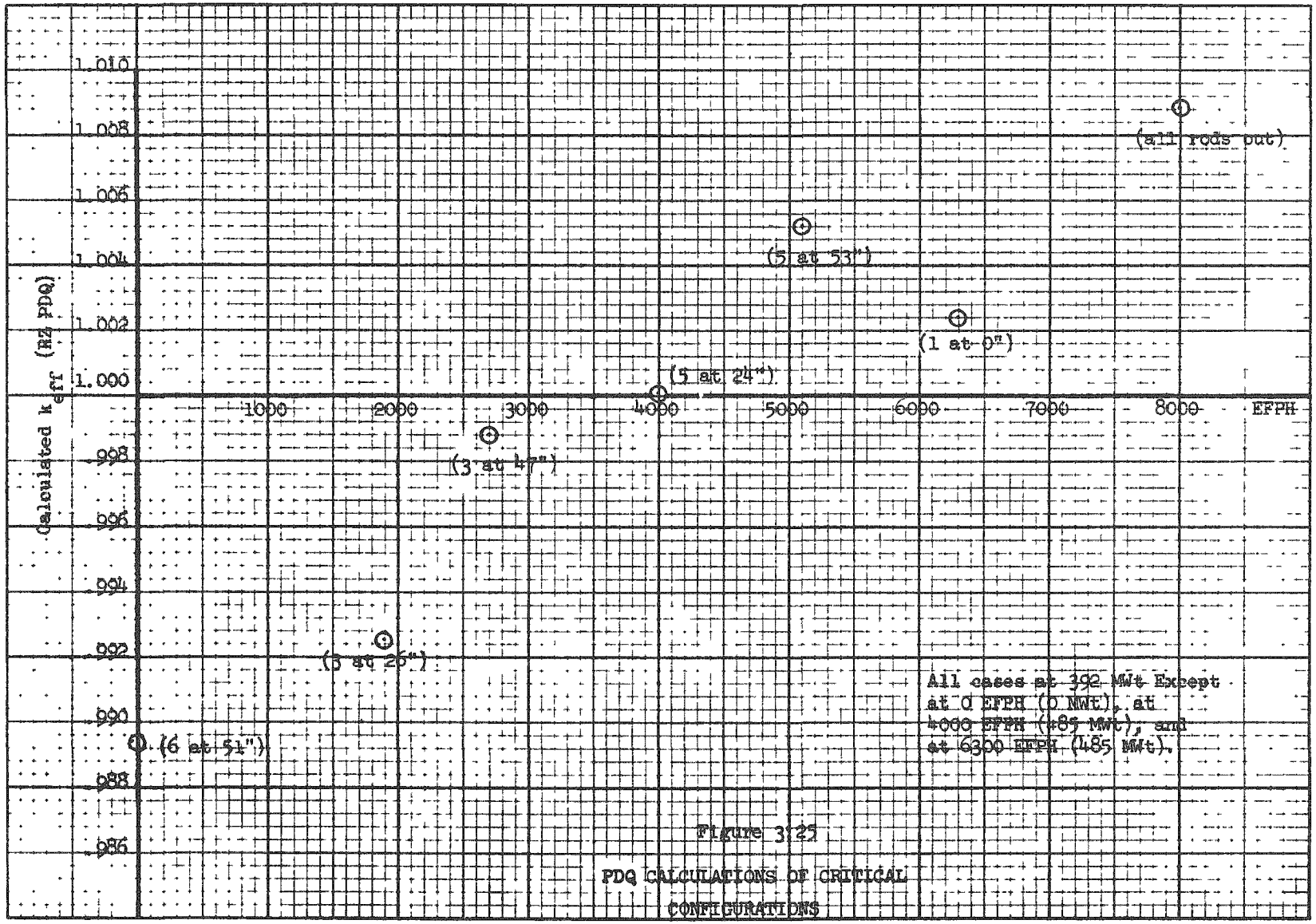

Figure 3.2.3

PDQ CALCULATIONS OF CRITICAL CONFIGURATIONS

which results from the use of a low lumped fission product cross section, is also seen. The agreement between experiment and calculations indicates that control rod worths are well predicted by the model.

3.8 Xe-135 Poisoning

Poisoning of the core by the fission product Xe-135 gives rise to a loss of about 2% to 2.5% in reactivity in Yankee. This reactivity loss accounts for about 25% of the total reactivity loss during operation at power throughout core life. Accurate prediction of the reactivity tied up in Xe-135 is therefore of significant importance in attempting to calculate core lifetime.

Calculations were performed of equilibrium and transient Xe-135 poisoning and compared with experimental data. The effects of fuel depletion on Xe-135 poisoning were evaluated. An analysis was performed of statistical weight effects under steady state and transient conditions. Xenon oscillations were not predicted and have not occurred during Core I operation.

To facilitate the calculation of Xe-135 poisoning with time, a transient code, called HISTORIAN, was programmed for the IBM-7090 computer. The program solves the time and flux dependent differential equations for the concentrations of I-135 and Xe-135 in the core. A power history consisting of step functions in the power level are input to the code. The calculational model is based on two-energy group constants. The program allows for fissions in the isotopes U-235, U-238, Pu-239, Pu-240 and Pu-241. The output consists of a tabulation of I-135 and Xe-135 atom concentrations and the reactivity tied up in Xe-135 as a function of time. The HISTORIAN program solves the space-independent I-135 and Xe-135 equations and therefore it does not take account of non-uniform distribution effects. Provision is made for a statistical weight factor to be input to HISTORIAN; however, this statistical weight is assumed constant in time.

In order to evaluate the effect on Xe-135 poisoning of the non-uniform spatial distribution of I-135, Xe-135 and fluxes, calculations of Xe-135 transients were also performed with the CANDLE II one-dimensional depletion code using very short time steps. A perturbation theory analysis of statistical weight factor based on in-core instrumentation data was also performed.

3.8.1 Variation of Equilibrium and Peak Xe-135 Poisoning with Burnup

The HISTORIAN code was used to calculate the variation in equilibrium and peak Xe-135 poisoning with lifetime. The results are plotted in Figure 3.26. The calculation used a unity statistical weight factor. The decrease in Xe-135 poisoning with burnup is due to the use of a fission yield for Pu-235 fission [27,28] which is lower than that for U-235 fissions (0.060 versus 0.063 total yield), and to the increase in thermal absorption of the core with burnup.

Due to the high reactivity worth of Xe-135, no direct measurements of equilibrium poisoning are possible. Measurements of Xe-135 poisoning in Yankee have consisted of differential Xe-135 worth during the Xe-135 transient after a shutdown. Power reduction at the various shutdowns have not occurred rapidly, but have taken place during periods of up to one hour. The first data point was usually obtained one-half to one hour after shutdown. It is therefore difficult to directly derive an equilibrium poisoning from the data during the transient. However good experimental values have been obtained for the peak poisoning after shutdown. These values and their statistical errors were obtained from a statistical fit to the Xe-135 decay curve from the peak to about 18 hours after the peak. Table 3.14 lists the experimental values of peak Xe-135 poisoning obtained in this manner, compared with calculated values.

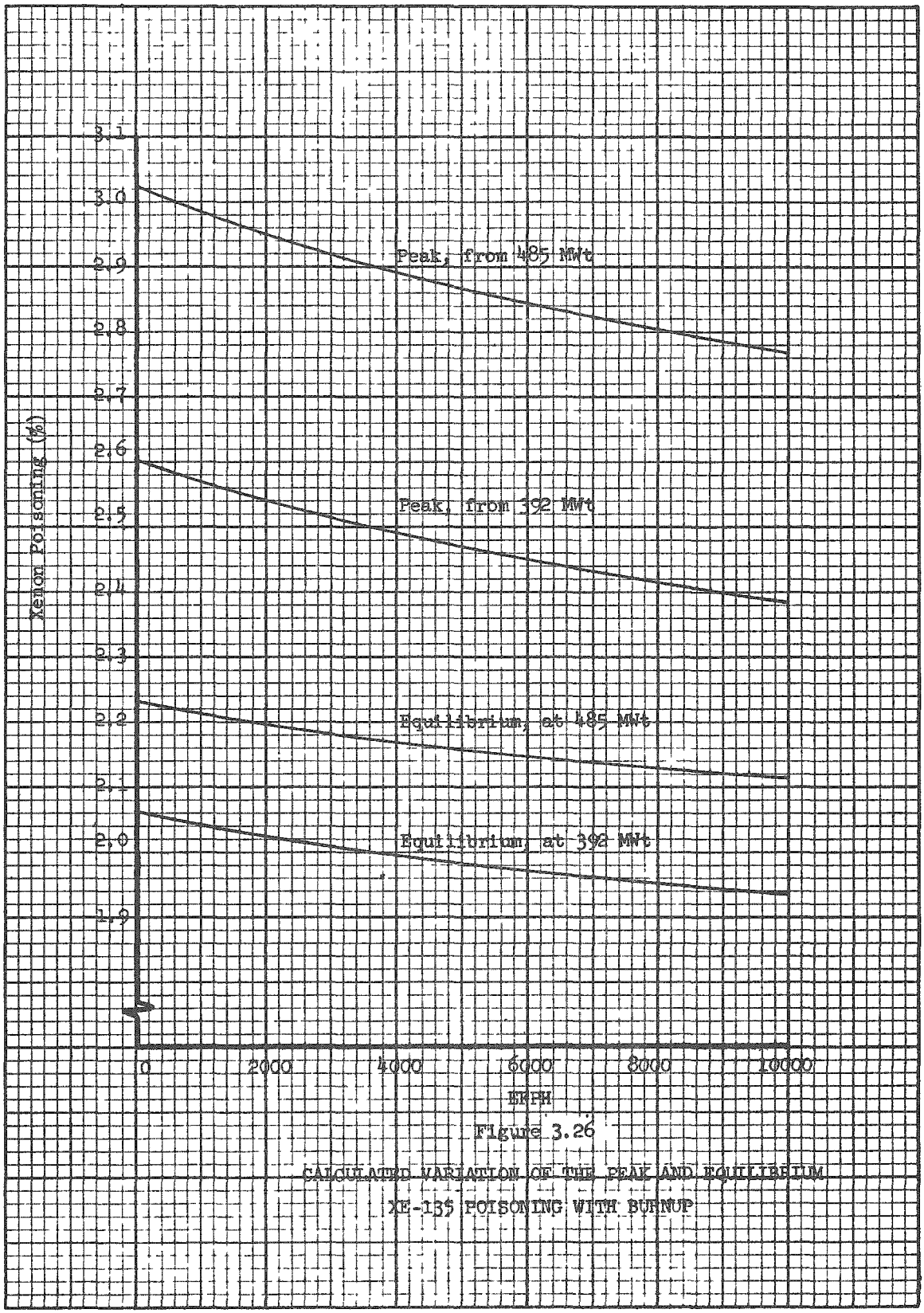

Figure 3.26

CALCULATED VARIATION OF THE PEAK AND EQUILIBRIUM XE-135 POISONING WITH BURNUP

Table 3.14

Calculated and Measured Peak Xe-135 Poisoning

EFPH	Power Before Shutdown (MWt)	Peak ρ^{Xe} (%) Measured	Calculated (HISTORIAN)	Calculated (CANDLE)
2000	392	3.21 ± .08	2.55	-
4000	485	3.50 ± .05	2.90	3.40
6400	385	3.00 ± .30	2.44	-
10,700	262	2.40 ± .04	1.85	-

It is noted that the point model calculations (HISTORIAN) underestimate peak xenon poisoning by as much as 20%. However, a spherical CANDLE calculation performed at 4000 EFPH agrees very well with experiment. This led to the conclusion that the underestimate in peak Xe-135 poisoning by HISTORIAN was due to the assumption of uniform (flat) power and Xe-135 distributions, that is, of a constant unity statistical weight factor. This is demonstrated in Figure 3.27 which shows a comparison of the measured and calculated (HISTORIAN and CANDLE) Xe-135 transient after the 4000 EFPH shutdown from 485 MWt. The HISTORIAN calculation uses a statistical weight factor of 1.00. The CANDLE calculation was performed with very short time steps. Both calculations assumed a step decrease in power from 485 to 0 MWt. The underestimate in the peak poisoning and the return time by the point model HISTORIAN calculation is evident. However, the CANDLE calculation agrees quite well with experiment. It is noted that, although the HISTORIAN and CANDLE transients are quite different, both calculations predict about the same equilibrium poisoning. This means that the statistical weight factor on Xe-135 poisoning is close to unity at equilibrium and increases during the transient after shutdown. This is further examined in the next section. Based on the

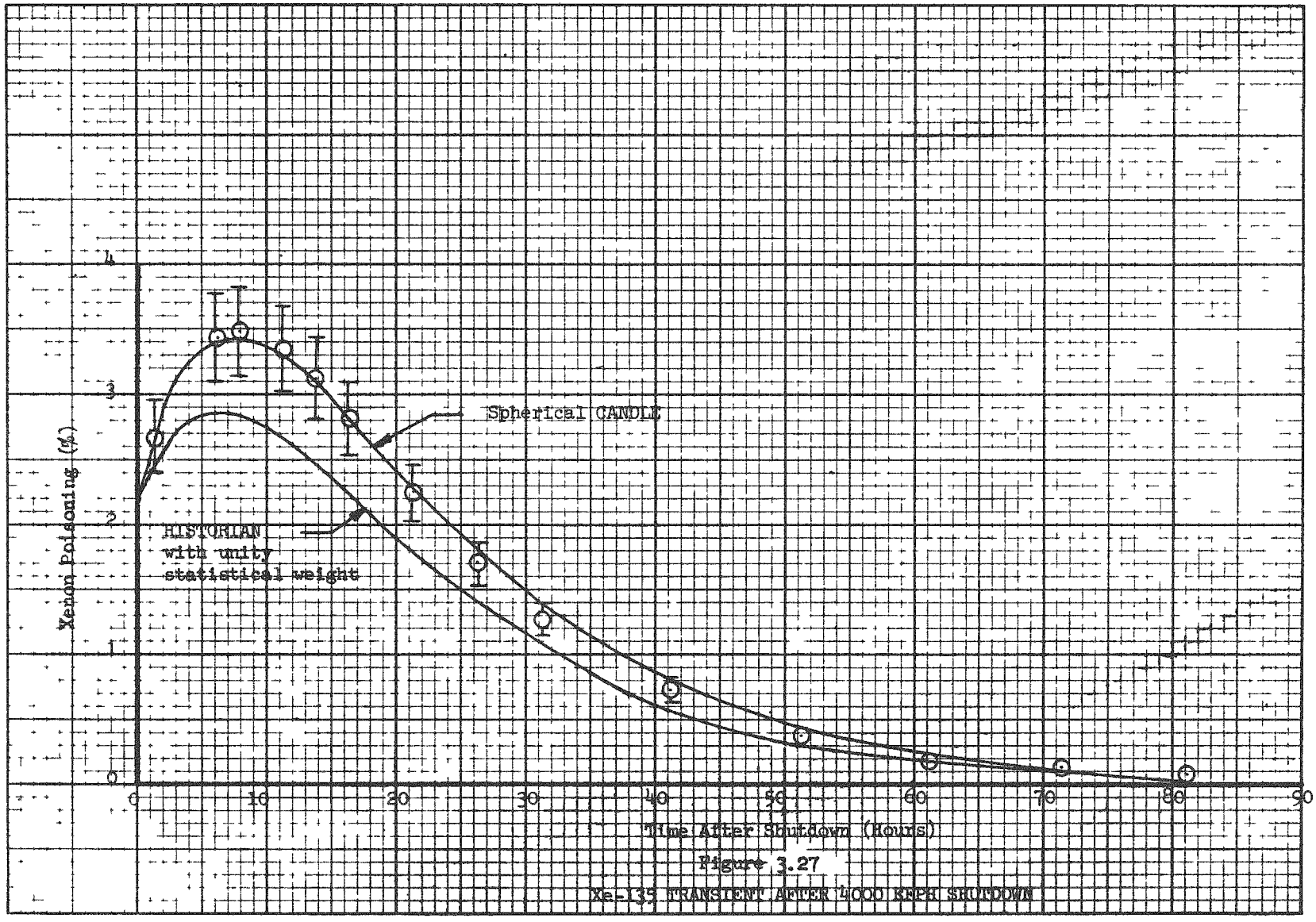

Figure 3.27

Xe-135 TRANSIENT AFTER 4000 KEPH SHUTDOWN

good agreement of the CANDLE calculation with experiment, and the agreement of CANDLE and HISTORIAN at equilibrium, it can be assumed that the equilibrium Xe-135 poisoning calculated by HISTORIAN and shown in Figure 3.26 represent to a good accuracy the actual equilibrium poisoning in Yankee.

3.8.2 Statistical Weight Factor on Xe-135 Equilibrium and Transient Poisoning

A two-group perturbation theory analysis of the statistical factor on equilibrium Xe-135 poisoning was performed based on in-core instrumentation data. The analysis was similar to that performed on the power defect and described in section 3.4.3. Equilibrium Xe-135 produces a change in the core thermal absorption in the form

$$\delta\Sigma_{a_2}(\bar{r}) = \frac{a(\bar{r})\,\phi_1(\bar{r}) + b(\bar{r})\,\phi_2(\bar{r})}{\frac{\lambda_x}{\sigma^x_{a_2}} + \phi_2(\bar{r})} \tag{3.22}$$

where

$$a(\bar{r}) = \sum_j \Sigma_{f_1}^j(\bar{r})\, y^j \tag{3.23}$$

$$b(\bar{r}) = \sum_j \Sigma_{f_2}^j(\bar{r})\, y^j \tag{3.24}$$

and j includes all the fissionable isotopes. The statistical weight factor on equilibrium Xe-135 poisoning is given by

$$W^{Xe} = \frac{\int \frac{\phi(\bar{r})\,\kappa(\bar{r}) + b(\bar{r})}{\frac{\lambda_x}{\sigma^x_{a_2} P_{Avg}} + I^x(\bar{r})}\, I^{x^3}(\bar{r})\, dV}{\frac{\bar{\phi}\,\bar{\kappa} + \bar{b}}{\bar{N}} \int \frac{1}{\frac{\lambda_x \bar{\epsilon}}{\sigma^x_{a_2} P_{Avg}} + 1} N(\bar{r})\, I^{x^2}(\bar{r})\, dV} \tag{3.25}$$

where

$$I^{x}(\bar{r}) = \frac{\dfrac{I(\bar{r})}{\xi(\bar{r})}}{\dfrac{1}{V}\displaystyle\int \frac{I(\bar{r})\,\epsilon(\bar{r})}{\xi(\bar{r})}\,dV} \qquad (3.26)$$

$I(\bar{r})$ is the flux wire activation in arbitrary units. The parameters κ, N, ϵ, and ξ are functions of burnup and therefore position in the core. The derivation of equation (3.25) can be found in the Appendix. The calculations implied by equation (3.25) were programmed as an additional option in the YADAR in-core instrumentation data reducing code.

The statistical weight factors on equilibrium Xe-135 poisoning are plotted in Figure 3.28 as a function of control rod removal for the programmed withdrawal sequence for an average power level of 392 MWt. The calculations predict a statistical weight factor on equilibrium Xe-135 poisoning which is very close to unity, with almost no variation as a result of control rod motion. The effect of non-uniform burnup is to reduce the statistical weight factor to unity. This effect may be attributed to the high burnup in regions of high flux and therefore high neutron importance. The reduced Xe-135 yield for Pu fissions and the reduced thermal flux relative to less depleted regions tend to counterbalance the neutron importance. The spherical CANDLE calculation described in section 3.8.1 predicted a statistical weight factor of 1.03.

Equation (3.25) reveals that the statistical weight factor on equilibrium Xe-135 poisoning is a function of the average core power. Figure 3.29 shows the variation of the statistical weight factor with average power level for three control rod configurations. The statistical weight factor is a sensitive function of power at low power levels. However, because of saturation of the Xe-135 equilibrium concentration, the effect of power on the statistical weight factors becomes negligible at high power levels.

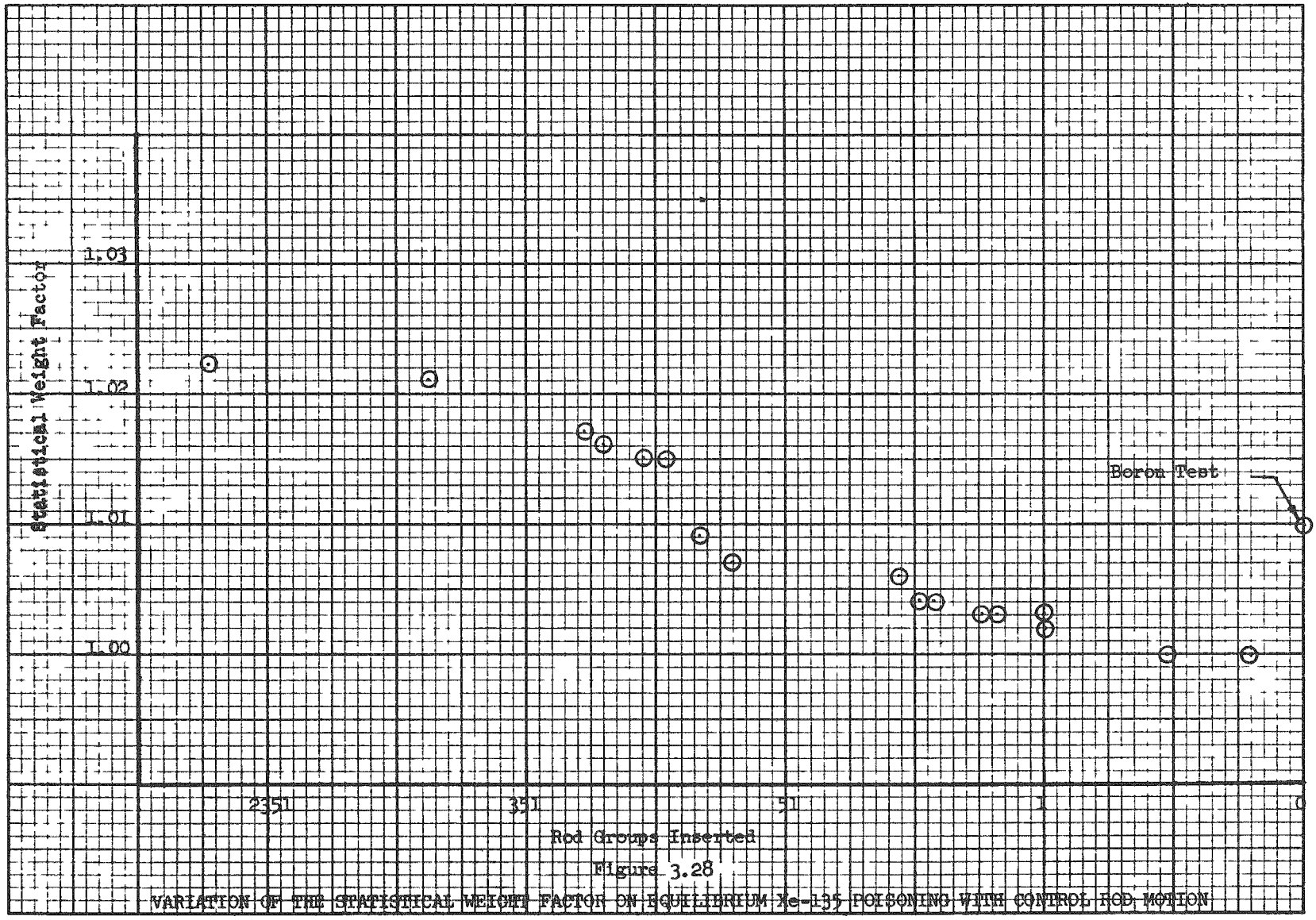

Figure 3.28

VARIATION OF THE STATISTICAL WEIGHT FACTOR ON EQUILIBRIUM Xe-135 POISONING WITH CONTROL ROD MOTION

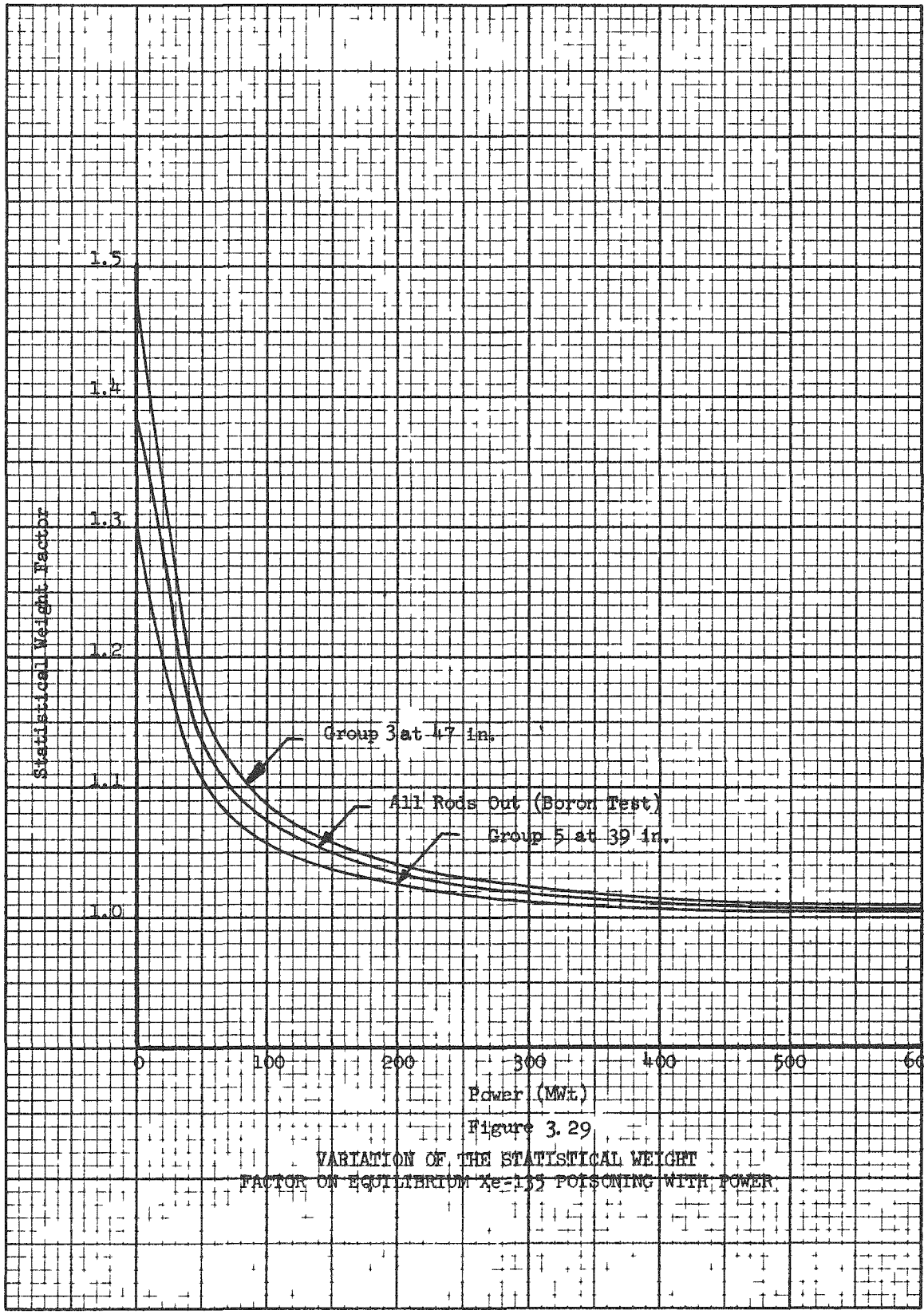

Figure 3.29

VARIATION OF THE STATISTICAL WEIGHT FACTOR ON EQUILIBRIUM Xe-135 POISONING WITH POWER

In order to evaluate the time dependence of the statistical weight factor during non-equilibrium conditions, non-uniform calculations of Xe-135 transients were performed with the CANDLE II code using very short time steps. Figure 3.27 showed the Xe-135 transient after the 4000 EFPH shutdown calculated by CANDLE in spherical geometry and by HISTORIAN. Figure 3.30 shows the variation in the statistical weight factor (defined as the ratio of reactivity calculated with a non-uniform model (CANDLE) to that calculated with a uniform model (HISTORIAN))with time. For comparison, the ratios of the measured Xe-135 poisoning to that calculated by HISTORIAN (with statistical weight unity) are also plotted on Figure 3.30. The statistical weight factor is seen to increase with time from a low value at time zero to a value of about 1.5 at the end of the transient. The calculated and the measured variation of the statistical weight factor agree quite well between about 2 hours and 16 hours after the shutdown.

Axial and radial CANDLE calculations with very short time steps were performed to study the time variation of the statistical weight factor during buildup of Xe-135 from zero at an average burnup of 4000 EFPH. The power history consisted of a step increase from 0 MWt to 485 MWt. Control in the CANDLE calculation was achieved by means of a uniform poison. The Xe-135 reactivity worth was obtained from the variation of the eigenvalue with time. A correction for Sm-149 buildup and fuel depletion was made by calculating the Sm-149 transient for a uniform power distribution and the reactivity loss in depletion using a burnup coefficient of $-.783 \times 10^{-5} \Delta\rho$/EFPH. (The maximum correction was 0.08% $\Delta\rho$ at 50 hours, which is only 3% of the equilibrium xenon worth). Figure 3.31 shows the statistical weight factor plotted against time after startup. The statistical weight factor on Xe is seen to vary with time, but it reaches a constant value after about 15 to 20 hours from startup. Because CANDLE carries out a one-dimensional calculation and because the effect

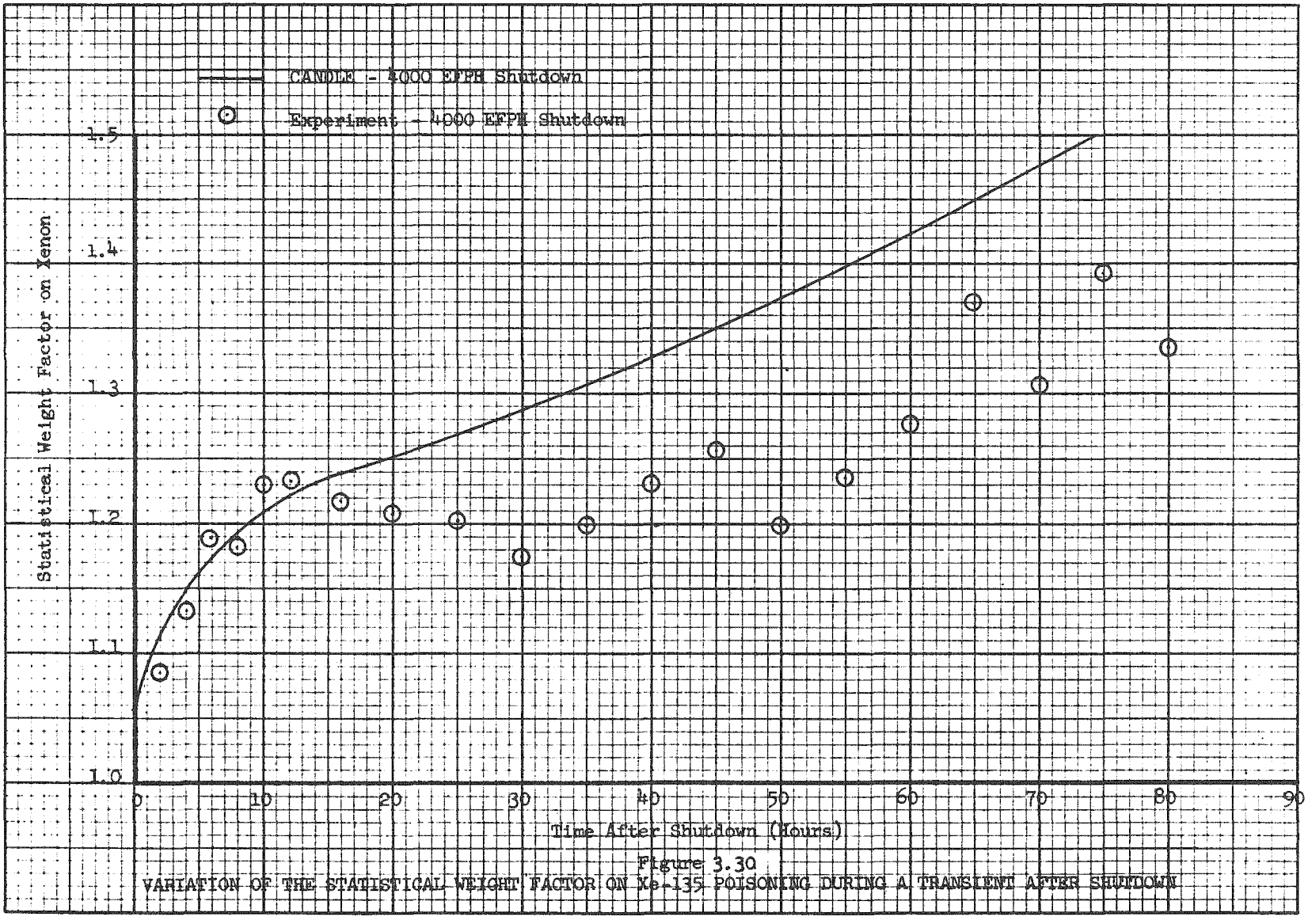

Figure 3.30
VARIATION OF THE STATISTICAL WEIGHT FACTOR ON Xe-135 POISONING DURING A TRANSIENT AFTER SHUTDOWN

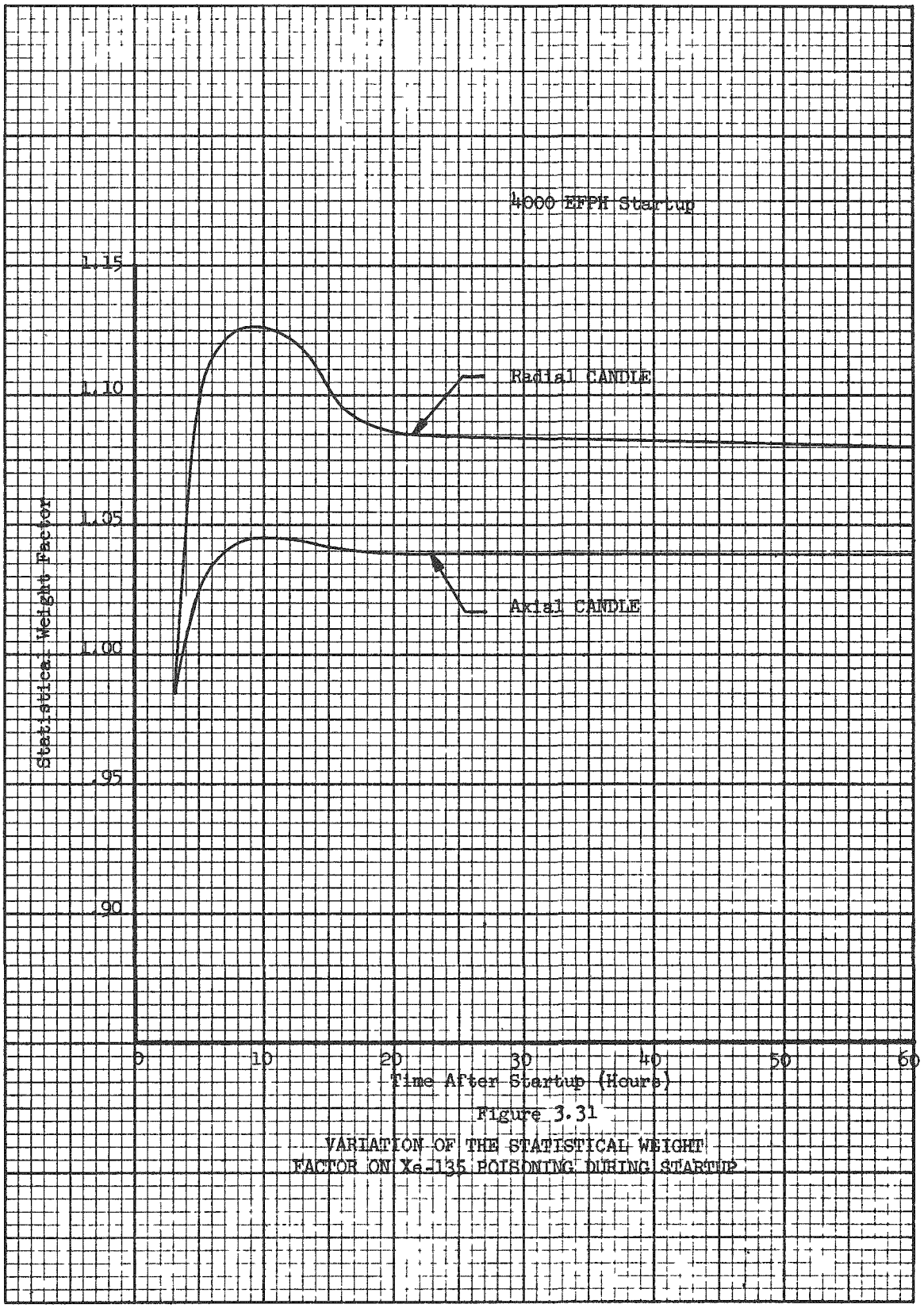

Figure 3.31

VARIATION OF THE STATISTICAL WEIGHT FACTOR ON Xe-135 POISONING DURING STARTUP

of control rods on power distribution and Xe distribution were not accounted for, these magnitudes may be different in a three-dimensional analysis. No account has been taken of the local Xe distribution in a fuel assembly. However, the variation in time of the statistical weight factor is probably qualitatively represented by the one-dimensional calculations. In conclusion, it appears that a uniform or point model for Xe-135 poisoning is adequate for the calculation of equilibrium Xe-135 poisoning, but the model will tend to underestimate transient poisoning because of variations in the statistical weight factor.

Figure 3.28 showed that rod configuration, or power distribution, had little effect on the equilibrium Xe-135 poisoning. However, with Xe-135 initially at equilibrium, a sudden change in the power distribution may cause a transient change in the Xe-135 reactivity effect until a new Xe-135 equilibrium distribution has been achieved. A significant removal of control rods from the core over a short period of time took place during boration at power on September 13, 1961. Prior to boration, group 1 was fully inserted and group 5 was at 46 in. Six hours later with 390 ppm boron in the coolant, group 5 was fully removed and group 1 was at 59 in. Group 1 was fully removed 36 hours later. Two-dimensional RZ PDQ calculations were performed in an effort to determine any change in Xe-135 reactivity worth which might result from the removal of the control rods from the core. The core was divided into 16 regions and the average burnup in each region was obtained from in-core instrumentation data. Two PDQ calculations were first performed at a zero power with no Xe-135 and no Sm-149. One problem had group 1 fully inserted and group 5 at 40 in. The other problem had 420 ppm boron with all rods removed. The power distributions obtained from these problems were subsequently used to determine the distribution of Xe-135 in the core. Three PDQ calculations at 392 MWt with non-uniform Xe-135 distributions were then carried out. The first calculation had group 1 fully inserted and group 5 at 40 in.

with the corresponding equilibrium Xe-135 distribution. The second calculation had 420 ppm boron with all rods removed, but with the Xe-135 distribution corresponding to the power distribution of the rodded core. This represents the conditions in the core right after a rapid removal of groups 1 and 5. The third calculation had 420 ppm boron with all rods removed and with the Xe-135 distribution corresponding to the unrodded power distribution. This represents the conditions in the core after boration, after Xe-135 has redistributed. Xe-135 was distributed in the core by adding to the thermal macroscopic cross section of each region a Xe-135 absorption cross section calculated according to equation (3.22).

Table 3.15 summarizes the results of the calculations. The variation in Xe-135 poisoning after removal of the control rod is small. The insensitivity of the equilibrium poisoning to the control configuration agrees with the perturbation theory calculations of Figure 3.28.

Table 3.15

Xe-135 Poisoning at 392 MWt Before and After Boration at Power

Core Condition	Xe-135 Poisoning (%)
0 ppm, 5 at 50, 1 in, equilibrium Xe distribution	- 2.09
420 ppm, all rods out, right after removal of the rods	- 2.06
420 ppm, all rods out, equilibrium Xe distribution	- 2.10

3.9 Sm-149 Poisoning

The calculation of Sm-149 transients has been programmed for the HISTORIAN code described in section 3.8. Because of the relatively long half life of Pm-149, Sm-149 transients are slow and the variations in reactivity due to Sm-149 poisoning with time are small. Measurements of Sm-149 poisoning are therefore very difficult since one cannot readily differentiate between Sm-149 poisoning and other slow reactivity mechanisms such as burnup and changes in statistical weight factors.

Figure 3.32 shows the variation in equilibrium and peak Sm-149 poisoning with burnup, calculated by HISTORIAN. The increase in Sm-149 poisoning with burnup is due to the high value of the Pm-149 yield for Pu-239 fission relative to that for U-235 fission (0.0113 versus 0.0189)[28,29]. An approximate measured value of peak Sm-149 early in core lifetime, based on operating data up to 50% equilibrium, has been published as 0.9% [30].

Figure 3.33 shows the calculated Sm-149 reactivity transient based on the actual power history between June 28, 1961 and August 22, 1961. On July 9, the plant was shut down for the scheduled 4000 EFPH shutdown. Reactor startup was initiated on July 23.

3.10 Fission Product Transients

The fission products which are usually considered explicitly in reactivity variation calculations are Xe-135 and Sm-149. After a prolonged shutdown Xe-135 eventually decays to zero and Sm-149 builds up to a peak because of the decay of Pm-149. However, other highly-absorbing fission products are produced by decay from a parent nuclide and in a high-flux reactor they may result in a significant poisoning effect. The fission product chains were studied in order to determine fission products with sufficiently high absorption cross sections and fission yields to cause significant reactivity variations. Eleven mass chains (mass numbers 83, 99, 103, 105, 113, 131, 143, 147, 151, 155, 157) were chosen for detailed analysis of their poisoning effect during the 4000 EFPH shutdown. These chains were chosen on the basis of high neutron absorption cross section,

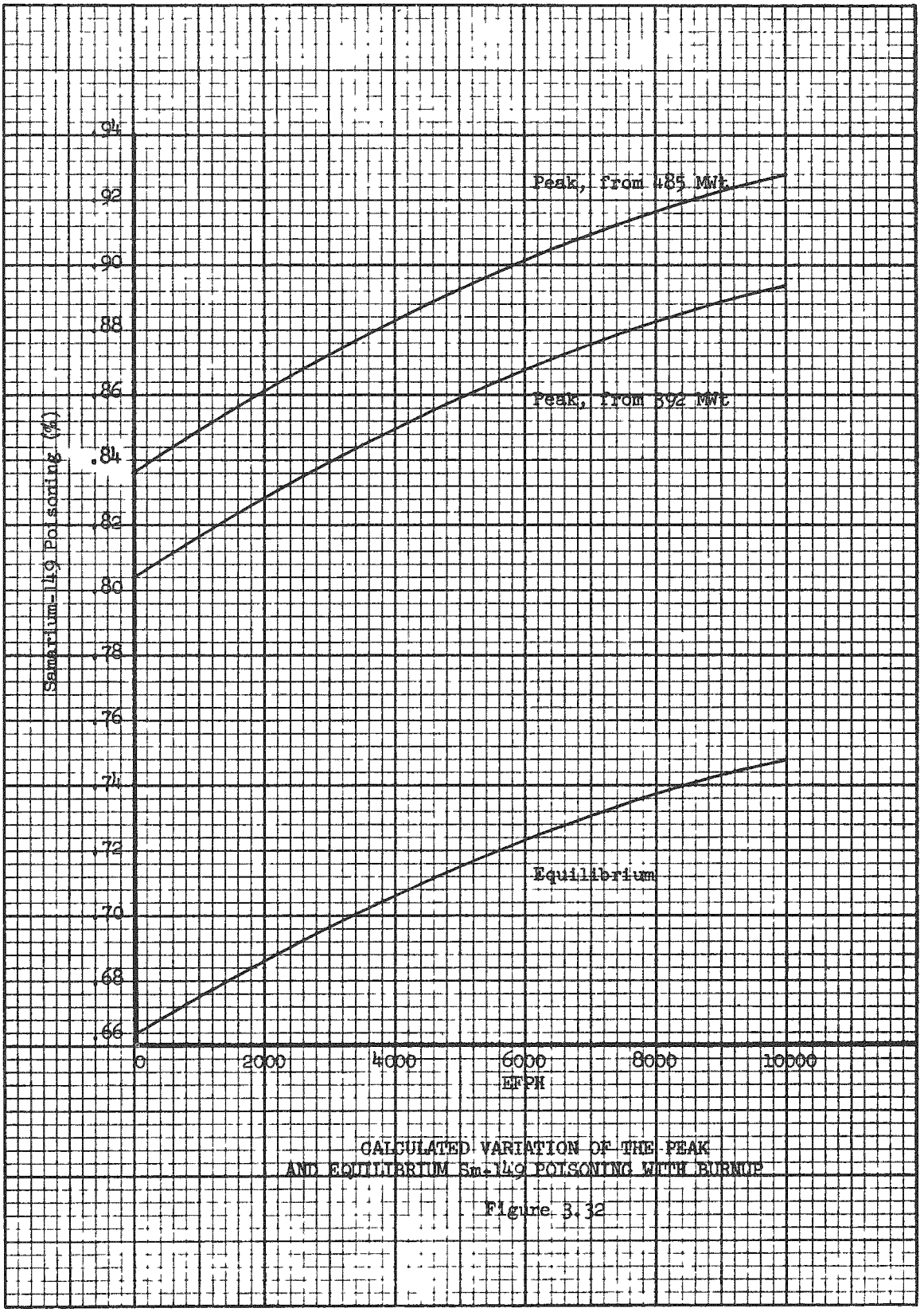

CALCULATED VARIATION OF THE PEAK AND EQUILIBRIUM Sm-149 POISONING WITH BURNUP

Figure 3.32

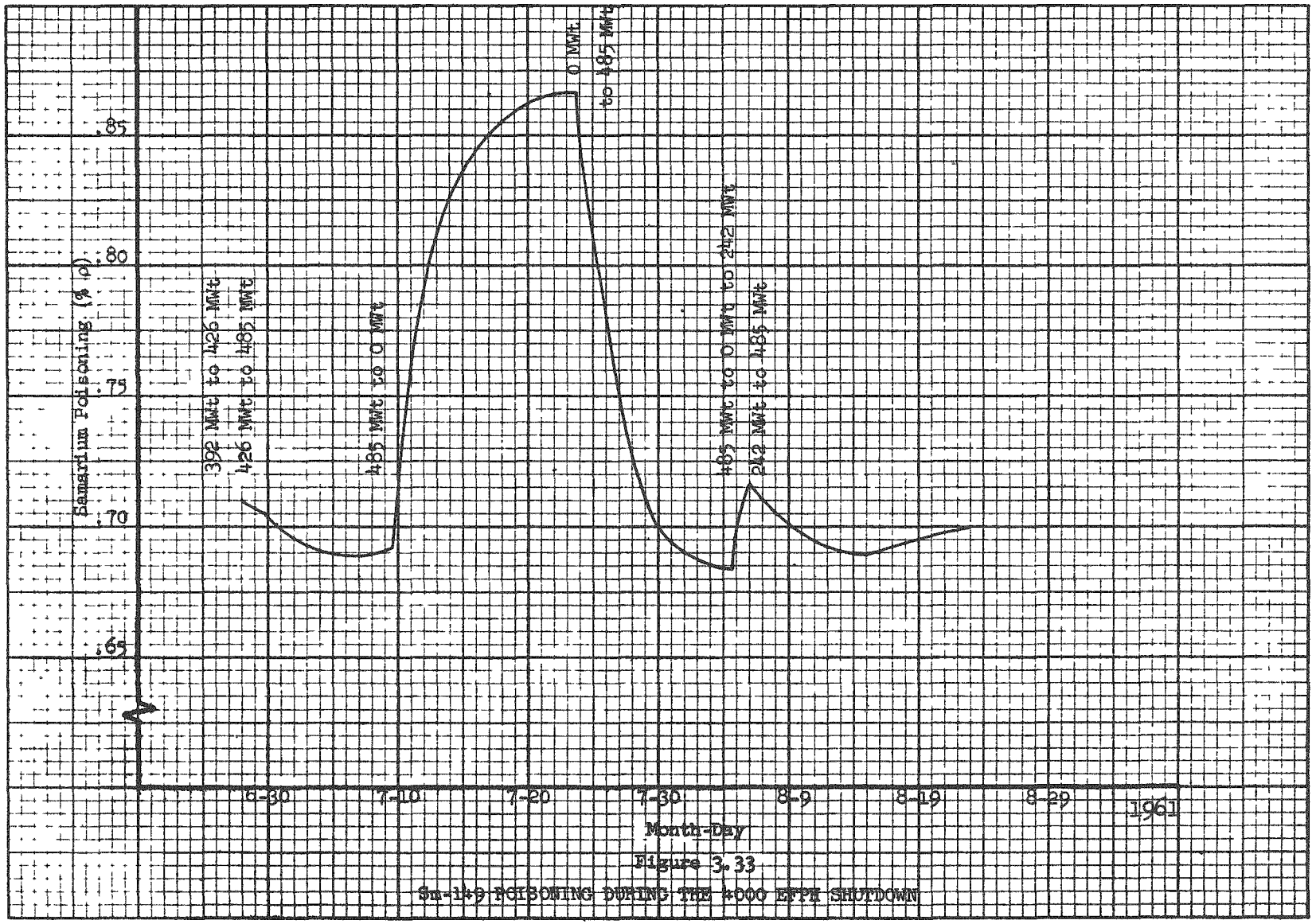

Figure 3.33

Sm-149 POISONING DURING THE 4000 EFPH SHUTDOWN

significant fission yield, and a half life of the order of one hour to 40 days. The differential equations which describe the time behavior of the members of the fission product chains given above are, to a good approximation, similar in form to either the Pm-149 - Sm-149 equations or the I-135 - Xe-135 equations. The HISTORIAN code described in section 3.8 was therefore used to calculate the poisoning effect of these fission product chains by inputting to the code the fission yields, absorption cross sections and half lifes appropriate to each chain. Fission yield, absorption cross section and half life data were taken from references 27, 28, 29, 31, 32 and 25. The calculations were performed for the period between June 28, 1961 and August 28, 1961. Reactor shutdown occurred on July 9 with subsequent startup on July 23. Table 3.16 gives the results in terms of the poisoning previous to shutdown, the peak poisoning after shutdown, and the minimum poisoning after the return to power. Of the 11 chains, only chain numbers 113, 151, and 157 were in equilibrium at the time of the shutdown so that only these chain numbers went through a minimum poisoning upon returning to power.

The reactivity variations shown in Table 3.16 are very small. The total increase during the shutdown in poisoning effect of these 11 chains is 5×10^{-4} ρ. This compares to an increase of 18×10^{-4} ρ in Sm-149 poisoning during the shutdown.

It is observed that the reactivity tied up in Sm-151 is 0.33% $\Delta\rho$ which is almost half the reactivity tied up in Sm-149. Although the variation of the Sm-151 concentration during a shutdown is negligible, the initial buildup of Sm-151 at beginning of life should be considered together with the buildup of Sm-149. The buildup of Sm-151 during a shutdown may become important at higher power levels, since the increase in atom concentration is directly proportional to the power level.

Table 3.16

Reactivity Variations of 11 Fission Product Chains

At the Time of the 4000 EFPH Shutdown

Fission Product	Poisoning Before Shutdown (% ρ)	Peak Poisoning After Shutdown (% ρ)	Minimum Poisoning After Startup (% ρ)
Kr^{83}	.0112	.0113	-----
Tc^{99}	.0380	.0390	-----
Rh^{103}	.1430	.1521	-----
Rh^{105}	.0840	-----	-----
Cd^{113} *	.0116	.0117	.0116
Xe^{131}	.0982	.1065	-----
Nd^{143}	.1530	.1639	-----
Pm^{147}	.2089	.2209	-----
Sm^{151} *	.3308	.3363	.3296
Eu^{155}	.0269	-----	-----
Cd^{157} *	.0100	.0122	.0098

*In equilibrium before shutdown.

3.11 Np^{239} - Pu^{239} Transient

Pu-239 is formed as a result of neutron absorption in U-238 according to the reaction

$$\text{U-238} + n \longrightarrow \text{U-239 (2.35 m)} \longrightarrow \text{Np-239 (2.35 d)} \longrightarrow \text{Pu-239} \tag{3.27}$$

If the short-lived U-239 is neglected, the equations which describe the reactions in (3.27) are:

$$\frac{dN}{dt} = (\phi_1 \Sigma a_1^{28} + \phi_2 \Sigma a_2^{28}) - \lambda N \tag{3.28}$$

$$\frac{dP}{dt} = \lambda N - (\phi_1 \sigma a_1^{49} + \phi_2 \sigma a_2^{49}) P \tag{3.29}$$

where N is the Np-239 atom concentration and P is the Pu-239 atom concentration. The absorption in Np-239 is very small. In equations (3.28) and (3.29) resonance absorption in U-238 and in Pu-239 is represented by equivalent fast-group absorption cross sections.

In depletion calculations [20,21] one usually neglects the production and decay of Np-239 and assumes that Pu-239 is formed directly by neutron capture in U-238. However, during a reactor shutdown, the Np-239 will decay into Pu-239 with an accompanying increase in core reactivity.

The set of equations (3.28) and (3.29) is similar in form to the Pm-149 - Sm-149 equations. Their solution was obtained with the HISTORIAN code for the period following the shutdowns on July 9, 1961 (4000 EFPH) and November 2, 1961 (6400 EFPH). Figure 3.34 shows the variation in Np-239 and Pu-239 concentration during and after the 4000 EFPH shutdown. The Pu-239 concentration increased by 3.5% during the shutdown. The increase in Pu-239 concentration during the shutdowns results in a higher core reactivity at

Figure 3.34

Np-239 - Pu-239 TRANSIENT DURING THE 4000 EFPH SHUTDOWN

startup. The increase in Pu-239 concentration during shutdown is equivalent to a gain in reactivity of about 0.1% ρ at 4000 EFPH and 0.05% ρ at 6400 EFPH. This effect balances in part the increased poisoning effect of Sm-149 and fission products during shutdown.

3.12 Effect of the Non-Uniform Moderator Temperature Distribution on Core Reactivity

Most reactivity calculations assume a uniform moderator temperature distribution. However for operation at power, some core regions may have moderator temperatures which are significantly different from the average moderator temperature. Differences of the order of 20-25°F are very likely. With a temperature coefficient at power of about 2×10^{-4}/°F, this is equivalent to a 0.4% to 0.5% reactivity difference between these regions. A change in power distribution as a result of control rod removal or insertion will cause a redistribution in moderator temperature which may give rise to a change in core reactivity. RZ PDQ calculations of this effect were performed for the power distribution change which occurred during the boron test at power as a result of the removal of the control rods. The two cores analyzed were the core with rod group 1 inserted and rod group 5 at 50", and the core with all rods removed. Both cores were at 392 MWt at an average burnup of 5100 EFPH and no boron. The burnup was non-uniformly distributed in the calculation. The first set of problems assumed a uniform moderator temperature distribution. The power distributions from these problems were used to calculate the enthalpies and moderator temperatures for each core region for the two cores. A second set of problems was run with the calculated moderator temperature distributions. For the rodded core the core reactivity obtained with the non-uniform moderator temperature distribution was 0.03% lower than that obtained with the uniform distribution. The difference in core reactivity for the unrodded core was 0.14%. These calculations therefore indicate a drop in core reactivity of 0.11% due to the change in moderator temperature distribution caused by the removal of rod groups 5 and 1. This effect may explain in part the loss in reactivity which occurred during the boron test at power (see section 2.3).

3.13 Plate-Out on Fuel Rods

It is impossible to know conclusively whether plate-out on the Yankee fuel rods occurred during Core I operation, causing a reduction in core reactivity. However, it is instructive to compute the amount of plating needed to cause a given loss in reactivity. Elements most likely to plate-out and cause a significant reduction in reactivity are boron, after the core has been borated, and silver, indium, or cadmium released from the control rods by corrosion or erosion. A calculation was made of the amount of these elements needed to cause a 0.5% loss in reactivity.

The assumptions were made that the poison material was uniformly plated on the clad of all UO_2 rods in the core and that the plating was thin enough that no self-shielding effect existed. The calculations were performed for a depleted core with an average burnup of 4000 EFPH. The boron plating was obtained by two different techniques. The first calculation used a measured boron worth. A thermal disadvantage factor was used to account for the different thermal fluxes in the moderator and at the surface of the clad. The second technique was based on a calculated boron worth. The boron was homogenized in the core and thermal disadvantage factors were used to account for the dip in the flux in the fuel and the peak in the flux in the water moderator. This later technique underestimates boron worth by about 6% such that it calculates a boron plating somewhat higher than that obtained with the first technique. The second method of calculation was also used for Ag, In, and Cd. About 90% of the reactivity effect of Ag and In is due to the epithermal resonances of these elements. The epithermal effect on core reactivity of these elements was obtained by calculating a resonance escape probability using the resonance integrals for dilute solutions. Recent measurements [33] of the resonance integrals for dilute solutions give values of 841 barns and 3700 barns for Ag and In respectively. The measured resonance integral for boron is 280 barns.

Table 3.17 shows the results of the calculations.

Table 3.17

Calculated Plate-Out on Fuel Rods Required to Cause a 0.5% Drop in Reactivity

Element	Total Volume (cm^3)	Total Mass (gm)	Plating (mg/dm^2)	Thickness of Plating (10^{-6} cm)
B (amorphous state)	98.8	231	1.56	6.7
(crystal state)	69.4			4.7
Ag	340.6	3576	24.21	23.0
In	120.9	880	5.96	8.2
Cd	42.7	369	2.50	2.9
Control Rod (80% Ag - 15% In - 5% Cd)		1889	12.78	

The numbers in Table 3.17 refer to a 0.5% drop in reactivity for each poison material separately. The plating of control rod material assumes that the silver, indium, and cadmium released from the control rods and plated on the fuel remained in the ratio 80%-15%-5%. The release of the amount of boron given in Table 3.17 to the core water volume is equivalent to only 3.2 ppm in the primary loop. No statistical weight factor has been used in calculating the plating in Table 3.17. A higher concentration of plate-out on fuel rods located in the center of the core or in regions of high neutron importance would result in a greater loss in reactivity. A number of mechanisms of plate-out have been examined, but none have been found capable of providing plate-out to the extent calculated above, without improbable assumptions.

4.0 SUMMARY AND CONCLUSIONS

The reactivity characteristics of the Yankee Reactor Core I have been measured during operation of the core at power. An extensive analytical physics program, carried under the joint Yankee-Westinghouse Core I Follow Program, complemented the physics measurements. In addition to allowing a partial evaluation of the calculational methods through a comparison of calculated results and measured results, the program has led to a more thorough understanding of the reactivity characteristics of pressurized water, low enrichment UO_2-stainless steel power reactors. The excellent operating characteristics of the core have verified the technical feasibility and economic potential of this type of reactor, in addition to confirming the design predictions.

Although the Yankee plant was designed as a commercial operating plant, a large amount of valuable experimental data was obtained throughout core lifetime. The agreement between calculations and experiments was generally very good. In particular, the adequacy and usefulness of the MUFT-SOFOCATE-PDQ (or CANDLE) scheme for reactivity calculations was apparent. In instances where discrepancies existed, analyses have led to revisions or improvements of some of the analytical methods and/or the basic nuclear data. Further examination and evaluation of the spent core under the AEC sponsored Yankee Core Evaluation Program will provide very useful information that will extend the analyses given in this report and will provide further bases for improvements in the analytical methods of reactor design. The following conclusions may be drawn from the analyses of Yankee Core I reactivity characteristics.

1. The moderator temperature coefficient and the power coefficient were highly negative and experienced very little change in magnitude during the entire Core I lifetime. The withdrawal of control rods from the core as burnup proceeds tends to render the moderator temperature coefficient less negative while it appears that the net effect of plutonium and fission product buildup is to render the coefficient more negative. The combination of these two opposite effects results in a nearly constant coefficient throughout core life. Measurements have shown that the power coefficient is a sensitive function of power. Calculations indicate that the variation with power can be predicted on the basis of changes in the pellet-clad heat transfer characteristics.

2. Core lifetime and burnup rate are reasonably well predicted by one-dimensional diffusion theory calculations. These calculations however are sensitive to the values of U-238 resonance escape probability and lumped fission product poisoning.

3. The differential control rod worth is a sensitive function of burnup, power and fission product distribution in the core. Measurements, substantiated by calculations, have indicated the fallacy of relying on rod worth data obtained before power operation to obtain reactivity worth data.

4. A statistical weight analysis has shown that the variations in the power coefficient of the order of 15% were experienced in Yankee Core I as a result of non-uniform power distribution. Non-uniform distribution effects have been shown to have little influence on Xe-135 equilibrium poisoning. However, significant statistical weight factor variations occur during Xe-135 transients. Xe-135 oscillations were not predicted and have not been encountered during power operation.

5. Anomalous reactivity variations (both positive and negative) of the order of 0.5% $\Delta\rho$ have been observed during power operation. These variations have occurred during relatively long time periods and were characterized by anomalous control rod motion or temperature variations with time. These reactivity variations were not predicted on the basis of conventional reactivity calculations. However, subsequent analyses have shown that such variations can be explained on the basis of statistical weight factor variations, changes in the power coefficient as a result of variation in the heat transfer characteristics of the fuel, plant chemistry effects and changes in control rod differential rod worth.

ACKNOWLEDGEMENT

The author wishes to express his appreciation to Mr. H. W. Graves, Jr., Manager of the Nuclear Engineering Section, Reactor Development, WAPD, for his continued interest and for many stimulating discussions and suggestions. The excellent work of Mr. J. E. Howard of the Yankee Atomic Electric Company in performing the experiments and obtaining the physics data and his assistance and cooperation in transmitting these data to WAPD is especially acknowledged. The assistance of Mr. W. S. Hudec who performed some of the analyses and of Mr. E. P. Mortimore who carried out many of the calculations is appreciated. The able efforts of Miss Joan Jesko in preparing both drafts and final version of the report are gratefully acknowledged.

APPENDIX

CALCULATION OF STATISTICAL WEIGHT FACTORS BY PERTURBATION THEORY

A statistical weight factor, W, on a reactivity perturbation is defined as the ratio of reactivity worth calculated with a non-uniform perturbation in a non-uniform core, to the reactivity worth calculated with a uniform perturbation in a uniform core, or

$$W = \frac{\rho^{(\text{non-uniform})}}{\rho^{(\text{uniform})}} \tag{A1}$$

A perturbation theory expression for the reactivity ρ will now be obtained from the space- and time-dependent two-group diffusion equation:

$$\nabla \cdot D_1(\bar{r}, t) \nabla \phi_1(\bar{r}, t) - \left[\Sigma_R(\bar{r}) + \Sigma_{a_1}(\bar{r}) \right] \phi_1(\bar{r}, t) + \frac{\nu}{\nu_o} \sum_j \left[\nu_1^j \, {}^j_{f_1}(\bar{r}) \phi_1(\bar{r}, t) + \nu_2^j \Sigma_{f_2}(\bar{r}) \phi_2(\bar{r}, t) \right] = \frac{1}{v_1} \frac{\partial \phi_1(\bar{r}, t)}{\partial t} \tag{A2}$$

$$\nabla \cdot D_2(\bar{r}) \nabla \phi_2(\bar{r}, t) - \Sigma_{a_2}(\bar{r}) \phi_2(\bar{r}, t) + \Sigma_R(\bar{r}) \phi_1(\bar{r}, t) = \frac{1}{v_2} \frac{\partial \phi_2(\bar{r}, t)}{\partial t} \tag{A3}$$

In equations (A2) and (A3) the cross sections are assumed to be independent of time. The superscripts j include all the fissionable isotopes of the core. $\frac{\nu}{\nu_o}$ is an eigenvalue which provides a means of adjusting equations (A2) and (A3) such that the calculated time behavior of the fluxes will correspond to the experimental time behavior [5].

Equations (A2) and (A3) may be written in matrix notation as

$$M\Phi = \frac{\partial \Phi}{\partial t} \tag{A4}$$

where the flux matrix, Φ, is defined as

$$\Phi(\bar{r}, t) = \begin{pmatrix} \phi_1(\bar{r}, t) \\ \\ \phi_2(\bar{r}, t) \end{pmatrix} \tag{A5}$$

and the differential operator matrix M is defined as

$$M(\bar{r}) = \begin{pmatrix} v_1 \left\{ \nabla \cdot D_1(\bar{r}) \nabla - \left[\Sigma_R(\bar{r}) + \Sigma_{a_1}(\bar{r}) - \frac{\nu}{\nu_o} \sum_j \nu_1^j \Sigma_{f_1}^j (\bar{r}) \right] \right. & v_1 \frac{\nu}{\nu_o} \sum_j \nu_2^j \Sigma_{f_2}^j (\bar{r}) \\ \\ v_2 \Sigma_R & v_2 \left[\nabla \cdot D_2(\bar{r}) \nabla - \Sigma_{a_2}(\bar{r}) \right] \end{pmatrix} \tag{A6}$$

Separability of time and space will now be assumed in the solution for Φ. The following asymptotic solution will be assumed for Φ.

$$\Phi(\bar{r}, t) = \phi(\bar{r})\, e^{\omega t} \tag{A7}$$

If equation (A7) is substituted into equation (A4), the following time-independent diffusion theory equation is obtained

$$M(\bar{r})\, \phi\, (\bar{r}) = \omega \phi\, (\bar{r}) \tag{A8}$$

where

$$\phi(\bar{r}) = \begin{pmatrix} \phi_1(\bar{r}) \\ \\ \phi_2(\bar{r}) \end{pmatrix} \tag{A9}$$

We now introduce an adjoint function $\phi^+(\bar{r})$ which is orthogonal to $\phi(\bar{r})$. $\phi^+(\bar{r})$ is a solution of the differential equation

$$M^+(\bar{r})\ \phi^+(\bar{r}) = \omega^* \phi^+(\bar{r}) \tag{A10}$$

where $M^+(\bar{r})$ is the transposed matrix of equation (A6) and ω^* is the complex conjugate of ω. The adjoint matrix $\phi^+(\bar{r})$ is defined as

$$\phi^+(\bar{r}) = \begin{pmatrix} \phi_1^+(\bar{r}) & \phi_2^+(\bar{r}) \end{pmatrix} \tag{A11}$$

Assume that the reactor system represented by equation (A8) and which is on a stable inverse period ω is perturbed. A perturbation differential operator matrix $P(\bar{r})$ is defined as

$$P(\bar{r}) \begin{pmatrix} \nabla \cdot \delta v_1 D(\bar{r}) \nabla - \delta \left[v_1 (\Sigma_R(\bar{r}) + \Sigma_{a_1}(\bar{r}) - \frac{\nu}{\nu_o} \sum_j \nu_1^j \Sigma_{f_1}^j(\bar{r}) \right] & \delta \left[v_1 \frac{\nu}{\nu_o} \sum_j \nu_2^j \Sigma_{f_2}^j(\bar{r}) \right] \\ \delta \left[v_2 \Sigma_R(\bar{r}) \right] & \nabla \cdot \delta v_2 D_2(\bar{r}) \nabla - \delta \left[v_2 \Sigma_{a_2}(\bar{r}) \right] \end{pmatrix} \tag{A12}$$

where the δ refer to changes in the parameters from the unperturbed condition.

The perturbed flux $\phi'(\bar{r})$ is the solution of the diffusion equation

$$\left[M(\bar{r}) + P(\bar{r})\right] \phi'(\bar{r}) = \omega'\phi'(\bar{r}) \tag{A13}$$

where ω' is the asymptotic inverse period of the perturbed reactor system.

Multiply equation (A13) by $\phi^+(\bar{r})$ and equation (A10) by $\phi'(\bar{r})$, integrate over all space and subtract.

$$\int \left[\phi^+(\bar{r})\, M(\bar{r})\, \phi'(\bar{r}) - \phi'(\bar{r})\, M^+(\bar{r})\, \phi^+(\bar{r})\right] dV + \int \phi^+(\bar{r})\, P(\bar{r})\, \phi'(\bar{r})\, dV = \int (\omega' - \omega^*)\, \phi^+(\bar{r})\, \phi'(\bar{r})\, dV \tag{A14}$$

Since $\phi'(\bar{r})$ and $\phi(\bar{r})$ satisfies the same boundary conditions, the first integral on the left side of equation (A14) is zero.

From equation (A14) we obtain

$$\omega' - \omega^* = \frac{\int \phi^+(\bar{r})\, P(\bar{r})\, \phi'(\bar{r})\, dV}{\int \phi^+(\bar{r})\, \phi'(\bar{r}) dV} \tag{A15}$$

In equation (A15) ω^* may be replaced by its real component ω. If equations (A9), (A11) and (A12) are substituted in equation (A15) we obtain an expression for the change in the stable inverse period of a reactor system caused by some perturbation P of the system.

$$\omega' - \omega = \frac{1}{R}\int \left\{ - \delta v_1 \left[\Sigma_R(\bar{r}) + \Sigma_{a_1}(\bar{r})\right] \phi_1^+(\bar{r})\, \phi_1'(\bar{r}) + \delta v_1 \left[\frac{\nu}{\nu_o} \sum_j \nu_1^j \Sigma_{f_1}^j(\bar{r})\right] \right.$$

$$\left. \phi_1^+(\bar{r})\, \phi_1'(\bar{r}) + \delta v_2 \left[\frac{\nu}{\nu_o} \sum_j \nu_2^j \Sigma_{f_2}^j(\bar{r})\right] \phi_1^+(\bar{r})\, \phi_2'(\bar{r}) + \delta v_2\, \Sigma_R(\bar{r})\, \phi_2^+(\bar{r}) \right. \qquad \text{(A16)}$$

$$\phi_1'(\bar{r}) - \delta v_2\, \Sigma_{a_2}(\bar{r})\, \phi_2^+(\bar{r})\ \ \phi_2^+(\bar{r})\, \phi_2'(\bar{r}) - \nabla \phi_1^+(\bar{r})\, \delta\left[v_1 D_1(\bar{r})\right]\ \cdot \phi_1'(\bar{r})$$

$$\left. - \nabla \phi_2^+(\bar{r})\, \delta\left[v_2 D_2(\bar{r})\right]\ \nabla \cdot \phi_2'(\bar{r}) \right\} dV$$

where

$$R = \int \left[\phi_1^+(\bar{r})\, \phi_1'(\bar{r}) + \phi_2^+(\bar{r})\, \phi_2'(\bar{r})\right] dV \qquad \text{(A17)}$$

To obtain an expression for the reactivity effect of the perturbation it will be required that the change in the inverse stable period of the reactor system as a result of the perturbation P be zero. This may be achieved by introducing a fictitious change in the eigenvalue ν/ν_o such that the total reactivity change due to the perturbation P and the fictitious change in the value of ν/ν_o is zero. The new value of the eigenvalue will be called ν'/ν_o. We can write

$$\delta v_1 \left[\frac{\nu}{\nu_o} \sum_j \nu_1^j \Sigma_{f_1}^j(\bar{r})\right] = v_1 \left[\frac{\nu}{\nu_o}\, \delta\left[\sum_j \nu_1^j \Sigma_{f_1}^j(\bar{r})\right] + \sum_j \nu_1^j \Sigma_{f_1}^j(\bar{r})\, \delta\left(\frac{\nu}{\nu_o}\right)\right] \qquad \text{(A18)}$$

$$\delta v_2 \left[\frac{\nu}{\nu_o} \sum_j \nu_2^j \Sigma_{f_2}^j(\bar{r})\right] = v_2 \left[\frac{\nu}{\nu_o}\, \delta\left[\sum_j \nu_2^j \Sigma_{f_2}^j(\bar{r})\right] + \sum_j \nu_2^j \Sigma_{f_2}^j(\bar{r})\, \delta\left(\frac{\nu}{\nu_o}\right)\right] \qquad \text{(A19)}$$

Since the reactor system has been left unchanged by the perturbation and the fictitious change of the eigenvalue, $\omega' = \omega$. Using equations (A18) and (A19), equation (A16) became

$$- \delta\left(\frac{\nu}{\nu_o}\right) \int \left[v_1 \left(\sum_j \nu_1^j \Sigma_{f_1}^j(\bar{r}) \right) \phi_1^+(\bar{r}) \phi_1'(\bar{r}) + v_2 \left(\sum_j \nu_2^j \Sigma_{f_2}^j(\bar{r}) \right) \phi_1^+(\bar{r}) \phi_2'(\bar{r}) \right] dV$$

$$= \int \Bigg\{ - \delta v_1 \left[\Sigma_R(\bar{r}) + \Sigma_{a_1}(\bar{r}) \right] \phi_1^+(\bar{r}) \phi_1'(\bar{r}) + v_1 \frac{\nu}{\nu_o} \delta \left[\sum_j \nu_1^j \Sigma_{f_1}^j(\bar{r}) \right] \phi_1^+(\bar{r}) \phi_1'(\bar{r})$$

$$+ v_2 \frac{\nu}{\nu_o} \delta \left[\sum_j \nu_2^j \Sigma_{f_2}^j(\bar{r}) \right] \phi_1^+(\bar{r}) \phi_2'(\bar{r}) \qquad \text{(A20)}$$

$$+ \delta \left[v_2 \Sigma_R(\bar{r}) \right] \phi_2^+(\bar{r}) \phi_1'(\bar{r}) - \delta \left[v_2 \Sigma_{a_2}(\bar{r}) \right] \phi_2^+(\bar{r}) \phi_2'(\bar{r})$$

$$- \nabla \phi_1^+(\bar{r}) \delta \left[v_1 D_1(\bar{r}) \right] \nabla \cdot \phi_1'(\bar{r}) - \nabla \phi_2^+(\bar{r}) \delta \left[v_2 D_2(\bar{r}) \right] \nabla \cdot \phi_2'(\bar{r}) \Bigg\} dV$$

But

$$\delta\left(\frac{\nu}{\nu_o}\right) = \frac{\delta\nu}{\nu_o} = \frac{\nu' - \nu}{\nu_o} = \rho \qquad \text{(A21)}$$

Equation (A20) can therefore be written

$$\rho = \frac{1}{F} \int \Bigg\{ - \delta v_1 \left[\Sigma_R(\bar{r}) + \Sigma_{a_1}(\bar{r}) \right] \phi_1^+(\bar{r}) \phi_1'(\bar{r}) + v_1 \frac{\nu}{\nu_o} \delta \left[\sum_j \nu_1^j \Sigma_{f_1}^j(\bar{r}) \right] \phi_1^+(\bar{r}) \phi_1'(\bar{r})$$

$$+ v_2 \frac{\nu}{\nu_o} \delta \left[\sum_j \nu_2^j \Sigma_{f_2}^j(\bar{r}) \right] \phi_1^+(\bar{r}) \phi_2'(\bar{r})$$

$$+ \delta \left[v_2 \Sigma_R(\bar{r}) \right] \phi_2^+(\bar{r}) \phi_1'(\bar{r}) - \delta \left[v_2 \Sigma_{a_2}(\bar{r}) \right] \phi_2^+(\bar{r}) \phi_2'(\bar{r})$$

(A22)

$$- \nabla \phi_1^+(\bar{r}) \delta \left[v_1 D_1(\bar{r}) \right] \nabla \cdot \phi_1'(\bar{r}) - \nabla \phi_2^+(\bar{r}) \delta \left[v_2 D_2(\bar{r}) \right] \nabla \cdot \phi_2'(\bar{r}) \Big\} dV$$

where

$$F = \int \left[v_1 \sum_j \nu_1^j \Sigma_{f_1}^j(\bar{r}) \phi_1^+(\bar{r}) \phi_1'(\bar{r}) + v_2 \sum_j \nu_2^j \Sigma_{f_2}^j(\bar{r}) \phi_1^+(\bar{r}) \phi_2'(\bar{r}) \right] dV \qquad (A23)$$

ρ is the reactivity associated with the perturbation P.

Equation (A22) for ρ is equivalent to the definition of ρ given by Henry [5].

The perturbations P produced by the Doppler effect and equilibrium Xe-135 poisoning were given by equation (3.15) and equation (3.22). The assumption will now be made that the fluxes are self-adjoint. This assumption was checked for Yankee by calculating the normal and adjoint fluxes in the depleted core with the AIM-5 code [12]. The fast and thermal fluxes distributions to be used in equation (A22) are obtained from in-core instrumentation data. The activation $I(\bar{r})$ which is obtained from the flux wires is that of Mn^{56} after absorption of a neutron by Mn^{55}. The following quantities are introduced.

$$\kappa(\bar{r}) = \phi_1(\bar{r}) / \phi_2(\bar{r}) \qquad (A24)$$

$$P(\bar{r}) = \beta(\bar{r}) \phi_1(\bar{r}) \qquad (A25)$$

$$\beta(\bar{r}) = \sum_j \left[\frac{\Sigma_{f_1}^j(\bar{r})}{C^j} + \frac{\Sigma_{f_2}^j(\bar{r})}{C^j} \quad \frac{1}{\kappa(\bar{r})} \right] \qquad (A26)$$

where C^j is the number of fissions per watt-sec in isotope j

$$\epsilon(\bar{r}) = \beta(\bar{r})\ \kappa(\bar{r}) \tag{A27}$$

$$\sigma(\bar{r}) = \sigma_{a_1}^{\text{Mn-55}} + \frac{\sigma_{a_2}^{\text{Mn-55}}}{\kappa(\bar{r})} \tag{A28}$$

$$\xi(\bar{r}) = \sigma(\bar{r})\ \kappa\ (\bar{r}) \tag{A29}$$

$$\kappa^+(\bar{r}) = \phi_1^+(\bar{r})/\phi_2^+(\bar{r}) \tag{A30}$$

$$M(\bar{r}) = \left[1 + \frac{1}{\kappa(\bar{r})\ \kappa^+(\bar{r})}\right] \tag{A31}$$

$$N(\bar{r}) = \left[1 + \kappa(\bar{r})\ \kappa^+(\bar{r})\right] \tag{A32}$$

If equations (3.15) and (3.22) are substituted in equation (A22) and if the quantities given in equation (A24) through equation (A32) are used together with the definition of equations (3.18), (3.19), and (3.26), an expression for ρ(non-uniform) in equation (A1) is obtained. By using core averaged values for the quantities in equations (A24) through (A32), an expression for ρ(uniform) is obtained. Equations (3.17) and (3.25) are then readily obtained with equation (A1).

REFERENCES

1. J. D. McGaugh and R. H. Chastain, "Power Density and Burnup Distributions in Yankee Core I", WCAP-6051 (1962).

2. "Yankee Atomic Electric Company - Technical Information and Final Hazards Summary Report", Volume I and Volume II.

3. J. M. Gallagher, Jr., H. W. Graves, Jr., D. Hunter and J. E. Howard, "The Startup Experiment Program for the Yankee Reactor", YAEC-184 (1961).

4. H. W. Graves, Jr., R. F. Janz, and C. G. Poncelet, "The Nuclear Design of the Yankee Core", YAEC-136 (1961).

5. A. F. Henry, "The Application of Reactor Kinetics to the Analysis of Experiments", Nuclear Science and Engineering, 3:52-71 (1958).

6. E. E. Gross and J. H. Marable, "Static and Dynamic Multiplication Factors and Their Relation to the Inhour Equation", Nuclear Science and Engineering, 7:281-291 (1960).

7. C. G. Bilodeau et al, "PDQ - An IBM-704 Code to Solve the Two-Dimensional Few-Group Neutron-Diffusion Equations", WAPD-TM-70 (1957).

8. H. Amster, R. Suarez, "The Calculation of Thermal Constants Averaged Over a Wigner-Wilkins Spectrum: Description of the SOFOCATE Code", WAPD-TM-39 (1957).

9. H. Bohl, Jr., E. M. Gelbard, and G. M. Ryan, "MUFT-4 Fast Neutron Spectrum Code for the IBM-704", WAPD-TM-72 (1957).

10. A. F. Henry, "A Theoretical Method for Determining the Worth of Control Rods", WAPD-218 (1959).

11. G. R. Keepin, T. F. Wimett and R. K. Zeigler, "Delayed Neutrons from Fissionable Isotopes of Uranium, Plutonium, and Thorium", Phys. Rev. 107, 1044-1049 (1957).

12. M. P. Flatt and D. C. Baller, "AIM-5 - A Multigroup, One-Dimensional Diffusion Equation Code", NAA-SR-4694 (1960).

13. J. E. Howard, Personal Communication.

14. W. H. Arnold, Jr. and R. A. Dannels, "The Doppler Coefficient of U-238 O_2" TRANSACTIONS OF THE AMERICAL NUCLEAR SOCIETY 3-1 (1960).

15. E. Hellstrand et al, "The Temperature Coefficient of the Resonance Integral for Uranium Metal and Oxide", Nuclear Science and Engineering: 8, 497-506 (1960).

16. E. A. McCabe, Jr., "Thermal Design Aspects of the Yankee First Core Fuel Rod", YAEC-106 (1960).

17. J. R. Dietrich, Editor, Power Reactor Technology, 5, 1 (1961).

18. D. F. Babcock, "Heavy Water Moderated Power Reactors - Progress Report", DP-725 (1962).

19. Yankee Nuclear Power Station, "Operation Report No. 10", October 1961.

20. O. J. Marlowe, P. A. Ombrellaro, "CANDLE - A One-Dimensional Few-Group Depletion Code for the IBM-704", WAPD-TM-53 (1957).

21. J. D. Callaghan, et al, "TURBO - A Two-Dimensional Few Group Depletion Code for the IBM-704", WAPD-TM-95 (1957).

22. D. S. Craig et al, "Long Irradiation of Natural Uranium", A/CONF. 15/P1205 (1958).

23. J. D. McGaugh, "A Study of Fuel Depletion and Control Rod Programming in the Yankee Reactor", YAEC-183 (1960).

24. "Technical Progress Report - Pressurized Water Reactor (PWR) Project for the Period from August 24, 1960 to October 23, 1960", WAPD-MRP-88 (1960).

25. J. D. Garrison and B. W. Ross, "Fission Product Capture Cross Sections", Nuclear Science and Engineering: 12, 113-134 (1962).

26. S. B. Gunst et al, "U-235 Fission-Product Poison Experiments", TRANSACTIONS OF THE AMERICAL NUCLEAR SOCIETY, 5, 1 (1962).

27. W. H. Fleming and H. G. Thode, "The Relative Yields of the Isotopes of Xenon in Plutonium Fission", Can. J. Chem. 34, No. 3, 193 (1956).

28. R. Wiles, J. A. Petruska and R. H. Tomlinson, "Some Cumulative Yields of Isotopes Formed in the Thermal Neutron Fission of Pu-239", Can. J. Chem, 34 No. 3, 227 (1956).

29. J. A. Petruska, H. G. Thode and R. H. Tomlinson, "The Absolute Fission Yields of Twenty-Eight Mass Chains in the Thermal Neutron Fission of U-235", Can. J. Phys. 33, No. 11 693 (1955).

30. D. Hunter, C. G. Poncelet, H. W. Graves, Jr. and J. E. Howard, "Evaluation of Reactivity Coefficient in the Yankee Reactor", TRANSACTIONS OF THE AMERICAN NUCLEAR SOCIETY, 4, 1 (1961).

31. S. Katcoff, "Fission Product Yields from U, Th, and Pu", Nucleonics, 16, No. 4, 78 (1958).

32. D. J. Hughes and R. B. Schwartz, "Neutron Cross Sections", BNL-325 (1958).

33. A. E. McArthy et al, "Neutron Resonance Integral and Age Data", Argonne National Laboratory, Reactor Physics Constants Center - Newsletter No. 1 (1961).